DIPLOMARBEIT

Quality Measurement on 3D Ultrasound Volumes Reconstructed from 2D Slices and its Application in Radiation Therapy

Ausgeführt am
Institut für Analysis und Scientific Computing
der Technischen Universität Wien

unter der Anleitung von
Ao. Univ.-Prof. i.R. Dipl.-Ing. DDDr. Frank Rattay
Institute für Analysis und Scientific Computing, Technische Universität Wien

Mag. Dr. Johann Hummel
Zentrum für Medizinische Physik und Biomedizinische Technik, Medizinische Universität Wien

durch
Reinhard Kerschner, BSc

Wien, 08. April 2015

Declaration

I hereby declare that this master's thesis is the product of my own independent work. I confirm not to have used resources other than those declared. All content and ideas drawn directly or indirectly from external sources are indicated as such. This thesis has not been submitted to any other examining body and has not been published in any other way.

Vienna, 8th of April 2015 Signature: .....

Abstract

Radiation therapy relies on exact patient positioning to spare organs at risk and thus be able to deliver higher and more effective radiation doses with fewer side effects to surrounding tissue. Thereby it is also possible to apply better dose distribution on the tumor. There are several methods available for patient positioning, which are discussed, but most of them imply additional radiation dose for the patient. There are also systems on the market which rely on ultrasound as imaging modality. As the system should be used to align patients suffering from soft tissue cancer for example in the region of the prostate, the advantage is the good contrast of soft tissue compared to systems using X-ray. This short overview suggests a new 3D ultrasound reconstructed from 2D ultrasound image slices. To use such a method several tools are of need which are presented and discussed. A tracker device tracks the position of the ultrasound probe during image acquisition. Thereby, by ultrasound calibration, the transformation between the probe sensor and the recorded image can be calculated. Therefore a software is used which performs calibration, recording of the images as well as reconstruction of the 3D volume out of the recorded 2D images. After reconstruction it is compared which of the US systems is better in quality and accuracy, the reconstructed 3D ultrasound or the classical 3D ultrasound. This is of importance for patient positioning as then the better method can be used. There are several ways to perform such a comparison. One of the most promising for the underlying application is 3D/3D ultrasound image registration. This is done via comparison of two separate recorded and reconstructed image volumes. Registration tries to align two images that way that both images, when possible, exactly overly and are congruent. Image registration then gives a transformation matrix which contains the translation and rotation of one image compared to the other. Out of this it is concluded which of the two systems is better in quality and thus more accurate. For comparison two different datasets where used. Results show an overall lower quality of reconstructed image volumes compared to general 3D ultrasound devices when using patient data. Using a figure phantom show better results but quality in terms of accuracy still remains behind general 3D ultrasound machines. Thus applicability in image-guided radiation therapy cannot be recommended as when using it patient positioning would be too inaccurate.

Kurzfassung

Genaue Patientenpositionierung ist ein wesentlicher Punkt in der Strahlentherapie, da es hierdurch ermöglicht wird risikogefährdete Organe auszusparen und somit effektivere Strahlendosen mit geringeren Nebenwirkungen zur Anwendung zu bringen. Dabei stehen verschiedene Methoden zur Patientenpositionierung zur Verfügung, welche kurz vorgestellt werden. Die meisten implizieren jedoch die Anwendung von zusätzlicher Strahlung. Es gibt jedoch auch Systeme die auf Ultraschall basieren. Dabei ist einer der Vorteile, gegenüber Systemen die auf Röntgenstrahlung basieren, der gute Bildkontrast von Weichgewebe. Um diesen Vorteil gewinnbringend zu nutzen wird ein neues System vorgeschlagen, welches 3D Volumina anhand von 2D Ultraschallbildern erzeugt. Zur Umsetzung dieser Methode werden verschiedene Materialien benötigt, welche diskutiert werden. Ein Trackingsystem verfolgt bei der Bildaufnahme die Position des Ultraschallkopfes. Dabei kann mittels Ultraschallkalibrierung die Transformation zwischen Ultraschallkopf und Bild berechnet werden. Für diesen Zweck wird eine Software verwendet, welche in der Lage ist die Ultraschallkalibrierung durchzuführen als auch Bilddaten aufzunehmen und die Rekonstruktion eines 3D Volumens aus den aufgenommenen 2D Bildern zu berechnen. Nach der Rekonstruktion wird verglichen, welches der Ultraschallsysteme die bessere Qualität und Genauigkeit liefert. Dies ist von hoher Wichtigkeit für die Patientenpositionierung, da hiermit auf die Anwendbarkeit in der Strahlentherapie des vorgeschlagenen Systems geschlossen werden kann. Dabei gibt es verschiedene Möglichkeiten eines Vergleichs. Die vielversprechendste Variante für den zugrundeliegenden Anwendungsbereich ist dabei die 3D/3D Ultraschall Registrierung. Dabei versucht die Bildregistrierung zwei Bilder derart auszurichten, dass sie, wenn möglich, exakt übereinanderliegen und deckungsgleich sind. Als Ergebnis folgt aus der Bildregistrierung eine Transformationsmatrix, welche die Verschiebung und die Rotation der beiden Bilder zueinander beinhaltet. Daraus wird anschließend geschlossen, welches der zwei Systeme die bessere Qualität und damit die höhere Genauigkeit liefert. Für den Vergleich wurden zwei verschiedene Datensets verwendet. Die Resultate zeigen, dass eine insgesamt niedrigere Qualität des rekonstruierten Bildvolumens, verglichen mit herkömmlichen 3D Ultraschallgeräten, erreicht wird, sofern Patientendaten verwendet werden. Wird jedoch ein Phantom mit verschiedenen Figuren verwendet, so bessert sich die Qualität in Bezug zur Genauigkeit, bleibt aber weiterhin hinter herkömmlichen 3D Ultraschallgeräten zurück. Daher ist die Anwendbarkeit in der bildgeführten Strahlentherapie nicht empfehlenswert, da die Genauigkeit des Systems für die hohen Anforderungen zu niedrig ist.

Contents

1 Introduction

In the last decade many progress was made in the field of radiation therapy. Besides brachytherapy external beam radiation therapy with linear accelerators is used. In the last years also synchrotron radiation is used to accelerate heavy particles and use such particle beams to treat cancer. The advantage lies in the application of the Bragg peak. Anyhow, several methods of treatment of cancer are available and radiation therapy is more and more often used. To support employees in the field of radiation therapy several new technologies have been invented. Image guided radiation therapy is such a technology which promises to spare organs at risk. This is also a huge advantage for the patient because radiation dose can be reduced. But for the application of this promising technology exact positioning is necessary. Different technologies in the field of navigation where invented and are used to assure exact patient positioning. For example computed tomography (CT) or magnetic resonance imaging (MRI) is used to get images of the patient anatomy. But there are also other imaging modalities available. One of these uses the treatment beam for generating images. Many of these technologies imply the application of additional radiation dose for the patient. But there is also a method where no additional radiation dose is necessary: ultrasound (US). Especially with respect to the treatment of prostate cancer ultrasound seems to be the perfect choice. It is an imaging modality using ultrasonic sound waves and generating an image from the reflected echoes of the tissue. One huge advantage is that it is capable of visualization of soft tissue. Imaging modalities (IM) using ionizing radiation are not very practical in imaging soft tissue. This is because radiation based imaging technologies are not able to visualize soft tissue. To still get sufficient and detailed 3D images 3D US is used. Such images can be registered to previously taken CT images in a next working step. Thereby a precise patient positioning is possible. There are different ways to produce 3D US images. One of them is the generation of 3D US images from 2D image slices. For the generation of 3D US images composed of 2D US images one has to use tracking systems to be able to add these 2D images to the correct position in the 3D volume. Hence also navigation is important for image guided radiation therapy.

This chapter is to introduce the fundamentals of the topics related to 3D US image generation for patient positioning in image guided radiation therapy for treating cancer. Therefore the principals of ultrasound are discussed. This topic includes transducers as well as image resolution and artifacts. Image resolution is important subtopic for quality measurement as it gives information of which degree details can be seen. For patient positioning and the generation of 3D US images navigation with tracking systems is important as well. As the application of 3D US image generation is mainly used in radiation therapy also the topic of radiation therapy is discussed. Not only interactions between ionizing radiation or particles and tissue are discussed. Also radiation biologic topics are evaluated. As registration is necessary for quality measurement a closer look is also taken to this matter. By this all important topics concerning the generation of 3D US images in the field of radiation therapy are debated.

1.1 Ultrasound

In medical imaging besides X-ray ultrasound (US) counts as the most often used imaging modality. Its application becomes more and more important because of its mobility and compared to other modalities its low costs. It is easy to use and offers good image quality. One big advantage is the missing ionizing radiation as only ultrasound is used. The technology of ultrasound evolves rapidly and thus more applications become possible. Compared to Computed Tomography or Magnetic Resonance Imaging ultrasound is a real time imaging technology. That is, the image can be seen immediately on the US device screen. In the following the fundamentals on how ultrasonic imaging works are discussed.

1.1.1 Fundamentals of Ultrasonic imaging

Long ago it was discovered that acoustic waves are transmitted in water but are reflected from an interface of body tissues or any other boundaries. The reflection depends on the acoustic impedance of the material. As all tissues are composed of water, excluding bone and lungs, sound waves are transmitted through this tissue but are reflected at tissue interfaces. With this principal images can be obtained by sending high frequency sound wave pulses into the body and recording the reflected sound waves. From the reflected echoes the shape of an organ can be determined. These recordings are processed and thereby an image is generated.

The human ear can hear sound in the range of about 16Hz to 20kHz. Ultrasound is then the sound generated by frequencies greater than the hearing limit. Ultrasound imaging uses frequencies in the range of 1 to 10Mhz. Sound in general also ultrasound travels as longitudinal wave which means that the medium moves in the same direction in which the wave travels. As propagation depends upon the elastic properties of the material also the pressure change depends on it. It is defined as

$$\Delta P = -\beta \frac{\Delta V}{V} \tag{1.1}$$

where β is the modulus of elasticity. Also an important measure is the speed of sound, which also depends on the elasticity of the medium in which the wave propagates. c is defined as

$$c = \sqrt{\frac{\beta}{\rho_0}} \tag{1.2}$$

where ρ_0 represents the density of the medium. The speed of sound in tissue ranges from 1450m/s for fat to 4080m/s for bone, as the density of bone is rather high. The average speed of sound is defined as approximately 1540m/s (Sawney, 2007). As biological tissue is not acoustically homogeneous, ρ_0 and c are not constant, some part of the wave is transmitted as the other part is reflected. The amount of reflection can be calculated by

$$R = \frac{(Z_1 - Z_2)^2}{(Z_1 + Z_2)^2} \tag{1.3}$$

whereas the amount of transmission is defined by

$$T = \frac{(2Z_1 Z_2)^2}{(Z_1 + Z_2)^2} \tag{1.4}$$

The acoustic impedance Z is defined as $\rho_0 c$. The higher the difference $Z_1 - Z_2$, the higher the reflection gets, that is, the higher the difference in speed of sound defined by the two materials, the more the incident wave is reflected (Sawney, 2007), see Figure 1.1.

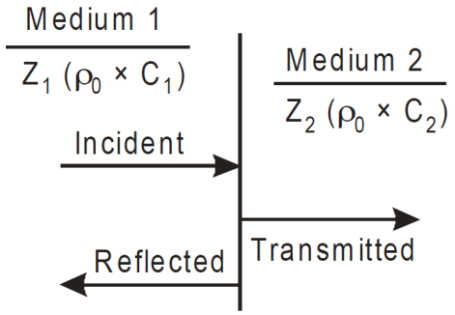

Figure 1.1: Incident, Reflected and Transmitted wave (Sawney, 2007)

As the difference of the acoustic impedance $Z_1 - Z_2$ for air and tissue is rather high, the complete energy is reflected. To minimize this reflection from the interface transducer and skin, a special gel is used. Otherwise it would not be possible to penetrate the body by ultrasound waves. Also important to know is, that the transmission and thereby the penetration depth is dependent on the transducer frequency. Higher Frequencies have shorter wavelengths which can penetrate less than longer wavelengths. To calculate the depth the wave can pass before it is reflected the speed of sound in the medium is necessary. The depth is defined as the product of the time the wave travels and the speed of sound. This information is used by the computer to generate the image.

1.1.2 Ultrasound Transducers

The transducer is the device generating ultrasound waves. It converts electrical energy into mechanical energy. The effect used for generating mechanical sound waves is the piezoelectric effect. Mechanical stress applied to a quartz crystal results in an electric field across the opposite faces of the crystal. The inverse is also true, so it is possible to apply an electric potential to a quartz crystal which results in mechanical deformation of the crystal. This deformation results in compression of the material which leads to a sound wave. When changing the electrical field with high frequencies it is possible to generate ultrasonic waves (Bronzino, 2006).

In the past many efforts were laid in the development of new transducers. In the beginning an image was made by manually moving the transducer across the region of interest. With such transducers real time imaging was not possible. Nowadays transducer arrays are used with which it is possible to rapidly steer the acoustic beam to generate images in real time. With linear arrays it is possible to focus the beam in a rectangular image region (Bronzino, 2006). To focus an acoustic wave different delays are applied across the transducer aperture. With such phase delays a dynamic focusing is possible. A Linear Phased Array contains several (128 and rising) array elements which dimension is less than one mm on one side. Each element has its own connection to transmit and receive electronics. Thus it is possible to steer each element particular. This procedure is explained in Figure 1.2. Each element can be seen as a point source that transmits a spherical shaped wave. The farthest element from the focus point is excited first while nearer elements are excited later. The phase difference is such, that each wave reaches the focal point at the same time (Bronzino, 2006). According to Huygen's principal, the amplitude at the focal point is the sum of all the waves from each array element.

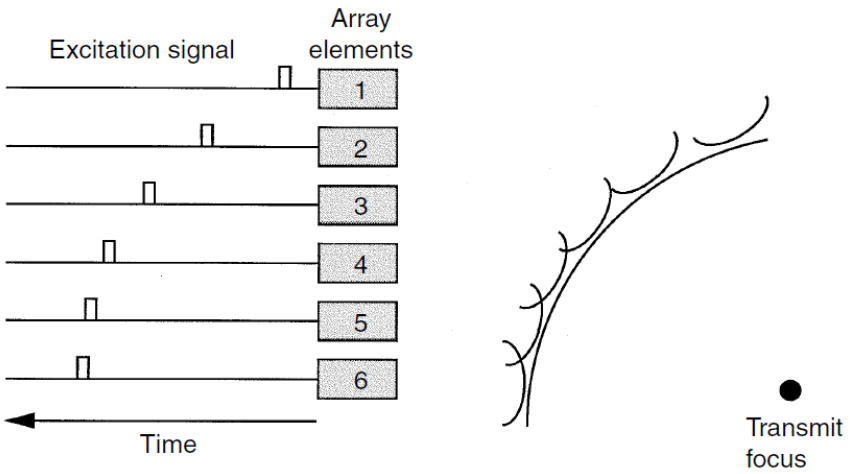

Figure 1.2: Focusing an acoustic beam using an phased array (Bronzino, 2006)

As transmitting and receiving at the same time is not possible, one has to differentiate between a transmission mode and a receiving mode. For receiving an echo the transducer works in receiving mode. In transmission mode the transducer sends a pulse with duration of one microsecond. Then it switches to receiving mode for about a millisecond. This is necessary the echoes to die out and not to interfere with another pulse sent from the transducer (Sawney, 2007).

There are different array-element configurations because different applications require different transducer types. These types can be seen in Figure 1.3 and are explained in the following (Bronzino, 2006).

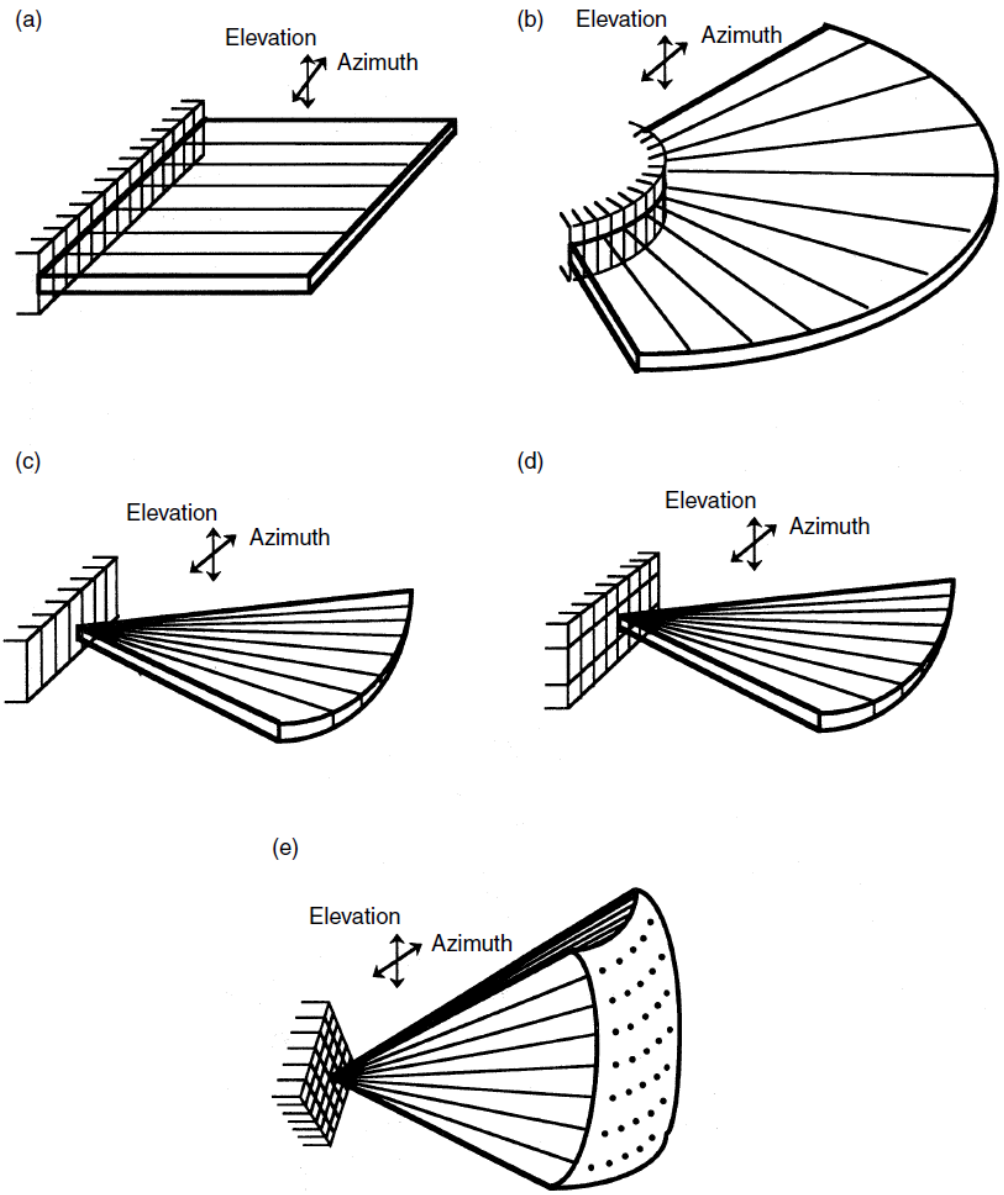

Figure 1.3: Different array configuration, (a) linear array, (b) curvilinear array, (c) linear phased array, (d) 1.5D array, (e) 2D array (Bronzino, 2006)

- The linear array has up to 512 elements where up to 128 elements are used at a given time. The scanning line is perpendicular to the face of the transducer. Because of the geometry the field of view is limited to the rectangular region directly in front of the transducer, which can be a disadvantage. On the other hand, such transducers have a high sensitivity because the beam is directed straight ahead.
- The curvilinear array scans a region that is sector shaped. As with the linear array the scan lines are perpendicular to the face of the transducer but a curvilinear array scans a wider field of view than a linear array. This is because of its convex shaped geometry of the curvilinear transducer.
- Linear phased arrays consist of 128 elements which are used to steer the ultrasound beam in the azimuth plane. Linear phased arrays scan a region wider than the

geometry of the transducer. This is an advantage when scanning through a restricted acoustic window like the rips.

- The 1.5D array is similar to the 2D array with the restriction that it has less elements in elevation plane. Because of these limitations, steering in this plane is not possible. Such transducers create a 1D beam. One big advantage is that dynamic focusing and phase correction can be implemented in both directions which lead to better image quality.
- 2D arrays have a large number of elements in both, azimuth end elevation dimensions. It is possible to focus steer the beam in both directions. As they scan a pyramidal region it is possible to create 3D images.

1.1.3 Image Resolution

Image resolution is important so separate small and closely structures, otherwise they cannot be seen in the ultrasound image. There are two different types of resolution, the axial resolution and the lateral resolution. The latter one is defined as the separation of small structures in the plane perpendicular to the beam axis whereas axial resolution is defined as the separation in direction of the beam axis. By focusing lateral resolution can be optimized. If the beam width is larger than the distance between to objects than these object cannot be resolved. Axial resolution depends on the pulse width. If the wavelength is larger than the axial distance of the structures, then these structures cannot be resolved (Sawney, 2007). To increase axial resolution the bandwidth is increased, so the pulse gets narrower (Bronzino, 2006). However, by increasing the frequency, absorption of the acoustic beam increases an depth penetration gets less. Depending on the application that is used different frequencies are used. When high penetration is necessary (e.g. cardiology, abdominal) frequencies in the range of 2 to 5MHz are used. If a higher resolution is needed, but penetration is not that important higher frequencies up to 20MHz can be used.

1.1.4 Artifacts

Ultrasound is an image modality that suffers from some artifacts. The most obvious artifact is noise also called speckle. It results from reflections of sound waves on microscopic inhomogeneity of the tissue. When changing the location of the transducer a change in the speckle can be seen. For an example of speckle see Figure 1.4. Shadowing is also a problem in ultrasound imaging. It results from objects that strongly reflect the sound waves. Thereby the transmitted energy is minimal which can be seen as shadows behind such objects. To reduce shadows in ultrasound imaging one can use a phased array transducer with which it is possible to scan through a window like the rips. But this does not always help. Another issue is multiple reflections which can occur between two strong reflectors. Such reflections are displayed as multiple echoes. The distance between each of the echo correlates to the distance between the two reflectors. (Birkfellner, 2014)

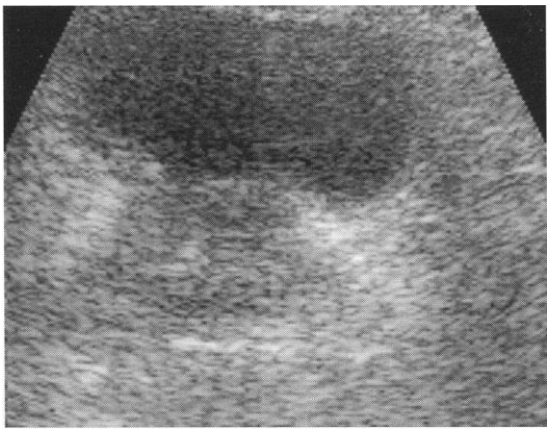

Figure 1.4: Speckle in an ultrasound image of the prostate (Birkfellner, 2014)

1.1.5 Operation Modes

During the decades ultrasound was used and the evolution of such devices yields several operation modes. The most often used mode used nowadays is the B-mode (brightness) but there are also other modes that were used. Historically the A-mode was the first mode ever which displays the amplitude of the echo along a single line on an oscilloscope. The M-mode followed the A-mode where the m stands for motion. The strength of the echoes is recorded and displayed as grey spots representing the amplitude. Objects that move are displayed as patterns of motion. Thereby for example the thickness of the heart valves can be determined. The B-mode is the most often used mode today where different amplitudes are represented by corresponding grey values. Today several B-mode lines are combined to generate a 2D image so it is used to display a grayscale image. Nowadays it is also possible to generate 3D images.

1.1.6 3D Ultrasound

The idea of 3D ultrasound is to generate a volumetric image of the tissue and it was invented to improve diagnostics from in 2D images rarely seen structures. It exists for more than 10 years and is used in several fields of medical applications. The most known clinical application is obstetrics but also cardiology, neurosurgery or urology are fields in which 3D ultrasound is used. There are different methods to obtain a 3D image. One approach is to use a wobbler. Thereby a motor wobbles a curvilinear array up and down to scan the missing dimension. Another approach is to use a two dimensional transducer. But as 2D arrays are difficult to build, they are rather expensive. This is why often wobblers are used. The last approach is to use tracking systems and add two dimensional images to a three dimensional volume. The tracker is used to scan the position of the ultrasound transducer. Its position is necessary to add the images correspondingly to the correct position of the 3D volume. This approach can be achieved using software and a normal linear or curvilinear transducer, so it is the cheapest possibility to produce 3D images (Birkfellner, 2014). But it should be kept in mind that this method is quite elaborate because a 3D tracking system and a workstation for calculating the 3D images is required. It is also necessary to calibrate the ultrasound image. There are also different ways to present the 3D volume data.

- Surface Rendering: The most known presentation of 3D images is with surface rendering. This is mostly used in obstetrics when the fetus is displays. Therefore there has to be a different impedance of the two media to have a sharp boundary. This boundary is then rendered as a surface and can be displayed
- Multi-planar reformation: This is a quite useful technique which enables the user to display a reformatted slice out of the 3D volume. It is possible to set different planes of interest and to set different angles of the plane.
- Transparent display: Using transparent display weak reflected boundaries are displayed transparent, so the user can see through the whole volume depending on the material impedance.

1.2 Navigation

Navigation is a task that helps the surgeon to improve surgical outcomes by the support of images that where taken prior to or during a surgery. It means the tracking of tools in space considering the anatomy of the patient. Development in medical imaging modalities such as Computed Tomography (CT) or Magnetic Resonance Imaging (MRI) led to an improvement in image quality which helps also for navigation tasks. It helps to plan surgical procedures and supports the surgeon to navigate during surgery. There are many computer assisted methods used in the medical field but it can be said that computer assisted navigation is the most established. The application of navigation was first used in neurosurgery but also in orthopedic surgery. By the years more and more applications got available and today it is an often used technique in the field of medicine and surgery. An important task of navigation is the precise planning of surgeries. The results can be directly transferred to the operation room. Tracked instruments can be displayed relative to the planed position using images taken pre or intraoperative. This is how navigation helps to make surgery more precise and it opens the door for novel surgery procedures (Oppelt, 2005). Navigation also plays an important role in image guided radiation therapy and radiotherapy where it is necessary to align the patients anatomy according to the planned position of irradiation. Navigation works well when the organ or tissue of interest is immobile, therefore surgery in the region of the brain is particularly well suited for navigation. But also orthopedic surgeries can be handled with navigation, for example prosthetics and osteosynthesis (Oppelt, 2005). Current research deals with navigation in soft tissue which is a hard task because of deformation of the organs. An interesting field using navigation in soft tissue is radiation therapy of the prostate. Here the prostate has to be aligned that way that it correlates spatially with images taken before the irradiation session. Therefor image registration is necessary. That means that corresponding anatomy of a reference image should be coincident to the current anatomy of the patient. Therefore before irradiation an image is taken and registered to the reference image.

1.2.1 Principals of Navigation

As mentioned before, navigation is based on the spatial relation between the actual patient anatomy and the one taken from a prior taken 3D image. Most often images are taken with CT

or MRI but also ultrasound is used. Correlation is established via registration. Thereby several fiducial markers in the image are identified as corresponding to anatomical landmarks of the patient. To acquire images during the surgery recently methods have been developed to do so. But the most often used image modality in the operation room is still ultrasound or X-ray using a C-arm X-ray unit. Only Ultrasound offers volumetric images in 3D. That is, only navigation using such ultrasound images is useful. Using such techniques automatic image registration procedures can be used to improve the workflow (Oppelt, 2005).

Navigation not only involves navigating in the widest sense but also includes several steps which also are important. Navigation should be seen as several steps building a workflow. Such steps are surgical planning based on pre-operative images, registration as one of the most important steps as well as guidance (Oppelt, 2005). Navigation is based on three major aspects:

- Visualization,
- Tracking and
- Integration

Visualization is the task where the surgical data is being monitored. This kind of data depends on the patient images. Data is displayed in real time and it should be ensured that current image data can be fused with pre-operative images. There are different methods to monitor such image data. An often used method is multi-planar reformation (MPR) but also 3D surface rendering is often used. Also planning data should be available. This is important for the surgeon to see the actual position of the tracked instrument superimposed with the planed access paths. This is also important when it comes to changes in the patient anatomy for example because of organ deformation which is not visible in the pre-operative image.

Tracking is important to give the surgeon a tool where the spatial position of the instrument is visualized on a monitor. So he can see the patient anatomy combined with the tracked instrument. Several technologies where developed and are used. Tracking is used for localization of tools such as needles or pointers and enable the display of these instruments in the image data. Used technologies are mechanical arms, optical systems or electromagnetic systems.

Integration is also important and should be kept in mind. It is important to integrate such technologies like intraoperative imaging and navigation in the workflow of the surgeon. Otherwise it would not be helpful and supportive to use them. An important prerequisite is an appropriate user interface, especially when interactive visualization, image processing or other techniques are required (Oppelt, 2005). Besides the improvement in surgical quality such systems only are accepted if they help to lower the cost for the healthcare system.

1.2.2 Tracking Systems

As navigation depends on the tracking of tools or instruments of the surgeon there is the need of the device which can fulfill this task. There are different types of tracking systems but the most used ones are optical trackers or electromagnetic systems. There are also other types of

systems but they operate in a niche and are not often used. Tracking systems consist of two different parts. The first one is a transmission unit while the second one is a sensor or several sensors rigidly attached to the surgical tools. The transmission unit of an optical tracking system consists of two or more cameras watching the sensors which reflect infrared light transmitted from the transmission unit. Electromagnetic transmission units create an electromagnetic field in which the sensors, small induction coils, are located. (Oppelt, 2005) In the following several types of tracking systems are listed and discussed:

- Optical trackers
- Electromagnetic trackers
- Mechanical tracking
- Ultrasonic trackers
- Passive HF trackers
- Inertial trackers

Optical tracking systems (OTS) consist of two or more cameras which track spherical balls reflecting infrared light transmitted from the transmission unit. Such systems are called passive systems. They offer wireless tools. But there are also active systems. The difference to passive ones is that not spherical balls are used but active infrared light emitting diodes (IR-LEDs). This is the reasons why tools from an active systems do not work without a wire connected to the transmission unit. The position of the sensor is determined via triangulation. This is possible because the sensor is seen by the transmission unit via two cameras. Thereby it is possible to calculate the relative position to the camera (Peters & Cleary, 2008). To derive the position relative to a fixed table it is possible to attach another sensor to a table. Thereby the camera can be moved without the need of recalibration (Oppelt, 2005). The accuracy of such an optical tracker depends on the length such a base unit which ranges from 0.5m to 1m. To achieve a high precision, the camera itself needs to be calibrated and temperature controlled. One disadvantage is that during surgery an uninterrupted line of sight is necessary for the base unit to track the sensors (Peters & Cleary, 2008). The system to be able to differentiate between different types of sensors a unique configuration of the markers is required. This configuration is known by the base unit and so it can differentiate between them. In order to determine the position and the orientation of the sensor at least three or more reflective spheres are necessary. An actual optical tracking system can be seen in Figure 1.5.

Beside optical tracking systems electromagnetic tracking systems (EMTS) are also often used. Thereby an electromagnetic field in the volume to track is established by the transmission unit. The field strength is then being measured by sensors which are made of small coils or flux gate sensors (Birkfellner, 2014). These sensors are connected to a base unit via a cable, so different sensors can be differentiated. Such systems do not require a free line of sight which is one advantage (Peters & Cleary, 2008). But the accuracy is not as high as with optical tracking systems. It also should be considered that the electromagnetic field may be distorted by conductive or ferromagnetic materials which lower the accuracy (Peters & Cleary, 2008). Sensors of electromagnetic tracking systems are very small which allows for usage of such systems within flexible instruments such as endoscopes.

Another method of tracking is mechanical tracking. Such systems consist of a passive arm with encoders on each joint. Since the position of each joint is then known by the encoder the position of the instrument tip can be determined. Such systems are very accurate but also bulky and difficult to sterilize. This is the reason why these systems are replaced by optical trackers more and more (Birkfellner, 2014).

Ultrasonic trackers are a variant of optical tracking systems only using ultrasonic waves instead of infrared light. Instead of the cameras many microphones are used which can track the sensors which emit ultrasound. Thereby the ultrasound emitters act like an optical beacon. Such systems suffer from the same disadvantages than optical trackers which is the need of a free line of sight. Also Changes in air humidity and temperature affect the accuracy of such systems. This type of tracking is not very widespread although such trackers are very cost effective (Birkfellner, 2014).

An interesting approach of a tracking system is passive HF-tracking. This system consists of small passive transponders. By a base unit an electromagnetic field is established which leads the transponders to emit a signal when exposed to this field. Because the signal emitted by these transponders permeates soft tissue and therefore no free line of sight is of need these small transponders can be implanted so that it is possible to track the position of internal organs during radiotherapy.

Inertial tracking is the last system to be presented. Acceleration can be integrated two times which leads to the position, when starting from a known starting point. When integrating the angular velocity this theory holds true for angulation. With this a change in rotation can be determined (Birkfellner, 2014). To measure acceleration an acceleration sensor is being used while angular velocity is measured by a special sensor. One problem of such a system is that integration yields to an inevitable drift over a longer period of time. This is the reason why such systems are not often used.

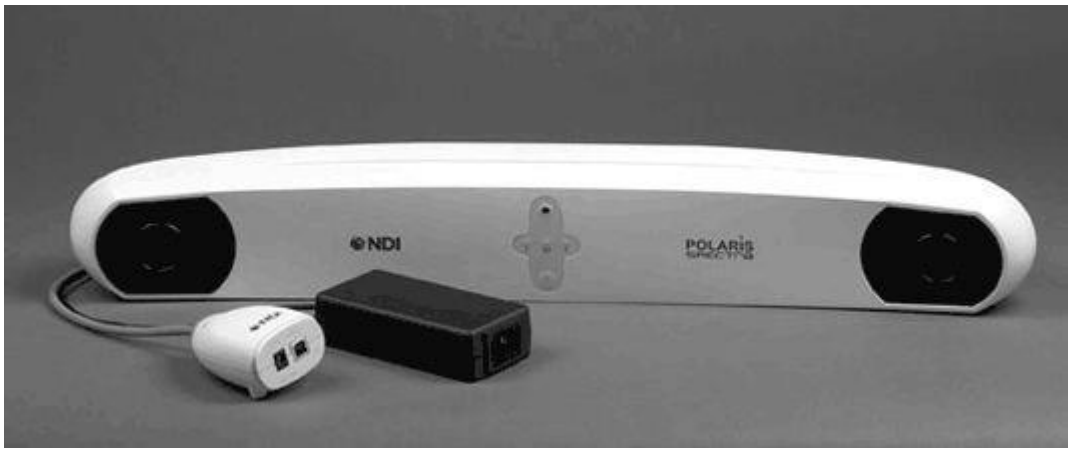

Figure 1.5: An actual optical tracker from NDI - the Polaris Spectra (MedicalExpo, 2015)

1.3 Radiation Therapy

Besides surgery and chemotherapy radiation therapy (RT) is a well evolved therapy to treat cancer. In surgery cancer cells are physically resected by removing the tissue. Chemotherapy

makes use of several chemical infusions to treat cancerous cells. Radiation therapy uses a completely new way of treatment. It makes use of ionized or non-ionized radiation to induce death of cancerous cells. To ensure sufficient radiation at the one hand and minimize side effects for the patient on the other hand many progress where made since the beginning of radio therapy in the early 20th century. The field of radio therapy evolved rapidly since then and offers now many possibilities to treat cancer without surgery or chemotherapy. There are two different methods in use which are

- External beam radiation therapy
- Brachytherapy

In external beam radiation therapy an external radiation source, for example linear accelerators (LINACs) are used. This radiation penetrates through the skin and hits the tumor which is being treated. There are different sources of radiation used. Nowadays the most used source is an electron source where electrons are being accelerated. But there also exists sources where photons are used. The disadvantage is, that it is difficult to spare out organs at risk, so a radiation treatment planning is necessary. The advantage is that this technique is noninvasive, so no surgery or other interventions other than irradiation is necessary.

In brachytherapy several so called seeds are implanted into the volume of interest. These seeds are radiation sources which irradiates the cancerous cells from within the body. In terms of location of the seeds distinction is made between several positions (Steiner, 2011):

- Surface,
- Intracavitary,
- Intravasculary and
- Interstitial

While the location on the surface indicates that such seeds are implanted on or in the skin, intracavitary positions are ones in natural cavities within the body. Intravasculary locations are within blood vessels and interstitial locations are within the tumor itself. For cancer treatment most often such seeds are implanted interstitial.

1.3.1 X-ray and Gamma-ray Interactions

Biological effects result from interaction of x-ray or gamma-ray so it is important to use those radiations to assure the death of cancerous cells. Distinction is made between directly ionizing radiation like particles (electrons, protons, alpha particles heavy) ions and indirectly ionizing radiation like photon radiation. As indirectly ionizing radiation is used with external beam radiation therapy or brachytherapy, it is important to discuss possible interactions of photons with matter. When x-ray or gamma-ray photons traverse matter they will interact with tissue in different ways. They can be scattered or be absorbed. X-ray and gamma-ray radiation is in the same energy range and therefore they are physically identical although they are produced

by different processes. During the interaction of a photon with tissue, or matter in general, the energy of the photon is partly or totally absorbed by the atom. Thereby secondary particles like electrons or positrons are created which them self can undergo ionization processes. This is the reason why photon radiation is called indirectly ionizing radiation.

Rayleigh Scattering

In Rayleigh scattering or also called coherent scattering, the total atom is excited by the incident photon which interacts with the atom. As opposed to Compton scattering or the photoelectric effect, where interaction occurs only with electrons, this interaction with the total atom is unique. During the scattering event the photon is absorbed by the atom and causes all electrons of the atom to oscillate in phase. This oscillation leads to a radiation by the atom which is of the same energy, but this emitted photon is of slightly different direction (Bushberg, Seibert, Leidholdt, & Boone, 2012). This can be seen in Figure 1.6. The average scattering angle depends on the energy so when x-ray energy increases also the angle of the scattered photon increases. Because no electron is ejected no ionization occurs. This interaction occurs in the energy range of 15-30keV and is therefore not of interest for radiation therapy where much higher energies are used (Steiner, 2011).

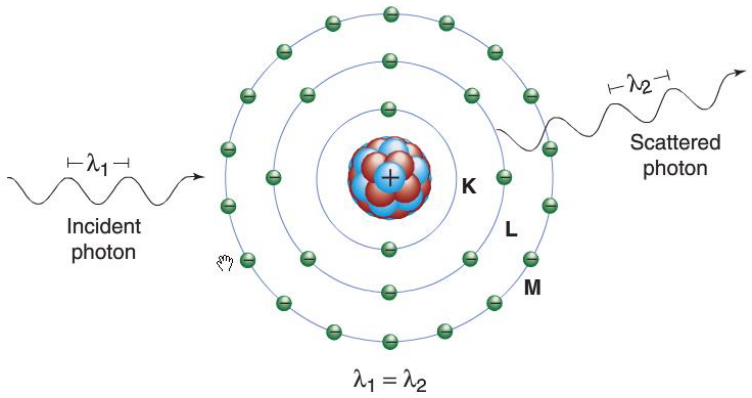

Figure 1.6: Incident and emition of a photon during Rayleigh scattering (Bushberg, Seibert, Leidholdt, & Boone, 2012)

Compton Scattering

Compton scattering is the process where the photon interacts with a valence-shell electron which are electrons of the outer shell of the atom. The electron is ejected from the atom and the scattered photon is emitted with less energy than the incident photon. The wavelength of the scattered photon is thereby longer. As energy must be conserved, the energy of the incident Photon (E_0) is equal to the sum of the energy of the scattered photon E_{sc} and the kinetic energy of the Compton electron which is emitted (E_{e-}) (Bushberg, Seibert, Leidholdt, & Boone, 2012). This relation is shown in equation (1.5).

$$E_0 = E_{sc} + E_{e-} \tag{1.5}$$

The process of Compton scattering, where an atom is being ionized by an incident photon can be seen in Figure 1.7.

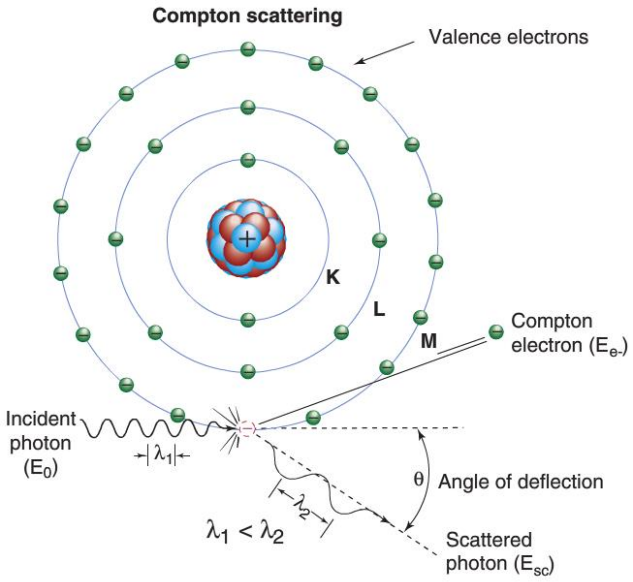

Figure 1.7: Ionisation of an atom from Compton scattering (Bushberg, Seibert, Leidholdt, & Boone, 2012)

Compton scattering, also called inelastic scattering, results in the ionization of the atom by emission of a so called Compton electron. This electron itself undergoes an ionization process and will thereby lose its energy in the surrounding material. The scattered photon may also undergo subsequent interactions like Compton scattering or photoelectric effect while traversing the media. It may be of interest to calculate the scattered photons energy which can be done from equation (1.6)

$$E_{sc} = \frac{E_0}{1 + \frac{E_0}{511keV}(1 - cos\theta)} \tag{1.6}$$

where θ is the angle of the scattered photon (Bushberg, Seibert, Leidholdt, & Boone, 2012). With this it can be said that with increasing incident energy the energy of the scattered photon decreases and the energy of the ejected electron increases. For the electron to leave the valence shell, the binding energy of the electron has to be less than the energy of the incident photon. Thus with increasing incident energy the probability of Compton scattering increases as well compared to Rayleigh scattering or photoelectric effect. The occurrence of Compton scattering also depends on the electron density. Because the number of electrons per gram is fairly constant in tissue, the probability of Compton scattering is nearly independent of Z (Bushberg, Seibert, Leidholdt, & Boone, 2012). This is due to the fact that the nucleus is shielded by the other electron shells. The probability of Compton scattering is independent of

the atomic number (Steiner, 2011). In fact the probability of Compton scattering is proportional to the density of the material.

Photoelectric Effect

At the photoelectric effect a photon is absorbed by the atom and a photoelectron is ejected. The energy of the photoelectron (E_{pe}) equals the energy of the incident electron (E_0) minus the binding energy of the ejected electron (E_b) which is written down in equation (1.7).

$$E_{ep} = E_0 - E_b \tag{1.7}$$

In Order a photoelectron to be emitted, the incident energy of the photon must be greater than the binding energy of the ejected electron. It is most probable that the binding energy of the photoelectron is closest to, but less than, the incident photon energy. In other words this means that photons larger than the K-Shell binding energy a K-shell electron will most probable be ejected. Thereby the photoelectric effect is an ionization process. When a K-shell electron is being ejected the K-shell will be filled by an electron of the L-shell and so on. The difference in binding energy is than released as characteristic x-rays. It is also possible that an Auger electron is released (Bushberg, Seibert, Leidholdt, & Boone, 2012). This process can be seen in Figure 1.8.

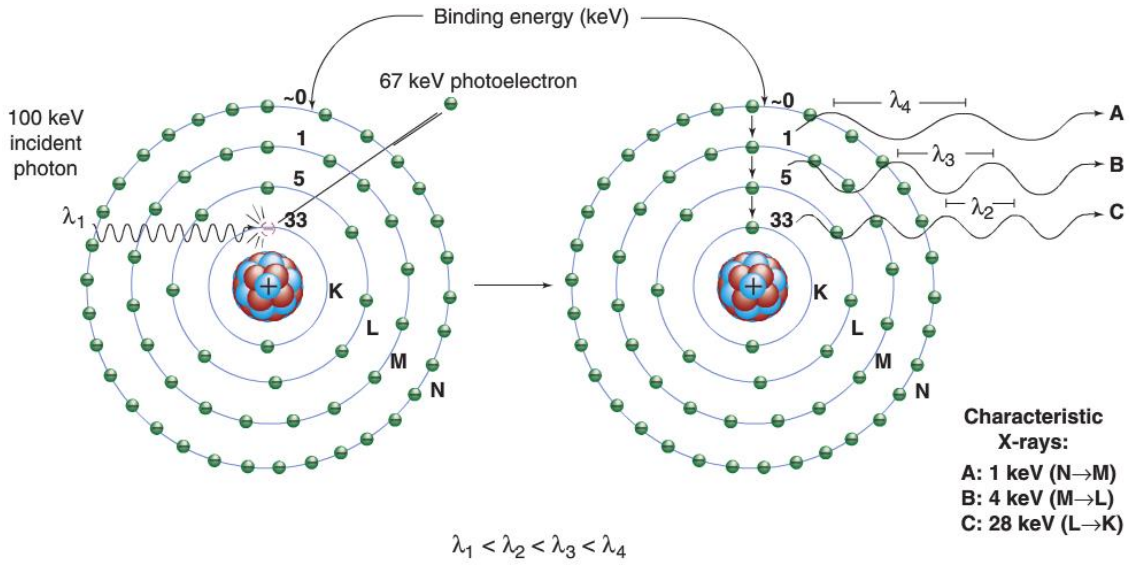

Figure 1.8: Photoelectric Effect (Bushberg, Seibert, Leidholdt, & Boone, 2012)

The probability of x-ray emission depends on the atomic number. As the atomic number decreases, the emission of characteristic x-rays also decreases. The probability of the occurrence of the photoelectric effect is proportional to the atomic number Z and inversely related to the energy E of the incident photon, see equation (1.8).

$$\mu_{photoelectric\ effect} \propto \frac{Z^3}{E^3} \tag{1.8}$$

From this context it can be seen, that with increasing energy the probability of occurrence of the photoelectric effect decreases rapidly. This decreasing does not take place continuously. These discontinuities are called absorption edges, for example K-edge for the K-shell or L-edge for the L-shell, see Figure 1.9. They appear when the incident energy exceeds the binding energy of the electron located in any shell. Thus the probability for a photon of energy just above the absorption edge to interact accordingly to the photoelectric effect is much greater than that for a photon of energy slightly below the edge (Bushberg, Seibert, Leidholdt, & Boone, 2012). The energy of the photon corresponds to the absorption edge with the binding energy of the electrons in a particular shell. Also a matter of interest is the fact that the atomic number has large influence on the energy of the absorption edge. Thus the higher the atomic number of the element is the higher the photon energy corresponding to a particular absorption edge is.

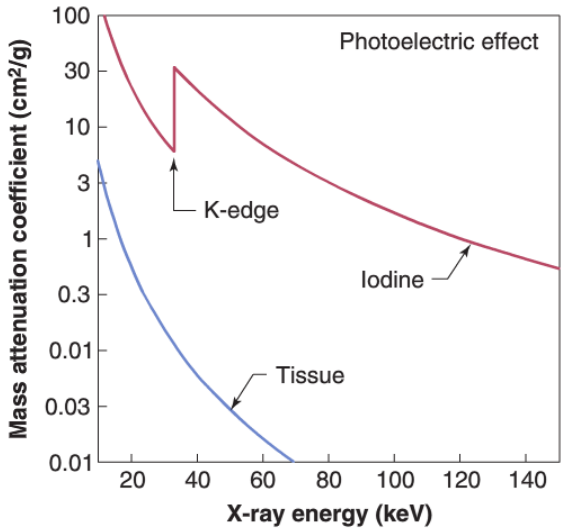

Figure 1.9: Photoelectric mass attenuation coefficients for tissue (Z=7) and iodine (Z=53). K-edge (Bushberg, Seibert, Leidholdt, & Boone, 2012)

Pair Production

Pair production is a process that only can occur when the photon energy exceeds the rest mass energy equivalent of an electron and a positron. This energy is 1.02MeV. The process is such that the x-ray or gamma-ray interacts with the electric field of nucleus of an atom and thereby an electron-positron pair is produced (Bushberg, Seibert, Leidholdt, & Boone, 2012). The photon is thereby absorbed as the conservation of energy has to remain valid. If the energy is higher than the threshold this energy is imparted to the both created particles as kinetic energy. The nucleus itself remains unchanged. Its presence is only necessary for the reason of energy and momentum conservation during the process of particle generation. The electron and positron lose their kinetic energy when exciting or ionizing other atoms. When the

positron comes to rest, a recombination process occurs, which means that the positively charged positron interacts with a negatively charged electron and two oppositely directed 511keV photons, the so called annihilation radiation, are produced. (Bushberg, Seibert, Leidholdt, & Boone, 2012). The whole process can be seen in Figure 1.10.

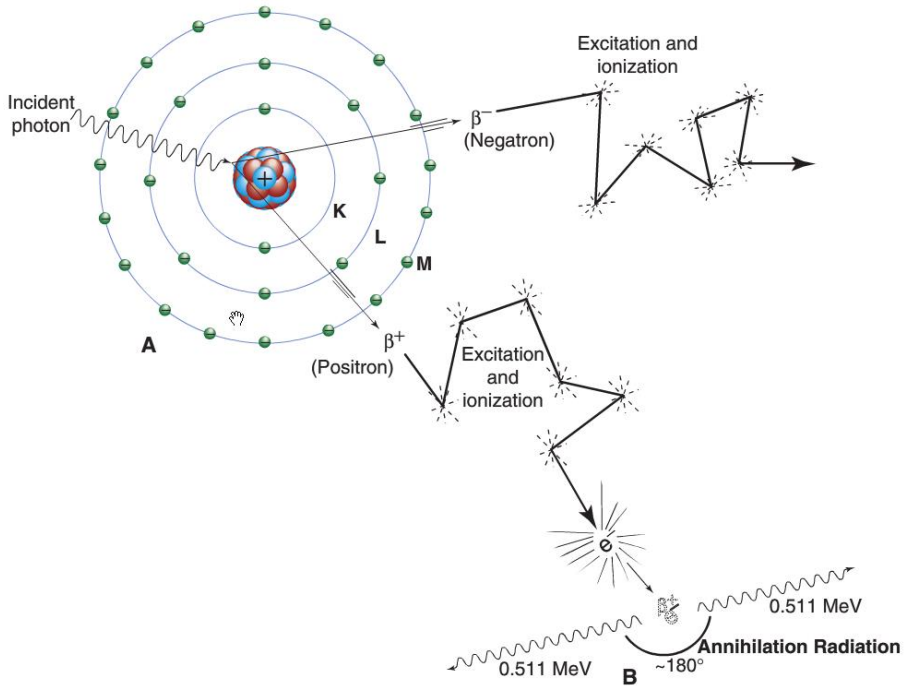

Figure 1.10: Pair production. A: pair production process. B: annihilation of of positron and electron producing two 511keV photons (Bushberg, Seibert, Leidholdt, & Boone, 2012)

The probability of pair production is proportional to the logarithm of the energy of the incident photon and the atomic number. Thus the higher the atomic number Z and the higher the energy the higher the probability of pair production (Krieger, 2009). This relation is written down in equation (1.9),

$$\mu_{pair\ production} \propto \frac{Z^2}{A} \cdot logE_0 \tag{1.9}$$

where Z is the atomic number, A is the mass number and E_0 is the incident energy. Pair production is the predominant process at very high energies. Pair production rarely can also takes place in the field of the electron shell, but it can occur. Because the mass of the electron is three orders smaller than that of the nucleus the electron leaves the shell. So two electrons and one positron deposit their kinetic energy in the absorber material by several collisions or excitations (Krieger, 2009). This process is called triplet production and occurs at photon energies higher than four times the rest mass energy equivalent. But it has to be mentioned that this process only occurs rarely.

Attenuation

Attenuation describes the removal of photons from an x-ray or gamma-ray beam as passing through tissue. It is caused by the processes discussed before. Rayleigh scattering occurs with low probability. At low energies the photoelectric effect dominates and it also depends on the atomic number Z. High energy photons lead to Compton scattering which dominates at low Z values like tissue (Z=7). The fraction of photons removed from a monoenergetic beam is called the linear attenuation coefficient μ and it is related to the thickness of the material. The number of photons removed from the beam can be expressed as

$$n = \mu N \Delta x \tag{1.10}$$

where n is the number of photons removed from the beam, μ is the linear attenuation coefficient, N is the number of incident photons and Δx is the thickness. But equation (1.10) is only valid for very small thickness. To calculate the number of photons removed from a beam traversing tissue of higher thickness equation (1.11) can be used. The relationship between the incident number of photons and those that are transmitted is exponential (Bushberg, Seibert, Leidholdt, & Boone, 2012).

$$N = N_0 e^{-\mu x} \tag{1.11}$$

The linear attenuation coefficient μ is calculated by the sum of all individual attenuation processes as written down in equation (**1.12**)

$$\mu = \mu_{Rayleigh} + \mu_{compton\ scatter} + \mu_{photoelectric\ effect} + \mu_{pair\ production} \tag{1.12}$$

The probability of an interaction depends on the one hand of the thickness of the material but on the other hand it also depends on the number of atoms x-rays or gamma-rays encounter per distance. This property is expressed by the density of the material. Thereby the higher the density the higher the number of atoms such rays encounter the higher the probability of an interaction with an atom. The measure considering attenuation and the density of the material is given by the mass attenuation coefficient which is the linear attenuation coefficient divided by the density of the tissue, see equation (1.13)

$$mass\ attenuation\ coefficient = \frac{linear\ attenuation\ coefficient\ [cm^{-1}]}{density\ of\ the\ material\ [g/cm^3]} \tag{1.13}$$

As mentioned earlier, the probability of the discussed interactions depends on the energy and the density. This relation can be visualized which can be seen in Figure 1.11. It can be seen that Compton scattering dominates for high energies interacting with low atomic number. The photoelectric effect only is relevant for relatively low energies used in diagnostics. Pair

production only appears at energies higher than 1.022MeV and increases with increasing energy (Bushberg, Seibert, Leidholdt, & Boone, 2012).

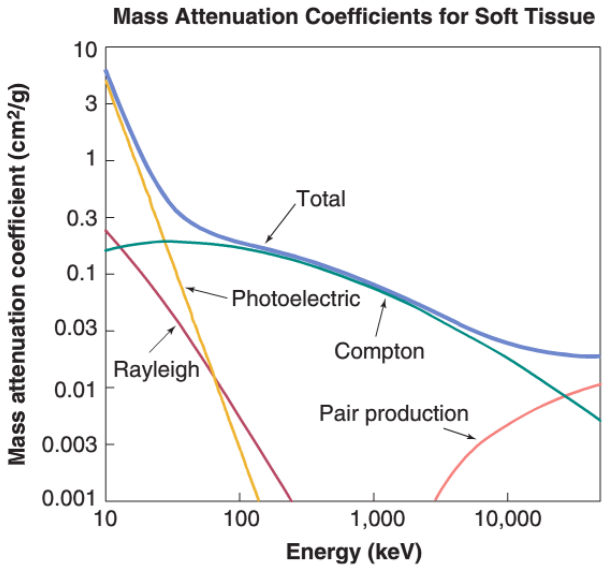

Figure 1.11: Graph of mass attenuation coefficient as a function of photon energy (for tissue) (Bushberg, Seibert, Leidholdt, & Boone, 2012)

1.3.2 Particle Interactions

Biological effects also result from interaction with particles like electrons or protons or even ions, so it is important to use also those radiations to assure the death of cancerous cells. As mentioned in the previous chapter, distinction is made between directly ionizing radiation like particles (electrons, protons, alpha particles or heavy ions) and indirectly ionizing radiation like photon radiation. As directly ionizing radiation is used with external beam radiation therapy, it is important to discuss possible interactions of particles with matter. When particles traverse tissue they will interact with matter in different ways. Depending on the energy of the incident particle, excitation or ionization occurs. Also the behavior of light particles like electrons and heavy particles like alpha particles or protons is different. Charged particles interact with matter by coulombic forces and lose energy by excitation, ionization or radiative losses (Bushberg, Seibert, Leidholdt, & Boone, 2012). Neutral particles like neutrons interact in another way. They only interact with the nucleus of the atom. When there is an interaction between charged particles and orbital electrons of the atom where the particle loses energy, excitation or ionization occurs. These losses are due to coulomb forces exerted on charged particles when they pass the atoms electric field which is generated by the atom's charged particles like electrons or protons.

Excitation

Excitation occurs when some of the incident particles energy is transferred to the atoms electrons. Thereby these electrons get into higher energy levels which orbit farther from the

nucleus. In comparison to ionization at excitation the energy transfer does not exceed the binding energy of the electrons. So excitation is a nonionizing process. The electron will return to its normal energy level by emission of the excitation energy (electromagnetic radiation). The latter process is called de-excitation. These two processes of excitation and de-excitation can be seen in Figure 1.12. (Bushberg, Seibert, Leidholdt, & Boone, 2012)

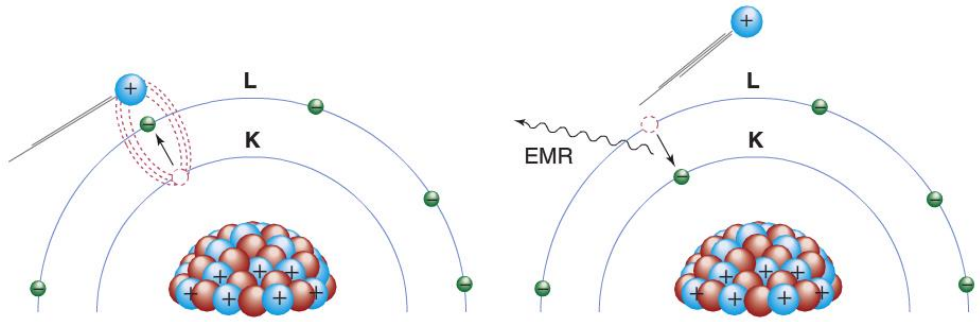

Figure 1.12: Excitation and de-excitation of an electron (Bushberg, Seibert, Leidholdt, & Boone, 2012)

Ionization

If the incident particle exceeds the binding energy of an electron in a corresponding shell, ionization occurs. This process is described by the ejection of the electron and hence the ionization of the atom. If the ejected electron has sufficient energy it can undergo further ionization processes which are then called secondary ionizations. Such electrons, ejected by secondary ionization, are called delta rays. The process of ionization is figured in Figure 1.13. The most energy is deposited through ionization. To name a value this lies at about 70% in soft tissue. But energy loss via excitation increases by decreasing particle energies because the energy does not exceed the binding energy of an electron in a corresponding shell. Equal probability of excitation and ionization is being observed at about 40eV. With further reduction of the particles energy ionization diminishes rapidly. Below the energy of ionization of liquid water at 11.2eV no ionization occurs and excitation is the process taking place (Bushberg, Seibert, Leidholdt, & Boone, 2012). It should be mentioned that at energies of about 10keV about 450 secondary electrons are being generated. It can be concluded that energetic electrons deposit most of their energy via ionization. Each of the secondary electron has a energy in the range of 10 to 70eV (Bushberg, Seibert, Leidholdt, & Boone, 2012).

Specific Ionization is the average number of primary and secondary generated ion pairs per unit length. It is expressed in ion pairs (IP) per mm. This number is proportional to the square of the electrical charge (Q) of the particle and inversely related to the square of the velocity of the particle, see equation (1.14).

$$SI \propto \frac{Q^2}{v^2} \tag{1.14}$$

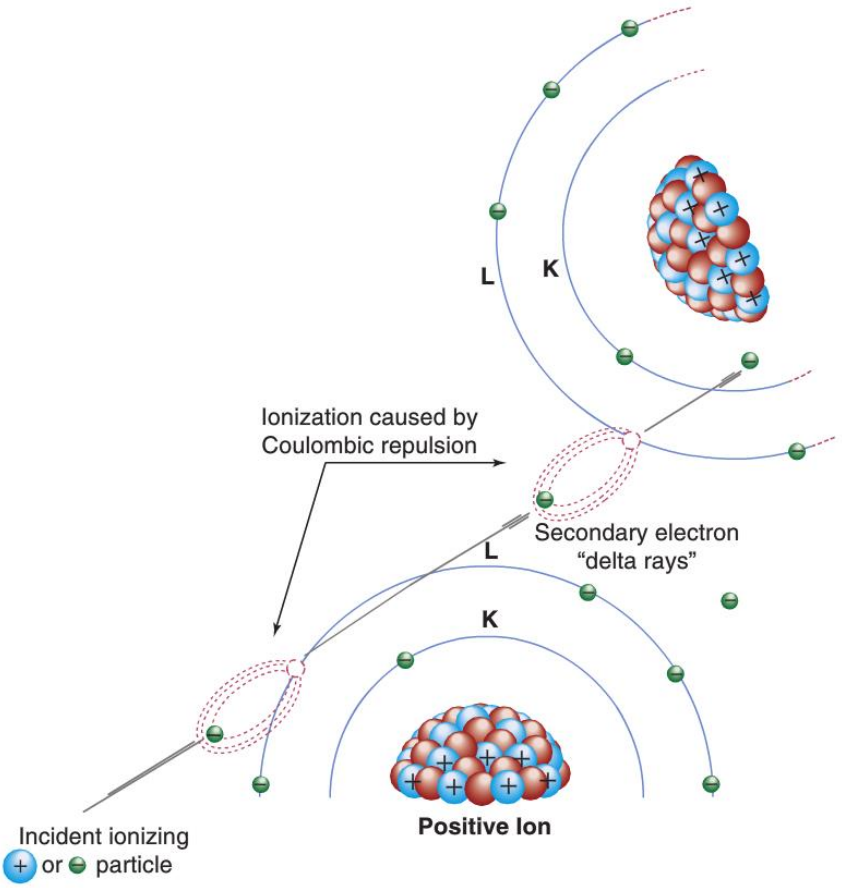

Figure 1.13: Ionization process with production of delta rays (Bushberg, Seibert, Leidholdt, & Boone, 2012)

The coulombic field depends on the charge, hence the larger the charge the greater the coulombic field. Particles with low energy slow down and the coulombic field can therefore interact at a given location for a longer period of time. Therefore the range of such particles in matter is limited. For alpha particles; the energy ranges from about 4.05MeV to 10.53MeV; the range is less than the diameter of several cells. The specific ionization of an alpha particle can be as high as 10 million ionization pairs per mm in soft tissue. As the particle slows down, the specific ionization increases to a maximum which is called the Bragg peak. This can be seen in Figure 1.14. Beyond the Bragg peak specific ionization decreases rapidly because the alpha particle becomes electrical neutral by acquiring electrons. Thus it loses its capability for further ionization. The reason why specific ionization is mentioned is because the Bragg peak has application in radiation therapy using particle beams. The advantage is that the dose on either side of the Bragg peak is substantially lower so it is much easier to spare organs at risk.

Scattering

Scattering is not only possible with photons but also with particles. Thus a scattering event causes a particle to be deflected from its original trajectory. There are two types of scattering:

- Elastic scattering
- Inelastic scattering

Elastic scattering occurs when the total kinetic energy of a scattered particle is unchanged. This type of scattering can be seen when two balls out of wood collide. When there is an energy loss during collision than the scattering event is said to be inelastic. This means that the kinetic energy of the scattered particle is less than the kinetic energy of the incident particle. (Bushberg, Seibert, Leidholdt, & Boone, 2012)

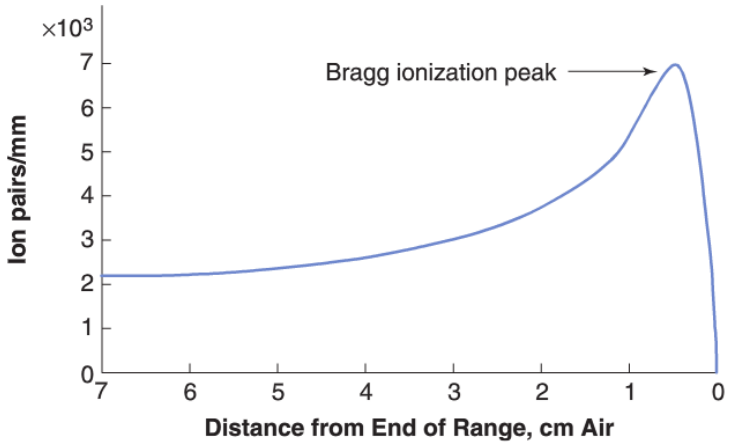

Figure 1.14: Specific ionization as a function of distrance in air; Bragg peak (Bushberg, Seibert, Leidholdt, & Boone, 2012)

Generation of Bremsstrahlung

The Process of generation of Bremsstrahlung is an inelastic interaction where the path of the negatively charged particle is deflected by the positively charged nucleus. This deflection occurs through coulombic attraction of the positively charged nucleus. This deflection is related to an energy loss of the deflected electron. As energy conservation remains valid this missing energy is emitted as electromagnetic radiation called Bremsstrahlung. The generation of this electromagnetic radiation is visualized in Figure 1.15. The total emission of Bremsstrahlung is proportional to the squared of the atomic number Z of the absorber and inversely related to the square of mass of the incident particle. This is the reason by the generation of Bremsstrahlung by electrons is about 6 orders higher than by protons or alpha particles because the mass of such heavy charged particles is too high. Bremsstrahlung is in the same energy range than x-ray radiation. Hence this is another process, beside the generation of characteristic x-ray via photoelectric effect, of generation of x-rays. The difference of these two generation processes is that by generating Bremsstrahlung a continuous spectrum of x-ray energies is emitted whereas characteristic x-ray radiation is of an individual energy only. (Bushberg, Seibert, Leidholdt, & Boone, 2012)

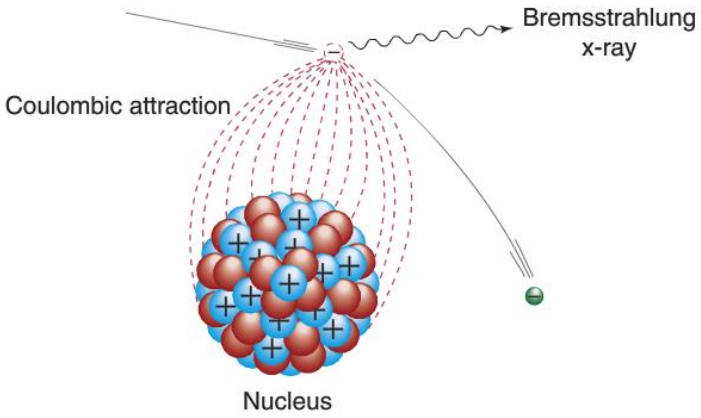

Figure 1.15: Generation of Bremsstrahlung as energy loss of the incident particle (Bushberg, Seibert, Leidholdt, & Boone, 2012)

Positron annihilation

A positron is the opposite particle of an electron and is a type of antimatter. While electrons become bound to an atom a positron cannot undergo binding conditions with matter. The end of a positron is reached when it collides and therefor interacts with an electron. If this is the case annihilation of the negatively charged electron and the positively charged positron pair occurs. Hence the complete rest mass is converted to energy which is being radiated via two oppositely directed 0.511MeV annihilation photons. It has to be mentioned that the angle between both annihilation photons is not exactly 180° but slightly less because the positron carries a small rest of momentum when it interacts with the electron. (Bushberg, Seibert, Leidholdt, & Boone, 2012)

Neutron interactions

The distinction of neutrons and protons or electrons is that they are uncharged and can thereby not undergo interactions resulting from coulombic forces. Rather they interact with the nucleus of the atom. Sometimes liberation of nucleic fragments occurs. Such fragments can be protons or other larger fragments like alpha particles. This can be seen in Figure 1.16. This kind of liberation often results in excitation and ionization; hence it is called a secondary process. As neutrons often interact with light nuclei as of hydrogen, oxygen or carbon another possible interaction is elastic scattering as known from billiard balls. Interactions in tissue most often take place with hydrogen bound to water. Thereby recoiled protons are produced. Another interaction is called neutron capture where neutrons are captured by atomic nuclei. This kind of interaction is combined with a larger energy release of up to 7MeV. This is due to the binding energy of the neutron. Hence the atom is converted into another isotope. The energy is emitted as gamma ray. One example is the production of deuterium. It occurs from capturing a neutron by a hydrogen nuclei and results in deuterium (2H) and the emission of a 2.22MeV gamma ray. This reaction is written down in equation (1.15).

$$^{1}H + {}^{1}n \rightarrow {}^{2}H + \gamma \qquad (1.15)$$

Nuclides produced by neutron capturing are not always stable and can be radioactive or unstable. Unstable nuclides are defined by its decay into other isotopes. Such neutron interactions are important for the production of radiopharmaceuticals which is the reason why it is mentioned. (Bushberg, Seibert, Leidholdt, & Boone, 2012)

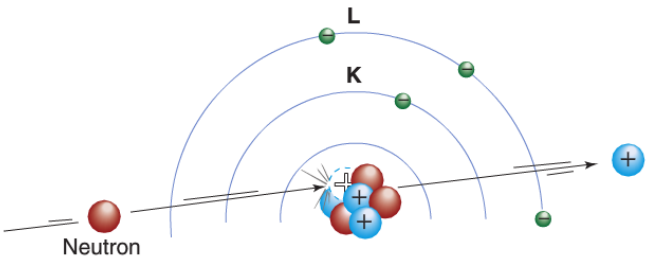

Figure 1.16: Liberation of a proton as energy loss resulting from collision (Bushberg, Seibert, Leidholdt, & Boone, 2012)

1.3.3 Radiation Biology

As discussed in the previous chapter, there are many interactions of radiation with tissue when irradiating it. By these interactions biologic effects are caused. The task of radiation biology is to identify these biologic effects and describe them. These biologic effects depend on the one hand on the absorbed dose (quantity) and the dose rate on the other hand on the type and energy of the radiation (quality). The radio sensitivity of tissue depends on several variables. Some of these variables are inherent to cells while others are dependent on the cells themselves when irradiating them. Not always defects at the molecular or cellular level can be detected or result in detectable effects. This is because it can take up to several weeks or even years some damage to appear (Bushberg, Seibert, Leidholdt, & Boone, 2012). As mentioned previously x-ray and gamma ray interactions or even the emission of energy during radionuclide decay result in the production of energetic electrons. Through interactions like excitation or ionization of these electrons they deposit their energy in tissue. These processes result in liberation of secondary electrons which itself can transfer their energy to tissue. For example, a single 30keV electron results in the production of about 1000 secondary electrons. Each of these secondary electrons has the potential to excite other atoms. They transfer their energy via vibrational, rotational or collisional interactions with water molecules. This results in damage of chromosomes or cell death which is desirable in radiation therapy. If ionizing events take place in the near region of the DNA, damage in multiple locations can be produced. Such multiple damaged sites (MDS) are very difficult to repair or are repaired incorrectly by the cell.

Formation of free radicals

Depending on the process of interaction distinction is made into direct or indirect. While direct interactions are defined as such where the biologic macromolecule or protein becomes ionized by a particle or photon passing its proximity, indirect interactions are defined as

where the damage is mediated via free radicals. Most cells in the body are composed of water, thus the majority of damage induced by radiation is caused by radiation interactions with water. Thereby water molecules are ionized and form H_2O^+ and e^-. The electron reacts with another water molecule and forms a negative charged water ion, see equation (1.16).

$$H_2O + e^- \rightarrow H_2O^- \tag{1.16}$$

These negative water ions are very unstable and form another ion called a free radical.

$$H_2O^+ + H_2O \rightarrow H_3O^+ + \cdot OH \text{ (Hydroxyl Radical)} \tag{1.17}$$

$$H_2O^- \rightarrow OH^- + H \cdot \text{ (Hydrogen Radical)} \tag{1.18}$$

Such free radicals are denoted by a dot next to the chemical symbol and are defined to have unpaired orbital electrons. Free radicals can be radical ions like H_2O^+ or H_2O^- or electrically neutral like $\cdot OH$. Hydroxyl radicals or hydrogen radicals can be created by the reactions written down in equations (1.17) and (1.18). But there are other reactions as well. The most important one is the following where H_2O is being excited by radiation and thus forms a hydroxyl and hydrogen radical as written down in the following equation.

$$H_2O \rightarrow H_2O^* \rightarrow H \cdot + \cdot OH \tag{1.19}$$

Free radicals are extremely reactive. They can combine with other free radicals to form nonreactive chemical species, water for instance when a hydroxyl radical and a hydrogen radical combine. In such a case no biologic damage occurs. They also can combine pairwise and form a highly toxic species, hydrogen peroxide for instance. But the probability of pairwise combination is low for low linear energy transfer (LET) radiation and the majority of reactions are due to hydroxyl radicals. Since oxygen stabilizes free radicals via a reduction of the probability of recombination to hydrogen or water. The lowering in recombination probability is due to combination of free radicals with oxygen. Thereby highly reactive oxygen species (ROS) are formed. One example is the production of a hydroperoxyl radical where the reaction path is written down in equation (1.20).

$$H \cdot + O_2 \rightarrow HO_2 \cdot \tag{1.20}$$

Free radicals can attack biomolecules (written as R for rest) in many different ways. Two of them are hydrogen abstraction (equation (1.21)) and $\cdot OH$ addition (equation (1.22)).

$$RH + \cdot OH \rightarrow R \cdot + H_2O \tag{1.21}$$

$$R + \cdot OH \rightarrow ROH \cdot \tag{1.22}$$

Repair mechanisms, such as radical recombination or hydrogen donation from thiol compounds, are inhibited in the presence of oxygen. This is because of the transformation into peroxyradicals. With less than approximately 10^{-5} seconds their lifetime is limited. But they can diffuse sufficiently far in the cell to produce damage. (Bushberg, Seibert, Leidholdt, & Boone, 2012)

It was shown that not only factors like dose, dose rate or the sensitivity to radiation of the biologic system affects biologic effects. Also the spatial distribution of the energy deposition is of interest. The LET takes this factor into account and describes the average energy deposition per unit path length of the incident radiation. All ionizing radiations can produce all types of biologic effects, but it is not ensured that the same effects occur. This means that the magnitude of the effect per unit dose differs (Bushberg, Seibert, Leidholdt, & Boone, 2012). To be able to compare the effectiveness of different types of radiation a factor called relative biological effectiveness (RBE) was introduced. It is defined as the quotient of the dose of the reference radiation (typically x-rays at 250keV) producing an effect and the dose of the test radiation that is necessary for producing the same effect. This relation can be seen in equation (1.23).

$$RBE = \frac{Dose\ of\ reference\ radiation\ required\ to\ produce\ effect\ X}{Dose\ of\ test\ radiation\ required\ to\ produce\ effect\ X} \tag{1.23}$$

As can be seen in Figure 1.17 the RBE is proportional to the LET. The large increase is due to higher specific ionization which can be achieved with high LET radiation. However, beyond approximately 100keV/µm there is a steep decrease of RBE. This is because of an excess of radiation energy. No more radiation is necessary to produce the maximum biologic effect.

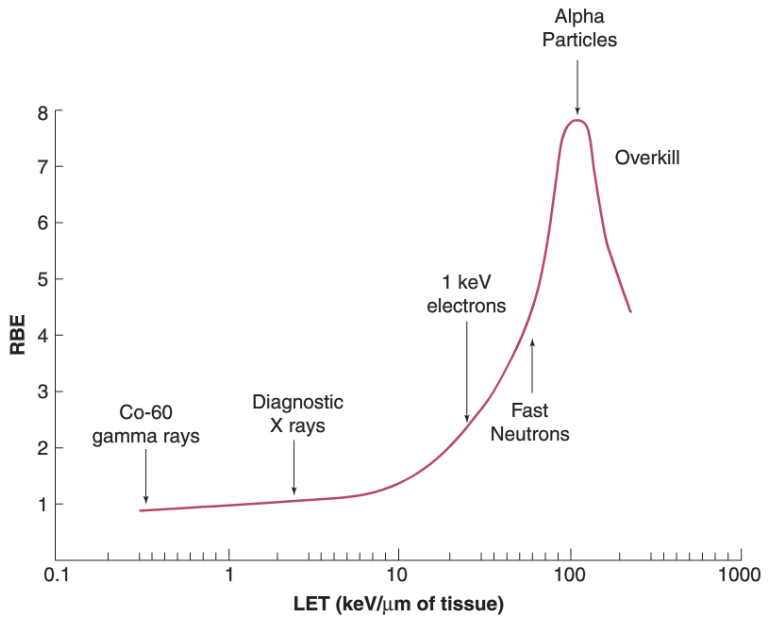

Figure 1.17: Relation of the RBE and the LET. (Bushberg, Seibert, Leidholdt, & Boone, 2012)

Radiation induced DNA damage

The most radiative sensitive targets of the cell are located in the nucleus of the cell. This is the region where deoxyribonucleic acid (DNA) is located as well. Hence it is to assume that damage to the DNA is the most serious one, since all proteins the cell needs to survive are stored within the DNA and are produced by proteins using the DNA. Without any replacement the cell inevitably undergoes cell death. By ionizing radiation the cell undergoes several structural changes. These changes can be:

- Hydrogen bond breakage
- Molecular degradation or breakage
- Intermolecular and intramolecular cross linking

Base pairs in the DNA are linked through hydrogen bonds thus a brakeage of such bonds lead to an irreversible change in the secondary and tertiary structure of the molecule. This leads to an impairment of gene transcription and translation (Bushberg, Seibert, Leidholdt, & Boone, 2012). The backbone of the DNA is linked via sugar-phosphate polymers. They form the two helical strands. When such a strand gets broken this is called a single strand break (SSB). Such a SSB results from the presence of OH radicals. If both strands of the double helix breaks at the same nucleotide pair this is called a double strand break (DSB). There may also take place other damages like base loss, base changes or cross-links between DNA strands (Bushberg, Seibert, Leidholdt, & Boone, 2012). Several examples of DNA damage can be seen in Figure 1.18. SSBs between the sugar and the phosphate can be repaired by rejoining, but in the presence of oxygen the damage is being potentiated by causing peroxidation of a base. Thereby a radical transfer occurs to the sugar preventing rejoining. A DSB occurs if two SSBs happen in the immediate vicinity. But also high energetic particles like alpha particles or protons can lead to a DSB. Such DSBs are very genotoxic lesions that can result in chromosome aberrations (Bushberg, Seibert, Leidholdt, & Boone, 2012). They cannot be repaired easily. This leads to a genomic instability because of incorrectly repaired DSBs. At an absorbed dose of one Gray (Gy) from x-rays will lead to a about 40DSBs, 1000SSBs and 3000 damaged bases per cell. As many cells are affected, this is a huge amount of damage. Such complex DNA lesions as base damage are less likely to be repaired correctly than an isolated SSBs or DSB. DNA damage is a quite common event for the cell because it experiences many DNA lesions per day even in the absence of radiation. These lesions are due to common cellular functions such as respiration (damage through ROS during metabolism). Also mitosis can be a source of DNA damage. Such damage is produced during base replication. That the mutation rate is low is due to effective DNA repair mechanisms. In some cases, when catastrophic mutations occur, the cell may undergo apoptosis or cell death. As many types of DNA repair mechanisms exist the chance of DNA repair is surprisingly high. But it has to be mentioned that the repair of damaged DNA depends on several factors like the stage of the cell cycle and the type and location of the lesion. These repair mechanisms are important for the healthy tissue to recover after a radiation therapy session. So it is important to apply the necessary dose for cancer treatment in fractions.

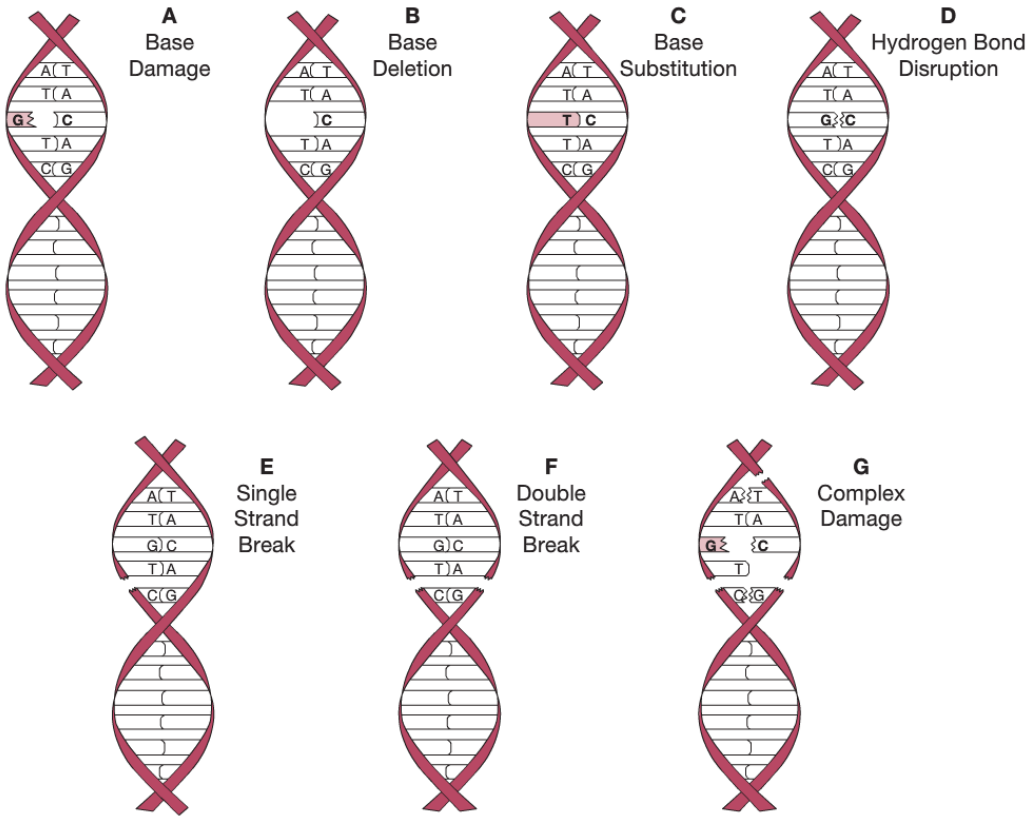

Figure 1.18: Examples of DNA damage (Bushberg, Seibert, Leidholdt, & Boone, 2012)

1.4 Image-Guided Radiation Therapy

In the early years of RT patients where positioned by estimating the location of the internal anatomy from the anatomy of the surface of the patient. As the internal anatomy is not always correlated with the surface anatomy there was the need for a more accurate system providing more precise alignment of the patient. Not only the patient positioning was cumbersome, also a much larger planning target volume (PTV) was chosen to consider geometric uncertainties and motion of the organ to treat. But such a large PTV is undesirable because thereby the risk for normal, healthy tissue is increased to suffer from radiation. To overcome these issues it is beneficial to measure such changes in the treatment room (TR) with several imaging techniques available. Thereby it is possible to reposition the patient (Dawson & Ménard, 2010). Not only during one treatment session repositioning is an issue, also inter-fractional variations are a problem. Intra-fractional variations result from respiratory motion, non-rigidity of the body, weight loss or radiation induced shrinkage of the tumor (Mohan, Dong, & Zhang, 2006). This is the field where image-guided radiation therapy (IGRT) has its application. Currently the standard procedure is to take a pre-interventional image with the use of CT. Such an image can be combined with PET or MR. The patient is than positioned according to the CT image acquired prior treatment (Vaezy & Zderic, 2009). Thereby it is to be assumed that patient anatomy does not change during treatment which is not often true. Regarding changes in the patient anatomy one can make use of IGRT technology. There exist

several image-guided intervention (IGI) strategies. These ranges from simple ones, where only the treatment setup is image guided to more sophisticated ones where also during treatment changes in the patient anatomy are considered and treatment plan can be adjusted online, which means adaption of irradiation during treatment (Mohan, Dong, & Zhang, 2006).

1.4.1 Patient Positioning

As mentioned, prior to each treatment session an image of the cancerous area is acquired. This image is compared to a reference image from which the reference location is determined. The most often used imaging modality for this process is CT. For the localization of the tumor fiducial markers, mainly gold seeds, are used (Vaezy & Zderic, 2009). To be able to position the patient after imaging markers are drawn on the skin. Also other reference points of the anatomy are used. These markers are then used during positioning while they are aligned to the isocenter of the treatment beam. This is done with the help of a set of laser beams which are orthogonal to each other. Planes generated by these lasers all intersect at the isocenter of the treatment beam, therefore alignment is possible. The isocenter is defined as the point where all treatment beams intersect regardless of the angle of the gantry or patient couch. As this procedure leads to uncertainties in the positioning other techniques are necessary to ensure patient alignment is correct. Otherwise realignment has to be done by assistance of newly developed technologies (Peters & Cleary, 2008). In the past years many efforts were laid to this topic and portal imaging systems were introduced. Thereby the treatment beam is used to image the anatomy of the patient.

Anyway, to ensure delivery of the conformal dose distribution and to eradicate uncertainties in target positioning intensity modulated radiation therapy (IMRT) and IGRT are used (Vaezy & Zderic, 2009). As mentioned previously, correct position of the patient is ensued by taking images of the patient anatomy and align the cancerous region to the isocenter. Correct positioning has to be done before each single treatment session. When the patient seems correctly aligned it is even possible that organs show motion of up to one cm relative to the external landmarks during treatment (Hoffmann, et al., 2010). Thereby alignment to external surface anatomy is not sufficient. To circumvent this problem it is possible to image the anatomy after patient positioning to ensure he is aligned correctly. As it is not possible to control the location of the tumor, this affects the accuracy of the delivery of radiation dose. To circumvent the thereby following requirement for larger treatment volume and thereby the increasing in radiation dose for surrounding normal tissue, which is unwanted, IGRT can be used (Kaar, et al., 2012). With the application of IGRT the PVT can be optimized. Thus maximal tumor control is achieved and complications can be minimized. Exact placement of the patient on the treatment couch enables safer delivery of more effective radiation dose with fewer side effects to healthy tissue. To achieve this several techniques have been invented and are available for use. So exact patient alignment by the use of IGRT can improve the outcome compared to conventional radiation therapy techniques. By this safety margins can be confined without affecting the conformity of the radiated volume. With this it gets possible to deliver dose with high precision (Bathia, 2012).

1.4.2 Imaging Technologies for IGRT

As mentioned in the previous chapter, patient positioning is an important task to optimize the PVT and thus to achieve maximum tumor control. Thereby complications can be minimized as well as the applied dose to normal tissue nearby the cancerous organ. By exact patient positioning also other side effects can be avoided. Hence image guidance is crucial for exact patient alignment. In cases where intra-fractional variation occurs, for example the prostate gets deformed when the rectum fills with stool, daily image-guidance is beneficial and should be routine (Vaezy & Zderic, 2009). In the last years many effort were laid in the development of imaging systems for exact patient alignment. As developments showed this efforts were worthwhile. During the last years several methods have been come to the market and were also applied in the field of IGRT. Several imaging techniques are used for IGRT as the following list shows (Vaezy & Zderic, 2009):

- Radiography
- Computed Tomography (CT)
- Magnetic Resonance Imaging (MRI)
- Positron Emission Tomography (PET)
- Ultrasound (US)

As there are several technologies using the aforementioned imaging modalities, they are being discussed in the following in more detail. Some of them are able to deliver high quality images of soft tissue while others are not. For example Electronic Portal Imaging Devices (EPIDs) use the treatment beam for imaging. As the treatment beam works in an energy range of MeV soft tissue cannot be resolved with high contrast. Hence other methods are used like x-ray imaging, CT or US.

Electronic Portal Imaging Devices

EPIDs are the most common plane imaging technology referring to IGRT. It is a technology that is shipped with the basic configuration of linear accelerators (LINACs) and is routinely used nowadays. The advantage of this approach is that it utilizes the treatment beam for imaging (Verellen, de Ridder, & Storme, 2008). Such systems replaced older film based verification systems used with ^{60}Co-units and LINACS. As the energy of the treatment beam reaches in the MeV range, soft tissue cannot be displayed with such a technique. The resulting contrast is too low to allow accurate patient positioning and position verification. Only dense tissue or material like bone or metal seeds can be visualized. As EPIDs can be used for dose measurement, they become very useful for quality assurance (Verellen, de Ridder, & Storme, 2008).

X-Ray Imaging Systems

Mounted x-ray tubes on the treatment delivery system were introduced to obtain also 3D volumetric images. To achieve this multiple gantry positions are required. To circumvent gantry movement for imaging an additional x-ray tube and detector perpendicular to the

treatment beam was introduced. These x-ray beams intersect then at the isocenter of the treatment beam. This system has an inherent disadvantage which is the additional dose but due to daily treatment dose this fact becomes less important (Verellen, de Ridder, & Storme, 2008).

Another system using x-ray imaging is the room-mounted x-ray imaging system. Two x-ray sources are fixed on the floor whereas the detectors are mounted on the ceiling. Such a setup can be seen in Figure 1.19. Thereby a high precision can be achieved, provided a proper calibration has been established (Kaar, et al., 2012). Such a system is suitable for tracking bony structures or fiducial markers implanted to the patient. Such markers have to be radio-opaque to be visible on the images. Tracking can also be proceeded during treatment which is a huge advantage comparing other systems. Using the integrated optical tracking system and reflective markers on the patient it is possible to correct for rotational and translational errors, provided a robotic treatment couch is available. One disadvantage is the transparency of soft tissue for x-rays resulting in a poor imaging contrast of soft tissue like the prostate. If no bony landmarks are nearby fiducial markers have to be implanted. This invasive intervention causes additional side effects for the patient (Kaar, et al., 2012).

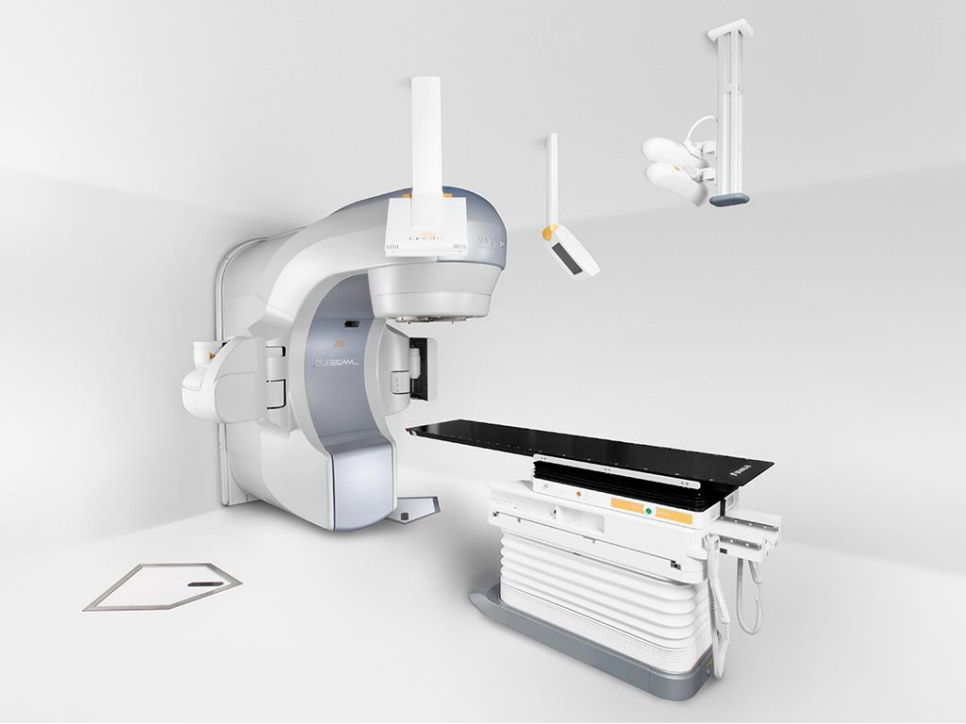

Figure 1.19: Setup of the Exac-Trac system by Brainlab (Brainlab AG, 2015)

One commercial available system is the system by Brainlab called Exac-Trac. The Setup of this system is compatible to several LINACs and hence widespread in installation. The Exac-Trac system also suits an optical IR-tracking device which is integrated to monitor motion in real-time. By this, tracking can also occur during treatment to detect intra-fractional shifts of the cancerous organ. Such shifts can then be corrected using a robotic treatment couch. With such a system, the Vendor claims, a precise patient setup within up to 1mm can be achieved.

Cone-Beam CT

To be able to visualize soft tissue, and define thereby the spatial relation between the target and organs at risk, a CT can be used. Most often such a CT is mounted on rails to be able to transport the patient to the bore of the CT. But there also exist solutions where the patient couch is moved along the bore. Another system is to mount an x-ray tube on the gantry of the LINAC. On the opposite site of the gantry a flat-panel detector is rigidly attached to the system. While the gantry rotates around the patient, several x-ray images are acquired. Such systems can be used to acquire cone-beam volumetric CT images (CBCT). CBCT delivers excellent spatial resolution in all 3 dimensions as opposed to conventional CT where the resolution of one dimension depends on the thickness of the slices and the pitch with which the patient is moved through the bore (Verellen, de Ridder, & Storme, 2008). These CBCT solutions offer sufficient soft tissue visualization while avoiding the necessity of surrogates in localization of the target. For rendering the 3D volumetric images a specific reconstruction algorithm is used (e.g. Feldkamp algorithm). To get rid of inaccuracies from the movement of the gantry they can be measured. Reconstruction algorithms offer then the possibility for correction of such unwanted movements. The advantage of such a system is the much better soft tissue contrast compared to EPIDs. But this advantage is of cost of additional radiation dose for the patient (Kaar, et al., 2012). Other weaknesses are the sub-optimal precision in movement of the gantry (gantry sagging) as well as the scatter radiation from the patient to the imagers. It should be also noted that the x-ray system has a different isocenter than the treatment beam so it has to be calibrated with respect to the treatment isocenter (Verellen, de Ridder, & Storme, 2008).

Helical Tomotherapy

The approach of helical tomotherapy combines add-on sequential tomotherapy (Accuray, 2015) with helical CT scanning. A CT detector array system is mounted on the opposite site of the gantry to the treatment beam exit. The continuously rotating gantry thereby allows for MVCT images. It can be compared with a conventional CT system where the x-ray tube has been replaced by a 6MeV LINAC. CT image acquisition is done with all leaves open. The patient is imaged in slices like conventional CT. The only difference is that these slices are very narrow. With such a system also dose verification is possible (Verellen, de Ridder, & Storme, 2008). For dose verification small beams, created by a binary collimator, can be switched on and off separately. The helical tomotherapy approach is a treatment modality in which IMRT is delivered. Simultaneously the patient is slowly translated through the bore. During delivery of the treatment the source describes a helical trajectory around the patient, hence its name. Compared to other systems the patient flow is rather low and the acquisition costs are high. These facts are drawbacks of such a system. (Kaar, et al., 2012)

Ultrasound

There also exist a radiation-free way of image acquisition using ultrasound. Such a system can be used for patient positioning when registering a US image to a pre-intervention CT image. Registration can occur manually or fully automated as suggested in (Kaar, et al., 2012). From

registration results a transformation which is then used for patient positioning on the treatment couch. There is no requirement of surrogate for visualization of the target. On the other hand this system only delivers the possibility of pre-interventional imaging so images cannot be acquired during beam on (Verellen, de Ridder, & Storme, 2008). Another disadvantage is the deformation of the organ of interest during US imaging because some pressure has to be applied to get high image quality. As found out in several studies the accuracy of such a system is low compared to seed-marker based IGRT in the region of the prostate. Nevertheless, it is a cost-saving system not requiring any additional radiation dose. There also exist commercial systems like the B-Mode Acquisition and Targeting (BAT) by best nomos (Best nomos, 2015). SonArray is a system deliverd by Varian Medical Systems (Varian Medical Systems, 2015). Another system was presented by Elekta AB. Their system is called Clarity and compared to other systems it makes use of image segmentation techniques. Elekta AB thus claims improved accuracy (Elekta AB, 2015). As all these systems still require human interaction during the imaging and positioning process it is beneficial daily imaging and positioning is done by the same physician for all the delivered fractions. One huge advantage is that such systems are cost-saving and no additional radiation dose is required.

Magnetic Resonance Imaging

Not only imaging using ultrasound delivers a radiation free imaging modality, also MRI has no requirement on additional radiation dose. Thus the next logical step is the usage of MRI for image-guided radiation therapy. The huge advantage of MRI is the superior soft tissue contrast compared to kV or MV based imaging systems. At the University of Utrecht (the Netherlands) a prototype of a combination of a MRI system and a LINAC is under construction (Verellen, de Ridder, & Storme, 2008). But there are two system inherent limitations. The first is interaction of the RF signal used for MR imaging with the RF pulses required for electron acceleration in the LINAC. The second problem is the influence of the strong magnetic field from the MRI system on dose absorption processes. Secondary electrons start to gyrate because of the Lorentz force (Verellen, de Ridder, & Storme, 2008). Such systems are very promising but still in development.

1.5 Image Registration

As IGRT makes use of several images, each being compared to a pre-interventional image, image formation is an important task in radio therapy. Images can involve the same image modality, like CT-CT or different image modalities can be used for registration, like CT-US. Image fusion establishes an anatomical correlation between images taken from different image series. Image fusion is often used very commonly in clinical situations. It is to improve the overall interpretability by more than the sum of the information gathered from the individual images. In IGRT image fusion, also called registration, is used for the assignment of physiological process to the anatomy of the patient. This can be achieved using multi-modality registration like PET-CT (Oppelt, 2005). But the most important task is patient positioning via image formation. By registering two images a transformation matrix is calculated. By this matrix the translational and rotational shift can be derived. Hence the patient can be aligned correctly with high precision using image fusion, provided the

registration procedure between two images was successful. As mentioned previously, there are two main strategies for registration:

- Multi-modality registration
- Single-modality registration

Multi-modality registration is used to combine complementary information provided by different modalities. Such information includes anatomy derived from CT, MRI or US images as well as functional information using MRI, PET or SPECT. Single-modality registration, in contrast, is used to register anatomical images from two different images using the same image modality, for example CT-CT or US-US. But also functional images can be registered pairwise like MRI-MRI or PET-PET (Oppelt, 2005).

Usually registration is done by several different registration algorithms. This is the case when no geometrical relationship between two images is known. On the other hand registration can also be done by calibration when there is a fixed geometrical relationship between a reference image and the image to be fused. Such a geometrical relationship exists for mechanically combined imaging modality systems as positron emission tomography (PET) and CT. Another possibility to get the geometrical relationship is to track of the imaging devices with an appropriate tracking system as discussed in chapter 1.2 Navigation (Oppelt, 2005).

1.5.1 Types of Registration

As there exist several types of geometrical influences considering degrees of freedom (dof), translation, shearing or deformation, there is the need for several registration methods and algorithms. Rigid registration is confined to find the spatial transformation of translation and rotation only. Thereby six dof are covered, three for translation and three for rotation. If shearing and scaling are involved then the registration is said to be affine. Thereby six additional dof are of interest, three for each shearing and scaling. When anatomic structures like organs get deformed, rigid registration is useless and another type of algorithm is necessary. This type is called non-rigid which implies that rigid registration would not work flawless. These types of registration are depicted in Figure 1.20.

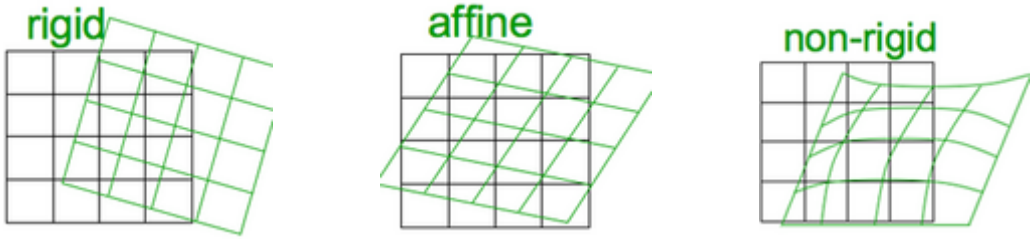

Figure 1.20: Different types of image registration (Slicer.org, 2015)

1.5.2 Merit Functions

A merit function is a type of a cost measurement or a cost function. In registration merit functions provide a measure on the similarity of images. To provide its function a merit function should fulfill several requirements (Birkfellner, 2014):

- When two images are aligned in an optimal manner it should yield an optimum value. Therefore the properties of a merit function for registering from the same modality and the merit function of an intermodal registration are completely different.
- To be able to distinguish images that are only slightly off from those completely different, the range of convergence should be as wide as possible.
- There exist two different types of merit functions: intensity-based or gradient-based.

A merit function is, in general, a measure of mutual dependences between different variables. In the case of intensity-based merit functions, the intensity values are considered the random variables which are compared at a given location of image elements which are assumed to be of the same anatomical region. A merit function assumes a common frame of reference while the moving image moves by means of translation, rotation or other volumetric transformations (Birkfellner, 2014).

1.5.3 Methods of Registration

As several types of registration exist also several methods of registration are available. They can be classified according to their used merit function or their operational characteristics. Also the methods for optimizing the result can differ in many ways. The easiest method for registration is the manual interaction whereby spatial relationship between the model and the reference image is modified manually. But the interest lies in automatic registration methods. Such methods use feature-based or voxel-based methods.

Feature-based Registration

In both images - the moving image as well as the reference image - corresponding features are extracted. Such extraction can be performed in two different ways: manually or fully automated by automatic extraction algorithms. Most often the manually extraction is used, since the algorithm not often detects features exactly. But algorithms are getting better and better by time, so at the time of writing also extraction algorithms are able to extract structures sufficiently. After performing feature extraction registration can be processed. This is done with a merit function calculating the distance of each feature. Registration is processed by minimizing the distance for each feature while conserving the result of closely features. As a feature several landmarks like anatomical points or otherwise anatomic contours or surfaces can be used (Oppelt, 2005). After registration was performed successfully the translation and rotation can be observed by the transformation matrix. It can then be used for further processing.

Landmark-based Registration

Landmarks are structures that can easily be extracted and can involve several anatomic structures or implanted gold seeds for example. For such a algorithm to deliver correct results at least three different landmarks are necessary. These landmarks have to correspond between the moving and the reference image, otherwise registration would not work. Calculation of the spatial transformation is done in a deterministic way, so no iterative methods are used. Registration is then done via minimization of the distance of the corresponding landmarks. As a kind of landmark-based registration, surface-registration makes use of segmented areas. These segmentations represent the surface of the anatomic structure. Such a registration is useful when fast and accurate segmentation algorithms can be applied. Segmentation can be performed by the definition of an intensity threshold which then acts as surface. Also in surface-based registration the spatial transformation is determined by minimizing the distance of the surfaces from both images (Oppelt, 2005).

Intensity-based registration

If no anatomical structures or landmarks can be extracted, or a fully automated registration should be performed, intensity-based registration is the way to go. It avoids the task of identifying corresponding features or landmarks and requires less user interaction than other registration methods. Furthermore intensity-based algorithms are less susceptible for noise or truncation effects. Several distance measures are used as merit function (Oppelt, 2005):

- Cross correlation
- Mean square deviation
- Ratio image uniformity (statistical similarity measure)
- Correlation ratio
- Entropy and joint entropy

Such normalized mutual information measure show good results, even with inter-modality images. Intensity-based registration approaches use the voxel intensity as basic distance measure in order to achieve ideal matching of the registration (Oppelt, 2005). As with other registration methods, the spatial transformation matrix is determined by minimizing the distance measure.

Optimization

Optimization is a task where the parameters of the spatial transformation matrix are determined in a manner that the distance measure reaches a absolute minimum or maximum. The ideal transformation is that of global extremum of the distance measure. Sometimes only a local extremum is reached. This is a task for optimization. Another point is that this extremum should converge as quickly as possible. This is because optimization will have to be repeated for each modification (Oppelt, 2005).

2 Material and Methods

As mentioned in the previous chapter, ultrasound is an important imaging modality and offers high image quality at low costs. It is used in several fields of medicine and becomes more and more important also in radiation therapy. Its importance in RT is because of the possibility of 3D imaging without the need of additional ionizing radiation. Also as aforementioned, patient positioning is an important task in RT and IGRT. It allows for safer delivery of higher and more effective radiation dose with fewer side effects compared to other radiation therapy techniques. Thereby safety margins can be constrained without affecting the conformity of the radiated volume. For this important task several technologies for patient positioning are available, some of them also involving 3D US imaging. Ultrasound in IGRT is a radiation-free way to acquire images of sufficient quality of soft tissue and makes use of 2D or 3D US imaging devices. Such systems are suitable for the treatment of prostate cancer. Before each treatment a physician acquires an US image of the prostate which is then registered (see 1.5 Image Registration) to a pre-interventional CT image. The resulting spatial transformation is then used for realigning the patient on the treatment couch. Being a disadvantage, deformation of the organ of interest occurs because of the applied pressure during the imaging process. This leads to an overall lower positioning accuracy compared to seed-marker based IGRT concepts, as studies revealed. Despite these accuracy problems several commercial systems are available (see 1.4 Image-Guided Radiation Therapy). Nevertheless, such systems still acquires human interaction during the repositioning process. Accounting this issue, a promising development is in progress; see (Kaar, et al., 2012). The system setup of such a system is as follows. An optical tracking system is used in the CT room (CTR) and the treatment room (TR). It is calibrated to the laser system at each site. Also calibration of the US scan head is necessary. Therefor US calibration, as suggested in (Bathia, 2012), is applied. Immediately after the CT image has been taken an US image has to be taken too. This enables the transformation of a point in the US image to the laser coordinate system of the CTR. For positioning another US image has to be taken in the TR. Since the laser coordinate system in the CTR and the TR are defined to be identical, this allows for determination of the difference in patient alignment. The transformation can be determined via 3D/3D US-US registration. Since 3D-US imaging systems are expensive a system was suggested that makes use of 3D US image generation out of 2D US images. It was expected that the overall image quality can be increased by the use of such a system. This is to be ensured via measurement and comparison of the conventional 3D US system and the suggested system using 2D US images. For such a system several materials is of necessity which is to be discussed in this chapter. Also used methods are introduced and discussed to get familiar with the implementation of the suggested 3D US imaging system using 2D US slices. For realization of the generation of 3D volumetric images out of 2D images the so called PLUS software, where PLUS stands for Public software Library for Ultrasound imaging research, was used.

2.1 PLUS Library

The PLUS library is an open source library for ultrasound-guided intervention systems and offers many possibilities for IGI. Although other libraries for IGI exist, PLUS was developed from scratch because often important features were missing. One example of an existing

library is the SynchroGab software Library (Boisvert, Gobbi, Vikal, Rohling, Fichtinger, & Abolmaesumi, 2008). It is based on the open-source Visualization Toolkit VTK (Schroeder, Martin, & Lorensen, 2003) and works with a couple of Ultrasound and tracking devices. It contained algorithms for reconstruction of volumetric images from acquired 2D images but lacks algorithms for spatial and temporal calibration as well as recording capability. The Image-Guided Surgery Toolkit (IGSTK) is an open-source framework for image-guided surgery applications but it also lacks spatial calibration features and other functionalities (Gary, Ibanez, Aylward, Gobbi, Blake, & Cleary, 2006). Many other different frameworks for development for real-time tracking and acquisition of image data are available. The Computer-Integrated Surgical Systems and Technology Libraries (CISST) (Kapoor, Deguet, & Kazanzides, 2006) for example was developed at the Johns Hopkins University. The OpenTracker library (Spiczak, et al., 2007) and the Virtual Reality Peripheral Network library (VRPN) (Hudson, Seeger, Weber, Juliano, & Helser, 2001) were also available but these systems focus more on robotic systems and lack limited support for imaging as well as an interface to medical US imaging systems or US image calibration algorithms. Because all libraries mentioned lack any feature necessary the PLUS library was presented (Lasso, Heffter, Rankin, Pinter, Ungi, & Fichtinger, 2014). It offers access to various US imaging systems and tracking systems using a hardware-independent interface. It includes software, hardware and documentation needed for calibration and data processing as well as visualization and transfer operations.

2.1.1 Configuration and features

As the internal structure relies on pipelines, devices are used. Each hardware device or data processing algorithm is represented by a device. A device may provide an output channel to deliver data generated. Data is generated internally, collected from hardware devices, or data can be used from other devices received from them. Also channels are used. Each channel transfers a bundle of data streams. Each stream can consist of a single video frame and/or different kinds of attributes like transformations. Also virtual devices exist. They are used for various operations on their input channels. Such an operation can be fusion of multiple channels, disk storage or 3D volume reconstruction. The structure of the pipeline architecture can be seen in Figure 2.1. This knowledge of the structure is essential for correct configuration of the PLUS library, as configuration is done per device. Each device has to be configured separately. As US and tracking data are acquired by separate devices, fusion of this data is necessary. Fusion is done with the virtual mixer device which combines two different data streams to one combined stream. Therefore it is also necessary to resample this data before fusion because image data and pose data are acquired at distinct time points (Lasso, Heffter, Rankin, Pinter, Ungi, & Fichtinger, 2014). Because resampling of image data is a complex operation, because of its large size, only resample of position data is done. US image data is acquired either directly using compatible US devices or using a frame grabber unit. As with pose data, also an US imaging device is configured as a device, each separately.

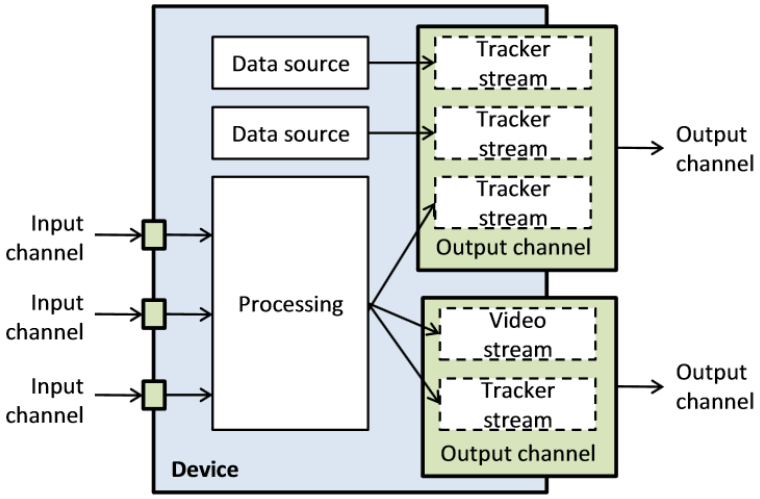

Figure 2.1: Example of the pipeline structure (Lasso, Heffter, Rankin, Pinter, Ungi, & Fichtinger, 2014)

All configurations of the hardware, like definitions of which hardware devices are used for acquiring US image data and tracking date, acquisition rate, connection settings and others, are specified in one single configuration file, hence configurations can be applied without modifying or rebuilding the software (Lasso, Heffter, Rankin, Pinter, Ungi, & Fichtinger, 2014). PLUS library includes calibration algorithms which allow for easy to use calibration. Calibration is needed for the correct spatial transformation between the image coordinate system and the transducer sensor (probe) coordinate system. If this calibration is missing no 3D volumetric image reconstruction is possible as it is not known where to add 2D US slices into the volume coordinate system. Hence calibration is an important task as elaborated in (Bathia, 2012). PLUS offers a fully automatic spatial and temporal calibration process where very less user interaction is necessary. The software also supports streaming of tracker data as well as acquired image data through OpenIGTLink, see (OpenIGTLink, 2015) for further information. This feature can be used to stream tracking and image data to 3D Slicer over an IP based network. One of the most important features of PLUS is the 3D volume reconstruction from 2D US image slices. Using the reconstruction algorithm also a hole-filling algorithm is available. PLUS offers support for several different frame grabbers, as the following list shows (PLUS Project, 2015):

- Framegrabbers: Epiphan, ImagingControls framegrabbers
- Video for Windows compatible devices
- Microsoft Media Foundation compatible devices
- Ultrasound systems (through digital interface, without framegrabber): Ultrasonix, BK, Interson, Philips (WIP) ultrasound scanners
- Medtronic StealthStation
- OpenIGTLink compatible devices

For image acquisition an Active Silicon VfW-frame grabber LFG4 (Active Silicon, 2015) was used as it was the only possibility to connect the Ultrasound imaging device to such a frame

grabber using the Composite Video output. This is due to the fact that no other connections are supported by the device. Also several tracking systems are directly supported by PLUS, as the following list claims (PLUS Project, 2015):

- Ascension electromagnetic trackers
- NDI optical and electromagnetic trackers
- Claron MicronTracker
- Medtronic StealthStation
- Prostate LDR brachytherapy steppers
- 3d connexion 3D mouse
- PhidgetSpatial and CHRobotics inertial sensors
- OpenIGTLink compatible devices
- daVinci surgical systems

For the calibration process and tracking of the US transducer an optical tracking system (NDI Polaris) was used. At the beginning also an electromagnetic tracking system (NDI Aurora) was used, but it appears to deliver rather inaccurate position data. It is assumed that this was because of metallic room environment, which lower accuracy of an electromagnetic tracking system like the NDI Aurora.

2.1.2 Applications

The PLUS library offers several applications which enable the user to apply the configuration process (fCal.exe) or offers the possibility of streaming features via OpenIGTLink (plusserver.exe). Also other applications for testing purposes are available.

fCal.exe

With fCal PLUS features an easy to use user interface which offers methods for configuration as well as several steps to apply the whole calibration process. It is also possible to start image and position data capturing as well as to apply volume reconstructions. The user interface is divided in several tabs, which the following list shows:

- Configuration
- Capturing
- Stylus calibration
- Phantom calibration
- Temporal calibration
- Spatial calibration
- Volume reconstruction

The graphical user interface is depicted in Figure 2.2. The tabbed structure can be seen on the left side of the user interface. Under configuration the device set can be chosen. Also the

connection to the configured devices can be established. Configuration is done with a simple text editor which can be started by clicking on the appropriate button left to the list of device sets. When the connection to a tracking system is established the configured tools can be displayed underneath the Connect-button.

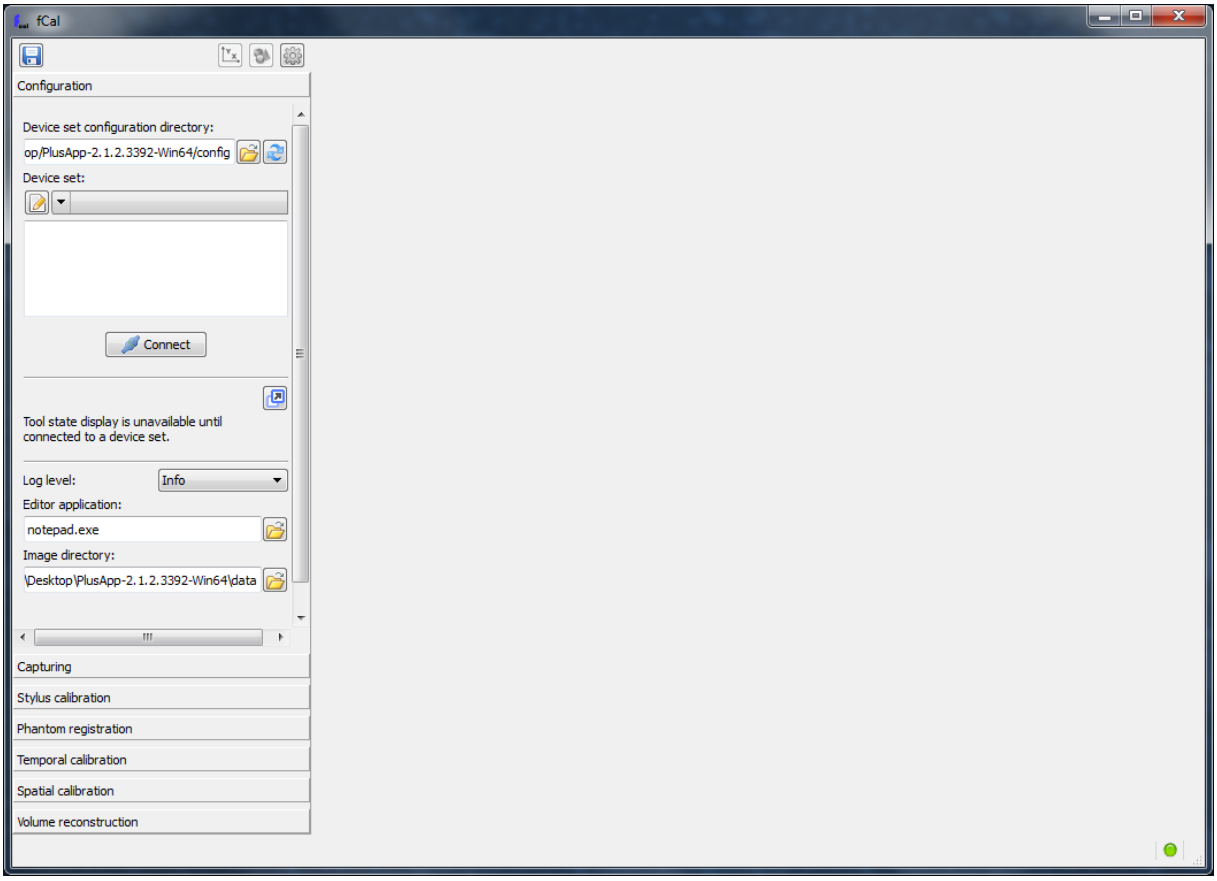

Figure 2.2: User interface of fCal.exe

PlusServerLauncher.exe

As PLUS offers a streaming feature using client/server architecture, there is an application available to configure and start/stop the server or client. This is done with the PlusServerLauncher. It does not offer any other functionality than configuration and starting or stopping the server. The server itself is a own application that offers all the functionality necessary for streaming of tracker data and image data as well as start or stop the recording of such data. Also a volume reconstruction feature is available, so the reconstruction process can be done on a fast workstation computer while data acquisition is done on a slower machine. The client/server architecture is also used when using 3D Slicer. Thereby it is possible to control the server application using a plug-in in 3D slicer that offers control features. The user interface of the PlusServerLauncher is depicted in Figure 2.3. As can be seen, there is only a dropdown list and a connect button available. All configurations available are listed within the dropdown list. Connection for the chosen configuration is established with the connect-button.

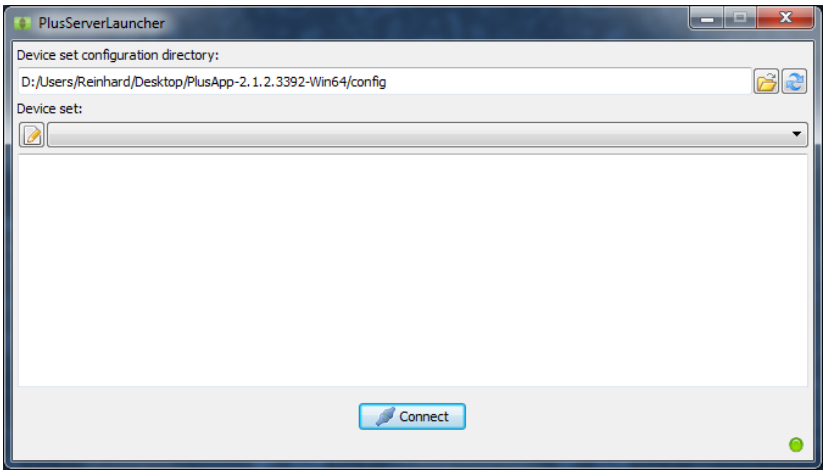

Figure 2.3: User interface PlusServerLauncher.exe

It is also possible to launch the PLUS server from the command line. The configuration file and other parameters can be consigned using command line parameters. But as with PlusServerLauncher an easy to use user interface is offered, there is no need for using the command line application. More information about the configuration of PLUS can be read on the PLUS webpage, see (PLUS Project, 2015).

2.2 3D Slicer

3D Slicer is a cross-platform application which is freely available. It is an open source software package for visualization and medical image computing. It offers image registration algorithms as well as segmentation features and 3D volume rendering for example of CT or MRI image data. Also 3D US images can be rendered. The software uses a module-based architecture which offers the ability for easy expansion with several extensions. Also the implementation of new workflow for image visualization, which is often used in IGRT, is possible. The user interface of 3D slicer can be seen in Figure 2.4. The blue marked area is the configuration area where the individual module can be configured. A module can be chosen using the drop down list tagged with the orange arrow. Several modules for many different applications are available. The red marked area corresponds to the 3D viewer for visualization of 3D image date and for rendering. It delivers the output of several modules and is accordingly coupled. The green area is used for visualization of 2D image data. It is used for visualization of anatomic structures in all three anatomic axes (axial, sagittal and coronal). Also the actual displayed slice of one image set can be identified or chosen by the slide control. Further settings for the visualization areas are available by clicking on the pin symbol, see Figure 2.5. For installation of additional plug-ins the Extension-Manager can be used. It can be activated using the view menu in the top menu bar.

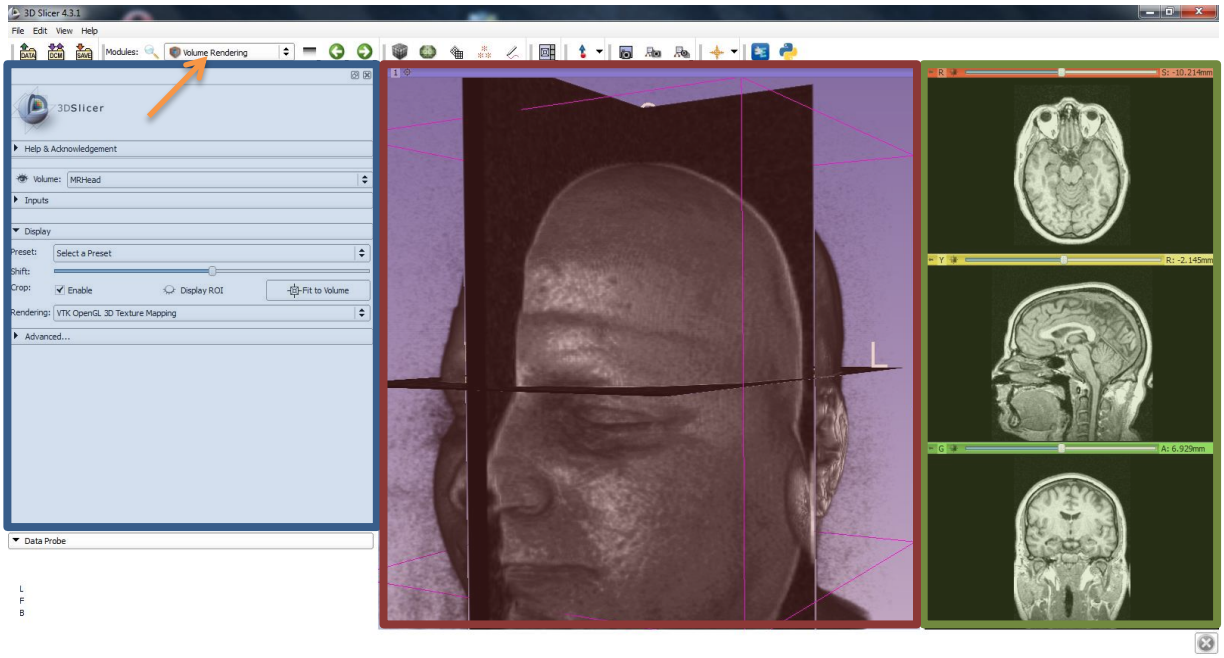

Figure 2.4: User Interface of 3D Slicer with marked modules

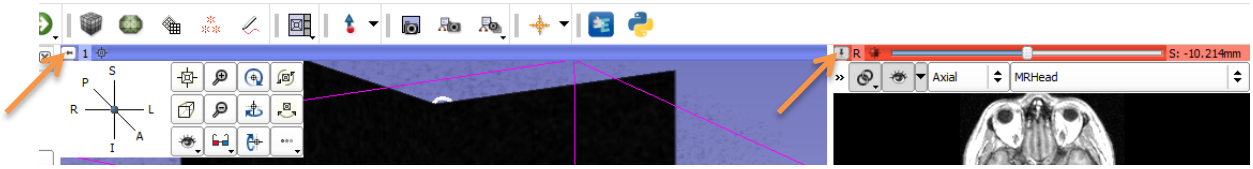

Figure 2.5: Additional configuration for the 2D/3D viewer via the pin symbol

2.2.1 Extensions

3D Slicer offers the possibility to be expanded via extensions. Thereby functionality not available in 3D slicer can be added with the installation of an additional plug-in. Many different extensions are available for installation in 3D Slicer and are afterwards available via the module selection control. From the extension manager there is one plug-in necessary which was installed. This extension offers the possibility of remote control the PLUS server application and other functionalities. But not all of the installed modules were used. The most frequent used and the reason for the installation of the SlicerIGT extension was the “Plus Remote” module. Its icon can be found under the category IGT in the extension manager. After installation of the SlicerIGT extension the appropriate modules can be found under the subcategory IGT of the module-dropdown list.

2.2.2 Used Modules

3D Slicer makes use of modules for tasks to be handled. There are more than 100 different modules available and several of them are necessary for data acquisition and reconstruction in 3D Slicer with PLUS server in the background. The following modules were used during data acquisition, reconstruction and measurement:

- OpenIGTLinkIF
- Volume Reslice Driver
- Plus Remote
- Volume Rendering
- General Registration (BRAINS)
- CheckerBoard Filter
- Transforms

OpenIGTLinkIF

The OpenIGTLinkIF module offers the possibility to establish connections using the OpenIGTLink-protocol. As PLUS server supports streaming of position and imaging data over the OpenIGTLink-protocol this is the module to use to connect 3D Slicer with the PLUS server application. A new connection is established via pressing the plus-button. Now it is possible to enter the network configuration settings like IP address and port. The connection can be activated by checking the active-setting. In the lower text-field received position data and image data is displayed. When calibration was done also the transformation can be viewed in the text-field.

Volume Reslice Driver

This module enables updates for a resclicing plane by a linear transform node. With this module it is possible to reslice a volume of the anatomic structure of the patient with a plane along the surgical tool. The result is then being displayed in the 2D and 3D viewer of 3D Slicer. This module also offers the possibility of displaying the US live image streamed via OpenIGTLink to 3D Slicer. To display the US live image in the 2D viewer the corresponding axis should be chosen. Under driver the appropriate image driver has to be chosen. The mode is configured as transverse. This tool is usefull for tracked surgical navigation using a tracking system, where position and orientation of the tool is being tracked by such a tracker. (Slicer.org, 2015)

Plus Remote

Plus Remote enables the user to remotely control PLUS over 3D Slicer. It uses an established connection over OpenIGTLink to the PLUS server to send commands. The module provides recording of 2D tracked ultrasound imaging data, the control of the volume reconstruction using PLUS server as well as live ultrasound volume reconstruction using a previous scout scan. The reconstructed 3D volumetric image is transferred through OpenIGTLink after volume reconstruction is complete by the PLUS server. This module only offers a graphical user interface for the control of the PLUS server. When data acquisition and 3D Slicer are running on different machines and tracked image data is being recorded it is not saved on the computer where 3D Slicer runs. Data is saved on the machine where the PLUS server is being executed.

Volume Rendering

This module allows for rendering of 3D volumetric image data. It enables the user to visualize previously reconstructed volumes by selecting the appropriate volume in the dropdown list. To activate the display the eye next to the dropdown list should be checked active. It is also possible to apply several presets of visualization but as this is not useful for volumetric US image data this feature was not used. It is important to mention that for rendering VTK GPU Ray Casting should be chosen when available. Otherwise the CPU is used for the rendering task which can take a while.

General Registration (BRAINS)

With the General Registration module it is possible to perform image fusion processes as discussed in 1.5 Image Registration. Thereby a fixed and a moving image have to be chosen. Slicer BSpline Transform and Initialization Transformation can be left blank. It is important to configure an output image volume otherwise no visualization of the registration result is possible. To evaluate the resulting transformation a Slicer Linear Transform has to be chosen. Under "Registration Phase" the dof can be chosen by checking one or more settings. Image registration is started via clicking on the Apply-button. The registration result, the output image volume, is represented by the moving image registered to the fixed image. No image fusion occurs. The resulting registration gets saved under the configured transformation.

CheckerBoard Filter

The CheckerBoard Filter module creates a checkerboard volume out of two volumetric images. The output image will show the two inputs alternating to the user specific checker pattern. This module is often used to compare the result of an image registration process. The second input is resampled to the same origin, spacing and direction before it is composed with the first input (Slicer.org, 2015).

Transforms

The Transforms module can be used for viewing, editing and creating transformation matrices. It is possible to display transforms resulting from image registration (see aforementioned module General Registration). The sliding controls offers direct visualization of translation and rotation the upper transformation matrix corresponds to.

2.3 Calibration

Before 3D volume reconstruction can be used it is necessary to perform the calibration process. Thereby the transformations of different coordinate systems are determined. The overall goal of calibration is to determine the transformation between the coordinate system of an object (e.g. image slice, phantom or stylus) and a marker rigidly attached to that object. A typical setup consists of a tracked US transducer and a reference sensor attached to the patient. For volume reconstruction the most important transformation is the one representing the translation between the image coordinate system and the transducer marker coordinate

system. Several coordinate systems are depicted in Figure 2.6. The whole calibration process of PLUS is established of several calibration steps. All these steps are necessary to be able to determine the transformation of the image coordinate system to the marker coordinate system rigidly attached on the US transducer.

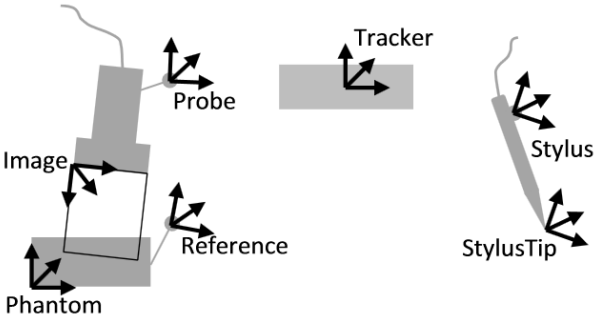

Figure 2.6: Coordinate systems of a typical US calibration setup (Lasso, Heffter, Rankin, Pinter, Ungi, & Fichtinger, 2014)

2.3.1 Details on Calibration

For 2D transducer calibration usually a set of different image planes have to be acquired. These data image an invariant geometric feature of a phantom. Therefore the phantom should offer different types of features, able to be clearly detected in the ultrasound image. Different types of phantoms are available. Then a set of transformation equations are constructed that match the known parameters of the phantom. These equations have then to be solved with respect to transformation parameters. Typical phantoms are built with nylon wires crossing each other and represent a plane which appears as a line in the 2D US image. The biggest challenge now is accurate identification of the phantom features in the ultrasound image (Lange, Kraft, Eulenstein, Lamecker, & Schlag, 2011). In a simple calibration process several different rigid transformations are used. The main idea of the calibration process is to measure or compute all rigid transformation to determine the one which is wanted (Lange, Kraft, Eulenstein, Lamecker, & Schlag, 2011). As the calibration process is processed to achieve the calibration from the ultrasound image to the transducer marker this transformation is ${}^{S}T_{US}$ as depicted in Figure 2.7. The position and orientation of the transducer marker is given by the transformation ${}^{Ca}T_{S}$ which is measured by tracking the marker in the camera coordinate system. Also the position of the phantom, represented by ${}^{Ca}T_{P}$, can be measured by tracking the marker rigidly attached to the phantom. If the position of the phantom in the ultrasound image ${}^{P}T_{US}$ is determined by imaging the phantom with the tracked transducer the transformation ${}^{S}T_{US}$ can then be calculated by

$$ {}^{S}T_{US} = {}^{Ca}T_{P}^{-1} \times {}^{Ca}T_{S} \times {}^{P}T_{US}^{-1} \tag{2.1} $$

as being mentioned in (Lange, Kraft, Eulenstein, Lamecker, & Schlag, 2011). To be able to determine the position of the phantom in the US image the phantom has to fulfill several

requirements. It has to have easily detectable, non-symmetric structures without imaging artifacts through echoes (Lange, Kraft, Eulenstein, Lamecker, & Schlag, 2011).

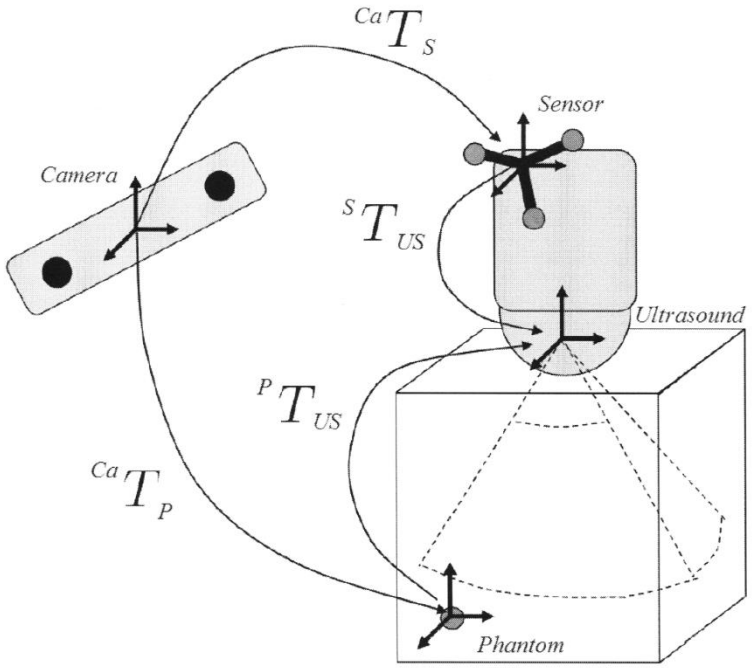

Figure 2.7: Different coordinate systems and their transformations used in an US calibration procedure. Revised from (Lange, Kraft, Eulenstein, Lamecker, & Schlag, 2011)

2.3.2 Calibration Procedure

As aforementioned, the calibration process builds upon different calibration steps. Each calibration step has to be performed to be able to calculate the transformation ${}^{S}T_{US}$ between the marker rigidly attached to the US transducer and the image coordinate system. The overall calibration process is subdivided in the following calibration steps:

- Stylus calibration
- Landmark registration
- Temporal calibration and
- Spatial calibration

Stylus Calibration

This part of the calibration, also called pivot calibration, is done to determine the translation between the marker attached to the stylus and tracked by the tracker and the stylus tip. The marker's coordinate system is usually named Stylus while the coordinate system of the tool tip is named StylusTip as can be seen in Figure 2.6. Determination of this translation is necessary to perform landmark registration as the next step of the whole calibration process. Pivot calibration is done via placing the stylus that way that it is visible to the tracker and the

stylus tip remains stationary relative to the reference marker which also has to be visible to the tracker. The stylus has to be swiveled while the tip still remains stationary which gives a sphere represented by the coordinates of the marker. Given this information it is possible to calculate the exact position of the tip of the stylus, thus giving the wanted translation. A performed pivot calibration using PLUS fCal.exe is depicted in Figure 2.8. The blue dots represent the whole sphere that is resulting from swiveling the stylus while the stylus tip still remains stationary. The green dot represents the stylus tip. When the stylus tip during the calibration process moves a bit the resulting sphere is not homogenous, resulting in a calibration error.

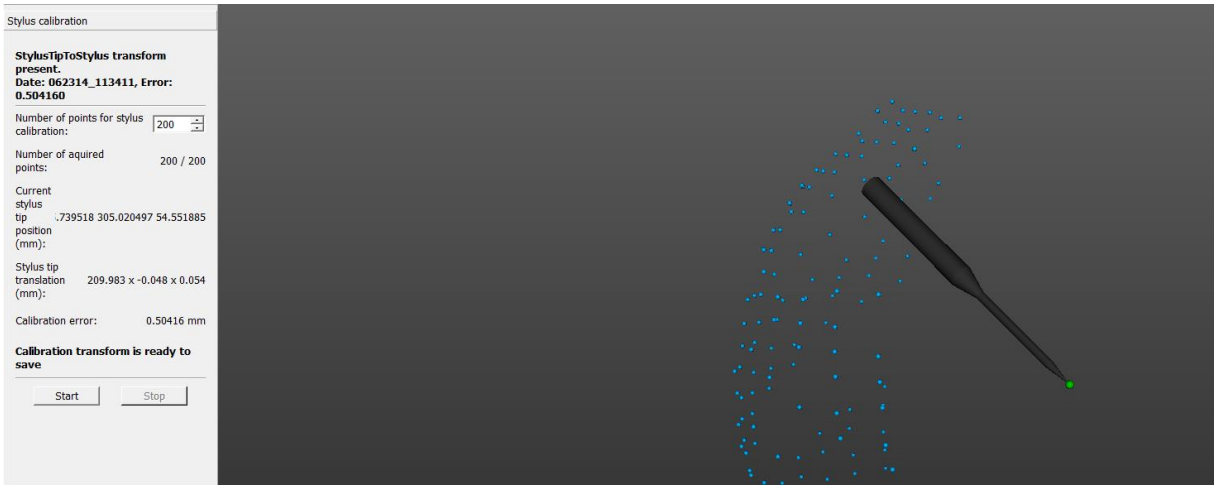

Figure 2.8: Performed stylus calibration using PLUS fCal.exe. (SlicerIGT, 2015)

Landmark Registration

In general landmark registration is used to calculate the transformation between an object and the marker attached to that object. The only necessity is that there are known positions of several landmarks. The more landmarks are used the better the resulting transformation in terms of accuracy can be. In this special case landmark registration is used to calculate the transformation between the phantom and the marker rigidly attached to the phantom, since only the marker is tracked via the OTS. But it is necessary to know the position of the phantom in the camera coordinate system. This is necessary to get the phantoms coordinate system in which wires are laid which are recorded during the last calibration step to acquire special information of the image plane. Landmark registration is performed by registration of specified landmarks on the phantom with the calibrated stylus tip. To the phantom eight of these landmarks are shaped. The positions of these landmarks are near the corners of the fronts of the phantom. Therefor these landmarks have to be touched with the tip of the stylus and registered in software. Figure 2.9 shows the front where the first four of eight landmarks are positioned. As can be seen, the landmarks have to be unsymmetrical to be able to determine the orientation of the phantom.

Figure 2.9: fCal phantom for calibration showing 4 of 8 landmarks

Temporal Calibration

The acquisition computer collects data from the position tracker and the US system, connected via a frame grabber. All these subsystems provide their own timestamp. Temporal calibration is then needed to correlate this timing information and to calculate a timing offset. That is, the position tracker delivers data faster (or slower) than the frame grabber. This offset is calculated via recording tracker and imaging data of the transducer while moving the US transducer continuously up and down. After recording a one dimensional position this information is extracted from both data sources. This information out of the tracker data is computed via projecting the 3D position to a perpendicular axis of motion. The 1D US image information is gained by placing a reflective object in the field of view of the transducer and extracts the position of this line. Both 1D data gives a quasi-sine over time. The phase shift of both sines gives the timing offset. As fixed stream the video-stream was chosen. The tracker stream was configured as moving system. The resulting sine structure from temporal calibration can be seen in Figure 2.10.

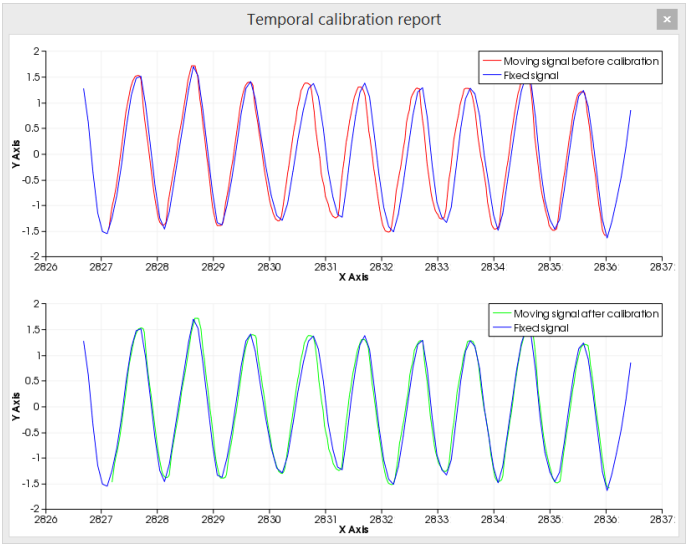

Figure 2.10: Resulting sine-structure after temporal calibration (SlicerIGT, 2015)

Spatial Calibration

The last step of the calibration procedure, spatial calibration, is used to determine the transformation ${}^{S}T_{US}$ between the coordinate system of the marker attached to the US transducer and the US image. It is the most challenging calibration. There are several potential methods available for spatial calibration (Mercier, Lango, Lindeseth, & Collins, 2005). PLUS uses a method where N-shaped wires are laid in the phantom as can be seen in Figure 2.11. This calibration method is used as suggested in (Carbajal, Lasso, Gómez, & Fichtinger, 2013; Chen, Thurston, Ellis, & Abolmaesumi, 2009). The fiducials are configured, so the coordinates of the wires are given to the calibration software. Hence the coordinates of the N-wire shaped configuration is known by the software. It is important that the N-wire shaped configuration is unsymmetrical to be able to determine the orientation of the phantom. These wires are slowly scanned with the transducer so that the software can segment the wires by the coordinates given in the configuration. As should be clear, it is important that the whole N-wire configuration is scanned with the US transducer. Hence the whole N-shaped wires should be visible in the US images during the whole spatial calibration process. Otherwise segmentation cannot be executed correctly because of missing wires in the image. It is also important that during the calibration process the marker of the phantom and the one of the US transducer can be seen by the OTS. As the position of the phantom is known in the OTS coordinate system – achieved by landmark registration – and the N-wire configuration is known by the calibration software, the relative position of the N-shaped wires are also known in the OTS coordinate system. By segmenting each wire and knowing the position of each wire in the phantom the constant but unknown transformation ${}^{S}T_{US}$ can be computed by equation (2.1). The transformations ${}^{Ca}T_{P}^{-1}$ and ${}^{Ca}T_{S}$ can be determined by measurement with the OTS. Hence the missing transformation between the marker attached to the transducer and the US image can be calculated. After spatial calibration is performed the resulting transformation is written to the configuration file. The calibration error is displayed in the user interface. Hence it can be determined if recalibration is necessary or if the resulting transformation is accurate enough. Using this calibration method an accuracy of 0.6mm was achieved.

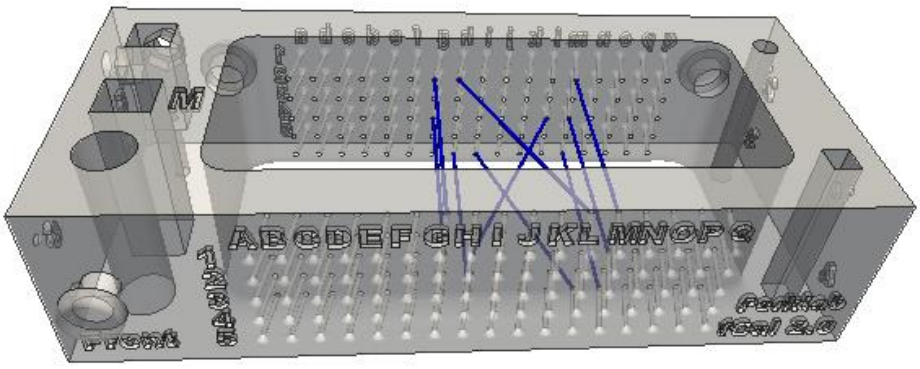

Figure 2.11: fCal phantom with N-shaped wires (PLUS Project, 2015)

2.4 Data Acquisition

Data acquisition involves the gathering of position date of the markers attached to the US transducer as well as image data from the US device. It is the previous step to volume reconstruction as without image data and position data no 3D volume can be reconstructed. Data acquisition can be achieved in two ways. On the one hand fCal offers the possibility to record pose data as well as imaging data while on the other hand gathering of the necessary data is also possible with 3D Slicer and the module Plus Remote which gets available with the installation of the SlicerIGT extension through the extension manager. To be able to use 3D Slicer for data acquisition an instance of Plus server needs to be up and running, as Plus Remote only offers command transfer to Plus server through OpenIGTLink protocol. It has to be mentioned that the data is not acquired by 3D slicer itself but by the Plus server. Plus Remote in 3D Slicer offers only the user interface for control of the running Plus server instance.

2.4.1 Data Acquisition Setup

As aforementioned, there are two possibilities for data acquisition. For this project it was chosen to acquire data with 3D Slicer and the module Plus Remote while an instance of Plus server is running. This setup of data acquisition applies also for volume reconstruction which is important to know as volume reconstruction requires a fast computer able of handling volume reconstruction. See more details on volume reconstruction in 2.5 Volume Reconstruction. As the computer where the frame grabber was built-in was rather outdated and not fast enough for real-time volume reconstruction it was chosen to use 2 different computers. One (named PC1) serving data acquisition of position data and image data as well as acting as server for streaming these data to an additional computer (named PC2) acting as client for the streaming data and as server for volume reconstruction. PC1 was setup that way that it runs a Plus server instance gathering position data of the OTS and image data of the US system. It was configured that way, that it acts as server to stream this data to PC2 using the OpenIGTLink protocol. PC1 therefore has no other function than acquisition of the necessary data and sending these data over the network to the second machine PC2. On the other hand PC2 was setup that way to run an instance of Plus Server as well as 3D slicer. The frame grabber was built-in to PC1 and is a VfW device. Plus Server therefor was configured such that it acquires the image data through the VfW API. The optical tracking system (NDI Polaris) was connected via universal serial bus (USB). The USB driver of the OTS emulates an RS232 interface, so Plus Server was configured that way to acquire position data with NDI Polaris through RS232. Using a virtual mixer device, Plus Server on PC1 was configured such to combine both data streams of the tracking system and the ultrasound device. This combined data stream was than configured to be sent through OpenIGTLink over the network. The Plus Server instance of PC2 was configured such that it connects to the Plus Server instance of PC1 over OpenIGTLink acquiring the pose and imaging data while streaming these data over the network. The Plus Server instance running on PC2 was setup that way to receive commands from 3D Slicer using the Plus Remote module. The whole setup is depicted in Figure 2.12.

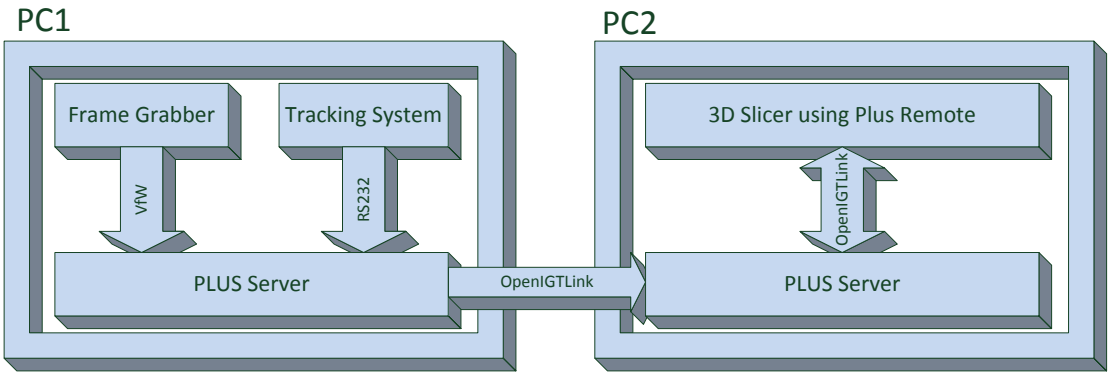

Figure 2.12: Data acquisition setup

2.4.2 Data Acquisition Procedure

To be able to reconstruct acquired 2D image data to a 3D volumetric image it is important to know the relative position of the region of interest. For test purpose a phantom in a water tank was used. To allow for determination of the pose of the phantom a reference sensor was used. As it was not possible to rigidly fix the reference marker to the phantom the marker was positioned in the nearby environment of the phantom. To assure the phantom did not move during data acquisition it was ensured that the phantom was not touched in any way. Hence, the relative position of the phantom was fixed in the coordinate system of the OTS. Thereby the absolute position of the phantom compared to the coordinate system of the reference marker was ensured to be constant. The reference marker was positioned in that way, that it could be seen by the tracking system. Also the rigidly attached marker on the US transducer was visible to the tracking system.

As mentioned previously, to gather the necessary data for volume reconstruction, two methods are available. Because of the easy to use graphical user interface (GUI) of 3D slicer and the module Plus Remote this possibility of data acquisition was used. Thereby it is not necessary to take care of saving and loading of the acquired data in a file as this is done automatically on the acquisition machine (PC2). First of all it was ensured that the Plus server instance on PC1 was connected to the configured devices like the OTS and the US device. It was also ensured that Plus server on PC2 was up and running and was connected to the Plus server on PC1. After this was achieved 3D slicer was set up that way that it connects to the Plus Server instance on PC2 using the 3D Slicer module OpenIGTLinkIF. To be able to visualize the live streamed US image in 3D Slicers 2D viewer the module Volume Reslice Driver was used. It was configured such that for the red 2D viewer “Driver” was set to “Image_Reference” and “Mode” was set to “Transverse”. After that was done the axial 2D viewer (red one) was configured to display the resliced image using the pin symbol and choosing reformat. As source “Image_Reformat” was selected. After these settings the US live image got visible in the red 2D viewer of 3D Slicer. After this configuration the system was ready to acquire pose and image data through 3D Slicer. To do so the module Plus Remote was selected. As a feature in the new version of Plus Remote, the OpenIGTLinkConnector gets selected automatically. Also the Capture Device ID as well as the Reconstructor Device is selected automatically. In the Recording tab it is possible to

configure a filename under which the recording gets saved on the acquisition computer (PC2). This is important for Volume reconstruction. To configure for another filename one has to click on the doubled arrow next to the “Start Recording” button. To start the recording of the acquired data one has to press the “Start Recording” button. The “Start Recording” command is then sent over OpenIGTLink to the Plus Server instance running to which 3D Slicer is connected (usually PC2 when using the aforementioned setup). When there is enough data acquired one has to stop recording. The appropriate command is send to the Plus Server instance and the data is saved under the configured filename. The GUI of the Plus Remote module is depicted in Figure 2.13. As can be seen, the doubled arrows are activated. Hence further configuration settings are visible.

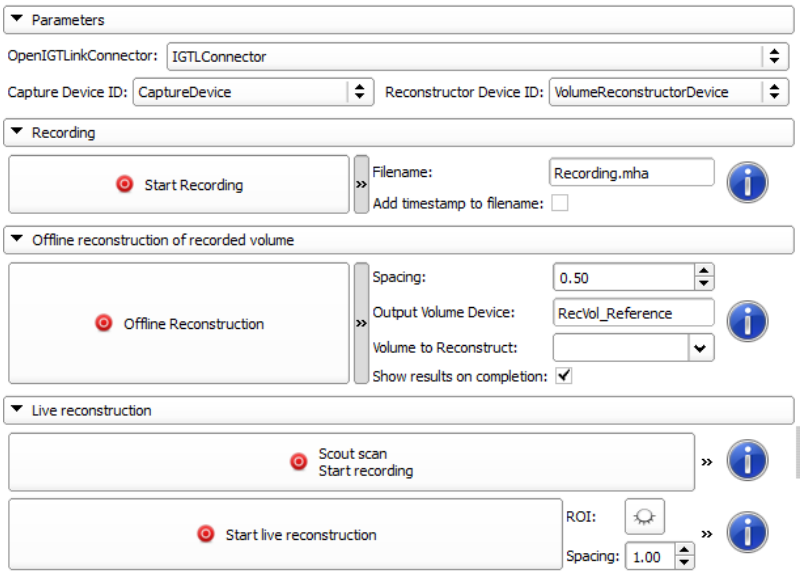

Figure 2.13: User interface of the module Plus Remote

2.5 Volume Reconstruction

Volume reconstruction is the process where a 3D volume is constructed from a set of 2D image slices which are sweeping across a region of interest. The 2D image data and the appropriate position data were acquired and recorded previously. Volume reconstruction can be achieved in two ways. On the one hand fCal offers the possibility to reconstruct a volume from a given recorded position data and US image data. The other possibility makes use of 3D Slicer and the module Plus Remote which gets available with the installation of the SlicerIGT extension through the extension manager. To be able to use 3D slicer for volume reconstruction an instance of Plus Server needs to be running. Plus Remote then sends commands through OpenIGTLink to the instance of Plus Server. It has to be mentioned that the resulting volume is not reconstructed by 3D Slicer itself but rather by Plus Server which then sends the reconstructed volume to 3D Slicer which is then to be displayed in the 3D viewer. Plus Server only offers the possibility of remote control the Plus Server by an easy to use GUI.

2.5.1 Details on Volume Reconstruction

The method of volume reconstruction PLUS uses is based on the proposal of (Boisvert, Gobbi, Vikal, Rohling, Fichtinger, & Abolmaesumi, 2008) as well as (Gobbi & Peters, 2002). The reconstruction procedure consists of several steps. The first one is the insertion of the 2D images into the 3D volume by iterating through each pixel of the acquired region of the 2D image and inserting the pixel value into the corresponding volume voxel. This describes the method "nearest neighbor interpolation". It is also possible to distribute the pixel value in the closest 8 volume voxels ("linear interpolation") (Lasso, Heffter, Rankin, Pinter, Ungi, & Fichtinger, 2014). While linear interpolation preserves more details of the original 2D image slice, it requires a higher resolution of the 3D volume. This method also lasts longer time to complete. Each voxel value is calculated by using the latest coinciding pixel value. Another option is to calculate a weighted average of all coinciding pixels and to use this value for the appropriate voxel. The latter method is called compounding (Lasso, Heffter, Rankin, Pinter, Ungi, & Fichtinger, 2014). To be able to remove acoustic shadows an option was added to compute voxel values as the minimum or maximum of coinciding image slice pixels. By this also artefacts by sweeping the transducer at the same region several times can be reduced. By using the "mean"-option it is possible to reduce random noise in the reconstructed image. While the reconstructed volume has uniform spacing along each axis, the spacing between the acquired 2D US images may vary. Not to get holes in the reconstructed image, it is possible to set the spacing of the reconstructed volume to the largest gaps between the acquired image slices. The disadvantage of this method is the resulting low resolution of the reconstructed volume. On the other hand, if the resolution of the computed volume is set to a higher value, than the method of simply pasting the 2D image slices to the volume will result in holes. To avoid such holes a lower resolution of the reconstructed volume can be chosen such that the largest spacing between the 2D images corresponds to the spacing in the volume, but this leads to lower details in the reconstructed volume. Therefore a hole-filling method was implemented in the reconstruction process of PLUS. This enables a high resolution volume and removal of holes by interpolation from nearby voxel values (Lasso, Heffter, Rankin, Pinter, Ungi, & Fichtinger, 2014).

2.5.2 Volume Reconstruction Procedure

As mentioned previously, to process volume reconstruction two methods are available. Because of the easy to use GUI of 3D Slicer and the module Plus Remote this possibility of volume reconstruction was used. Thereby it is not necessary to take care of saving and loading of the acquired data in a file as this is done automatically on the acquisition machine (PC2). It was ensured that Plus server on PC2 was up and running. After this was achieved 3D Slicer was set up that way that it connects to the Plus Server instance on PC2 using the 3D Slicer module OpenIGTLinkIF. After this configuration the system was ready to reconstruct a volume from before acquired position data and US image data through 3D Slicer. To do so the module Plus Remote was selected. As a feature in the new version of Plus Remote the OpenIGTLinkConnector gets selected automatically. Also the Capture Device ID as well as the Reconstructor Device is selected automatically. In the Offline Reconstruction tab it is possible to configure the spacing by activating the doubled arrow. For an accurate detail the

spacing was set to 0.5. Also the output volume can be named. As it is possible that several recordings are available it is necessary to choose the according recorded dataset from which the volume should be reconstructed. To start volume reconstruction one has to press on the "Offline Reconstruction" button. The user interface of the Plus Remote module can be seen in Figure 2.13. PLUS also offers the possibility of a live reconstruction. Thereby the volume is reconstructed during data acquisition. To do so, it is necessary to start a scout scan. Thereby a region of interest gets defined by sweeping the transducer over the region to be scanned. This can be done in a fast way, as only position data is important for the construction of the basic volume in which afterwards each slice is pasted. To display the reconstructed volume one has to select the Volume Rendering module from the module selection. Furthermore the appropriate volume has to be selected from the volume dropdown list. A reconstructed volume for test purposes can be seen in Figure 2.14. It is the N-wire shaped phantom which was used for calibration. The Hole-filling algorithm was configured to be deactivated. For spacing 0.5 was configured in the Plus Remote module.

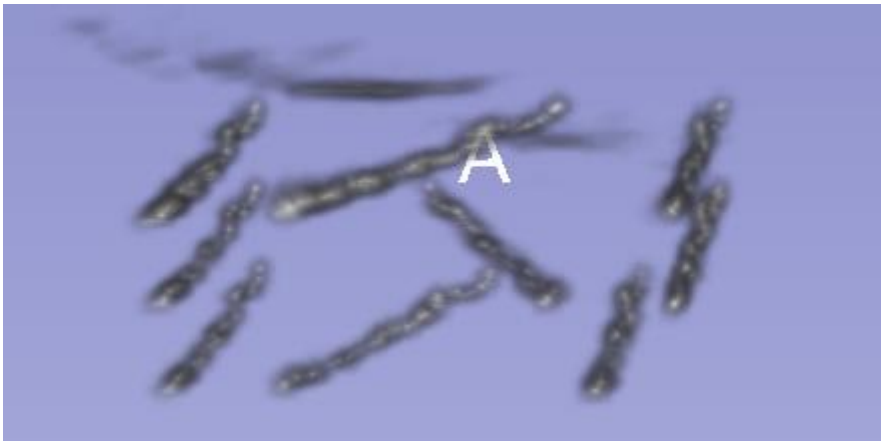

Figure 2.14: Reconstructed N-wire shaped phantom

2.6 Quality Measurement

Quality measurement is the essential part of this thesis. The aim of this part is to measure the quality of reconstructed 3D US volumes compared to general 3D US volumes. The idea is to have a measurement number that can be compared to conventional 3D US volumes. Therefore a metric function is necessary. The metric thereby depends on the definition of quality, as quality as it is named is not defined. There are several possibilities of quality concerning images. One can mean the details that can be seen in an image. Thereby the lines per mm can be a measurement. This is a measurement of the contrast ratio available between two distinct fiducials in an image. Another one can mean the overall resolution of the image or the level of noise and speckle in an US image. Quality also can be a measurement in terms of accuracy. It can be said the less the misalignment error between two images the higher the quality of the images. This measurement relies on the distinguishability of an image as for registration it is important that several fiducials are perceptible. If this requirement is not given, image registration may fail.

2.6.1 Details on Quality Measurement

As aforementioned, quality is not a distinct measurement. Therefore, to give quality a number, one has to define what is being meant with quality. For the concern to measure quality of reconstructed 3D US volumes compared to conventional 3D US images there are several methods available for quality measurement, as the following list shows:

- Peak signal to noise ration measure (PSNR)
- Structural similarity index measure (SSIM)
- Void Detectability Ratio (VDR)
- Quality in terms of accuracy

All methods can be used to get a measure of the overall image quality. The peak signal to noise ratio measure works by calculating the mean squared error (MSE). Afterwards the maximum range of the data type is then divided by the MSE. This measure gives thereby information about the noise level in an image. As every US image suffers from speckle and noise, this is no appropriate metric for determination of US image quality. The SSIM measures the similarity of an image compared to a reference image. As this is only suitable when modifying an image and compare it to the reference image, this metric is not useable for calculating a measurement on US images. The latter two metrics are available in Matlab and can be used to measure the quality of a regular image in Matlab (Mathworks, 2015). But as US images are used where no reference image is available and speckle is part of every image these metrics or not suitable for US quality measurement. While VDR is a contrast measure, the quality in terms of accuracy is a measure where the accuracy of the measured image in the reference coordinate system is taken into account. The VDR measurement works by measuring void in a phantom with cylindrical, artificial cysts in tissue-mimicking material. The better the void is perceptible compared to the material of the void, the better the image quality is meant to be. The VDR measure gives information about the detail perceptibility in an US image. The latter method in the previous list, the quality in terms of accuracy, makes use of error measurement during image registration. While one registers two images to one and another, the reference coordinate system is used as registration coordinate system. When registering two images it is attempted to make them congruent by using particular fiducials as discussed in 1.5 Image Registration. Thereby, when the image data position in the image coordinate system is not constant in both images, translation and rotation can be measured. Image registration results in a transformation matrix where the values of the deviation vector (most right vector of the matrix) represent the translation. Thereby the misalignment of the coordinate systems can be computed. It can be assumed that the lower the misalignment the better the anatomical structure fits to the reference coordinate system defined by image data and the better the image quality in terms of accuracy. For this assumption to be valid it has to be mentioned that the relative position of the phantom or the patient to the reference marker must not change. Otherwise the registration error increases by increasing distance of the US transducer to the reference marker. Therefore it is recommended to rigidly attach the reference marker to the phantom or patient if somehow possible.

2.6.2 Image Registration Cost Metrics

As in image-guided radiation therapy using ultrasound imaging image registration is used, the best metric to measure image quality would be the method using quality in terms of accuracy. Hence two recorded volumes are registered to each other using 3D Slicer and the "General Registration" module. It is important that the reference marker has not moved during data acquisition as if so the resulting registration error would state a wrong result. This is because each image is referenced to the reference marker coordinate system. For image registration one has to define a fixed and a moving image. The registration process then tries to align the moving image that way that it is congruent to the fixed image. For this to fulfill several merit functions are available. The default cost metric is the Mattes Mutual Information (MMI). This metric is used to maximize the number of coincident pixels with the same relative brightness value. It is computed as follows in equation (2.2)

$$S_{(\mu)} = -\sum_{i}\sum_{k} p(i,k|\mu) log \frac{p(i,k|\mu)}{p_T(i|\mu)p_R(k)} \tag{2.2}$$

where p is the joint, p_T the marginal test and p_R the marginal reference probability distributions (Mattes, Haynor, Veselle, Lewellen, & Eubank, 2003). The negative of the mutual information S between the fixed image and the moving image is thereby expressed as a function of the transformation parameter μ. This metric is best suited for images using different brightness ranges (Mathworks, 2015). This means registration can be achieved of different modalities like PET and CT. Another cost metric is Mean Square Error (MSE). The MSE of an estimator measures the squares of an error where the error is defined as the difference of an estimator and a predicted value. It is calculated as written down in equation (2.3).

$$MSE = \frac{1}{n}\sum_{i=1}^{n}(\overline{Y_i} - Y_i)^2 \tag{2.3}$$

Thereby $\overline{Y}$ is the predicted estimator whereas Y is the true value. In image registration the predicted value is represented by one image whereas the estimator is represented by the reference image. The third merit function makes use of Normalized Correlation (NC). NC is a measure of similarity and invariant to scaling. It is defined as in equation (2.4).

$$NC(A,B) = -1 \times \frac{\sum_{i=1}^{N}(A_i \cdot B_i)}{\sqrt{\sum_{i=1}^{N} {A_i}^2 \cdot \sum_{i=1}^{N} {B_i}^2}} \tag{2.4}$$

Thereby A_i and B_i are the i^{th} voxel of the images A and B. N is the number of voxels to be considered. The factor -1 is used to make the cost function optimal when a minimum is reached (Bathia, 2012). The use of this metric is limited to images acquired using the same image modality. Therefore it can be used for 3D/3D US registration. Another cost metric is the MIH which left unspecified. As MMI is the default selection, this setting is used for volume image registration.

2.6.3 Quality Measurement Procedure

For registration one has to choose a fixed and a moving image while the moving image is registered to the fixed image. To be able to evaluate the resulting transformation matrix it is important to configure such a transform. As each volume was consecutively numbered, the transformation was named such that the number of the fixed image was followed by the number of the moving image. As example, the fixed image volume was "Phantom 1" the moving volume was named "Phantom 2" whereas the configured transformation was named "Transform_Phantom_1_2". The same holds true for the output image volume which was configured as following: "Volume_Phantom_1_2". This helps to keep track of all transformations and output volumes as each volume was registered to each other. An initialization transform was not used, therefore this setting left blank. It was assumed that the type of registration was rigid with 6 dof, as during image acquisition no zoom setting was used. The configured distance was the same for all acquired images. Also skew was assumed not to be present. Therefore under the tab "Registration Phase" "Rigid (6 DOF)" was checked while the other types kept deactivated. All other settings were left as they were. To start the image registration process one has to press the apply-button. After the registration process is finished the output image volume gets displayed in the 2D viewer. The resulting transformation matrix is then available for further evaluation. Therefore the Transforms-module was used. It displays the whole transformation matrix as well as the translation from the deviation vector (the most right column of the transformation matrix). Also rotation is displayed separately. As rotation between the different images was not present, rotation left the unit matrix, as rotation is defined by a rotation matrix. If no rotation is present then the rotation matrix is represented by the unit matrix. To calculate the registration error and the overall accuracy of the registration and therefore a measure of the image quality the norm of the deviation vector was computed. To compare the registration result with the unregistered volume image the checkerboard filter was used. To be able to see more details of the registration result, the "Checker Pattern" was configured to 16 for each of the three axes. As "Input Volume 1" the fixed image volume was selected while as "Input Volume 2" the output volume of the registration process was selected. Thereby the result of the registration process gets visible to the user, as the moved image is depicted alternating to the fixed image. The alternation rate can be configured with the "Checker Pattern". The higher the alternation rate is the more details can be seen in the resulting checkerboard image. But it is important not to choose to high values. Otherwise it is difficult to compare the result. If the moving and the fixed image are close to each other then it can be said the registration to be successful.

2.7 Application in Radiation Therapy

As there are several methods for patient alignment in image-guided radiation therapy and some of them are based on ultrasound, none of these methods offers the possibility for automatic patient positioning. There is a system proposed by (Kaar, et al., 2013) which enables automatic patient alignment only by the use of 3D ultrasound images. It is proposed to apply 3D US in the therapy treatment room (TR) as well as in the computed tomography room (CTR). Not to lack a rigidly attached reference sensor to the patient the optical sensor at the CTR and the TR are calibrated with respect to the laser coordinate system at each site (Kaar, et al., 2013). Before applying the US to the patient a pre-interventional step is necessary. This is the calibration of the US transducer. The US images are taken immediately after the CT scan for treatment planning has been recorded. This enables the assignment of any point in the US image volume to the laser coordinate system (LCS) stretched in the CTR. The application of 3D US at each site allows for intra-modal image registration between both 3D US images, which is depicted in Figure 2.15. It can be seen that the link between the two rooms is the resulting transformation from image registration. The link is represented by the transformation matrix ${}^{US,T}T_{US,C}$ as can be seen in the arrow at the bottom of the graphic.

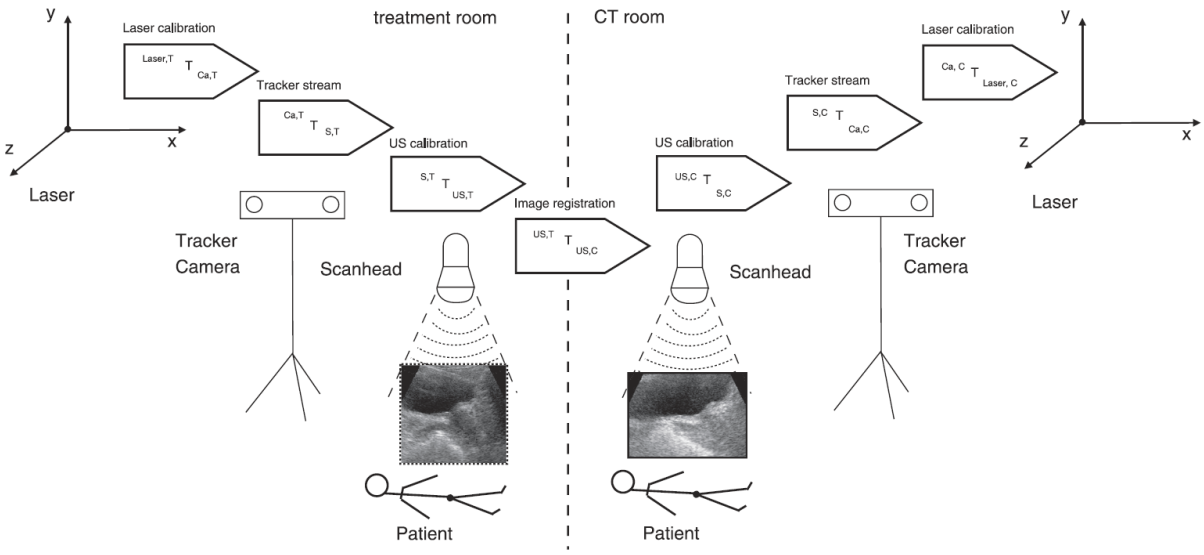

Figure 2.15: Transformation chain from TR to CTR. (Kaar, et al., 2013)

Since the LCS in the CTR and the TR are defined to be identical, another US image taken in the TR allows for determination of any difference in patient position (Kaar, et al., 2013). Determination of the shift can be obtained by 3D/3D US registration. To calculate the transformation of the position of a point P_{TR} in the treatment room given in the TR coordinate system to a point P_{CTR} in the CTR coordinate system the equation (2.5) has to be computed (Kaar, et al., 2013)

$$P_{TR} = {}^{Laser,TR}T_{Ca,TR} \times {}^{Ca,TR}T_{S,TR} \times {}^{S,TR}T_{US,TR} \times {}^{US,TR}T_{US,CTR} \times {}^{US,CTR}T_{S,CTR} \times {}^{S,CTR}T_{CA,CTR} \times {}^{Ca,CTR}T_{Laser,CTR} \times P_{CTR} \quad (2.5)$$

where the transformations ${}^{X}T_{Y}$ are represented by transformation matrices including six dof in position as well as in orientation. By this transformations translation and rotation are described, each of which has three degrees of freedom. ${}^{Laser,TR}T_{Ca,TR}$ and ${}^{Ca,CTR}T_{Laser,CTR}$ represent the transformation from the laser coordinate system at each site to the OTS coordinate system. ${}^{Ca,TR}T_{S,TR}$ as well as ${}^{S,CTR}T_{CA,CTR}$ give the transformation from the marker mounted to the US transducer to the OTS and are measured by the OTS. The transformations ${}^{S,TR}T_{US,TR}$ and ${}^{US,CTR}T_{S,CTR}$ give the translation and rotation of the 3D US image to the marker rigidly attached to the US transducer. These transformations can be determined by US registration. Last but not least the transformation ${}^{US,TR}T_{US,CTR}$ represents the position and orientation resulting from the 3D/3D US registration process. It is the transformation from the US image taken at the CTR to the US image taken at the TR. Equation (2.5) can be shortened to

$$P_{TR} = {}^{Laser,TR}T_{Laser,CTR} \times P_{CTR} \tag{2.6}$$

where ${}^{Laser,TR}T_{Laser,CTR}$ of equation (2.6) represents the whole transformation chain as written in equation (2.5). With this information given it can be seen readily that the transformation ${}^{US,TR}T_{US,CTR}$ from equation (2.5), which represents the transformation resulting from image registration, plays an important role in the whole transformation chain. With respect to this importance quality measurement is an essential part of the overall process of patient positioning. When using 3D US reconstructed from 2D slices, this measurement is not only important for automatic patient positioning but also for regular, still available US IGRT systems. The more accurate the image registration process succeeds the more accurate patient alignment can be performed. Hence the quality in terms of accuracy is an appropriate measurement to evaluate image quality for ultrasound-guided radiation therapy patient positioning. But not only image registration is important for patient alignment, also the calibration process of the US transducer plays an important part of the overall positioning process. If the US transducer calibration, resulting in the transformations ${}^{S,TR}T_{US,TR}$ and ${}^{US,CTR}T_{S,CTR}$, is inaccurate this also leads to an impairment of the patient positioning process. Not only the transformations ${}^{S,TR}T_{US,TR}$ and ${}^{US,CTR}T_{S,CTR}$ suffer from inaccurate US transducer calibration but also the transformation ${}^{US,TR}T_{US,CTR}$ suffers. More details on 3D ultrasound calibration are given in (Bathia, 2012). Finally also the exact measurement of the marker rigidly attached to the ultrasound transducer is important. If this part of the overall chain fails this leads to inaccuracies not only in the calibration process, but also in the translation ${}^{US,TR}T_{US,CTR}$ resulting from image registration. Thus it can be seen, that errors from one part of the chain result in errors of other parts of the chain, following the uncertainty analysis. Conclusively to the application of quality measurement in radiation therapy it can be said that quality measures of the images play an important role but is only a part of the error chain. Thus quality measurement is an important task for IGRT using US, as otherwise when not performing it, the patient may suffer from results of inaccurate alignment and thereby of radiation of non-cancerous tissue.

3 Results

Data acquisition was performed with a General Electric ultrasound device which was tracked by a NDI Polaris optical tracking system. As acquisition computer two Standard PCs where used, where the one was extended with an Active Silicon LGI4 frame grabber. The US device was connected to the frame grabber using a coax cable. The only interface useable for grabbing the US images was the C-video output of the US device. The setup was configured such as described in 2.4.1 Data Acquisition Setup. Thereby Plus server was configured on the PC extended with the frame grabber card as streaming server. The second PC was then used as acquisition device as defined in the PLUS documentation. As acquisition software 3D Slicer connected through OpenIGTLink to an instance of Plus server was used. As OpenIGTLink protocol uses a standard TCP/IP network link, it was ensured that the network load was minimal during the acquisition process. This was to ensure that no delays occurred. To control the Plus server instance the 3D Slicer module Plus Remote was used. Also volume reconstruction was initiated using the Plus Remote module. After volume reconstruction was performed, image registration within the process of quality measurement was executed. For image registration the module General Registration (BRAINS) was used as described in more details in 2.6.3 Quality Measurement Procedure. The image registration results were processed using the CheckerBoard filter to present these results.

3.1 Figure Phantom

As scanned object a figure phantom representing cones, a sphere and a pyramid was used. In sum 5 scans of the figure phantom and 5 images of the patient were taken. Each image was registered to each other image. These result in a total registration count of 10 registrations. Thereby the naming scheme used in 2.6.3 Quality Measurement Procedure was used. The results of registration processes of the figure phantom can be seen from Figure 3.1 to Figure 3.4. On the left the checkerboard represents the image volume before image registration. On the right the result after image registration is depicted. Image registration of Phantom_1_2 and Phantom 1_4 from Figure 3.1 show rather good registration results while the registration of Phantom_1_3 fell short of expectations. The same holds true for Phantom_2_3, Phantom_3_4 and Phantom_3_5. From the figures it can be seen that these registration results are rather poor. But on the other hand registration performed well for 6 out of 10 registration processes. But it has to be mentioned that the resulting checkerboard filter images are not telling the whole truth. To be able to make a statement one has to take care of the translation and rotation. It is important to take in consideration that the checkerboard filter images only represent a slice out of a volume which is generated by the checkerboard filter module. Hence it can only be argued that the registration result in the depicted slices fell short of expectations. It is possible that the registration results are better in another region of the volume. Nevertheless, the checkerboard filter images give some good overview of the results and allow for drawing a conclusion. As mentioned before, the poor registration results have not to necessarily manifest in the deviation vector of the transformation matrix resulting from image registration as can be seen in Table 3.1.

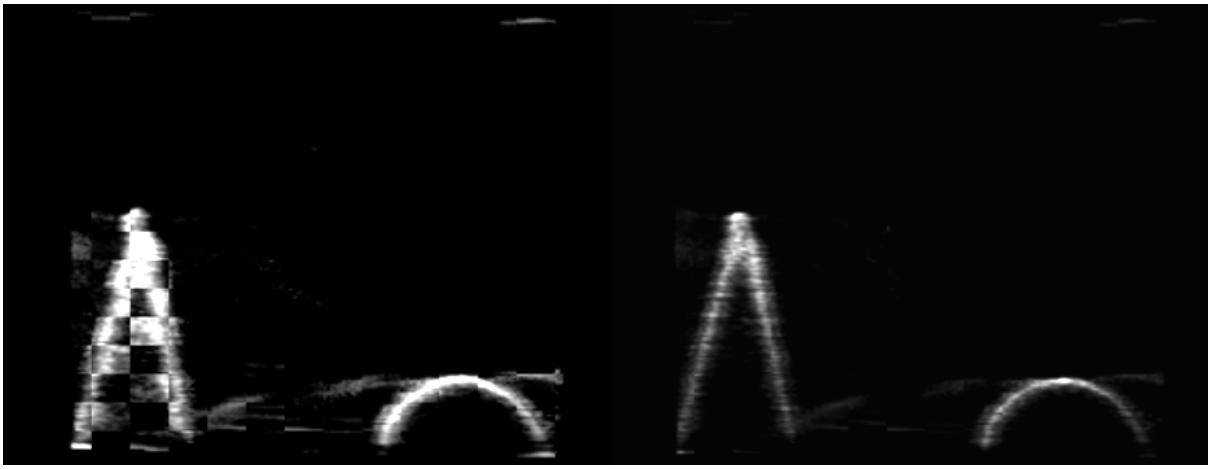

(a)

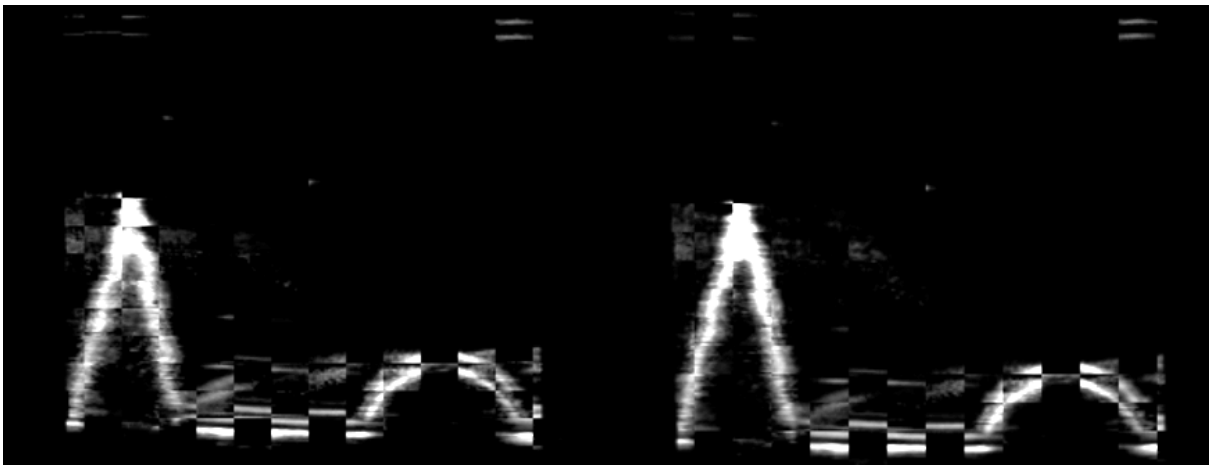

(b)

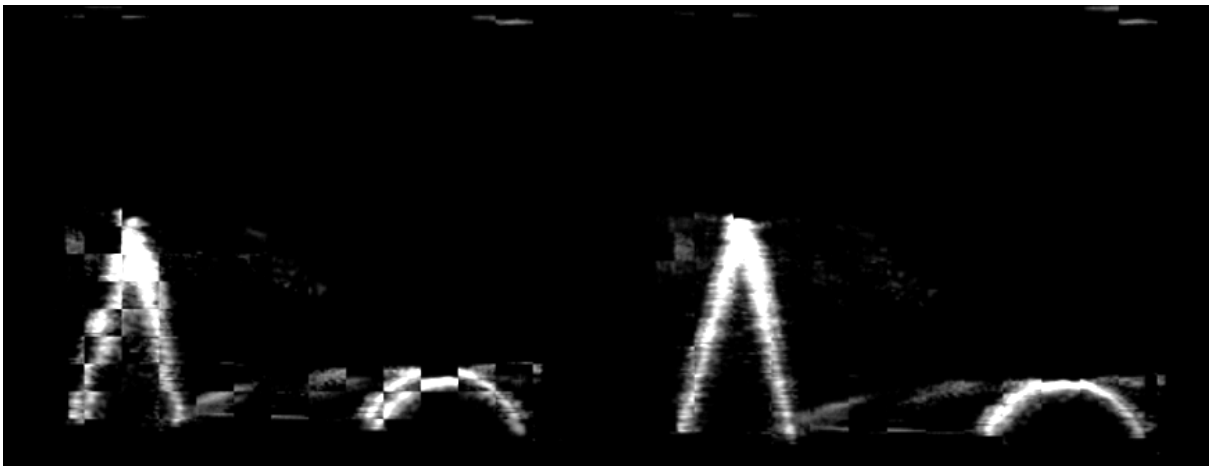

(c)

Figure 3.1: Image registration results of the figure phantom using checkerboard filter. The left image represents the checkerboard before image registration while the right image represents the checkerboard after image registration. (a): Phantom _1_2, (b): Phantom_1_3, (c): Phantom_1_4

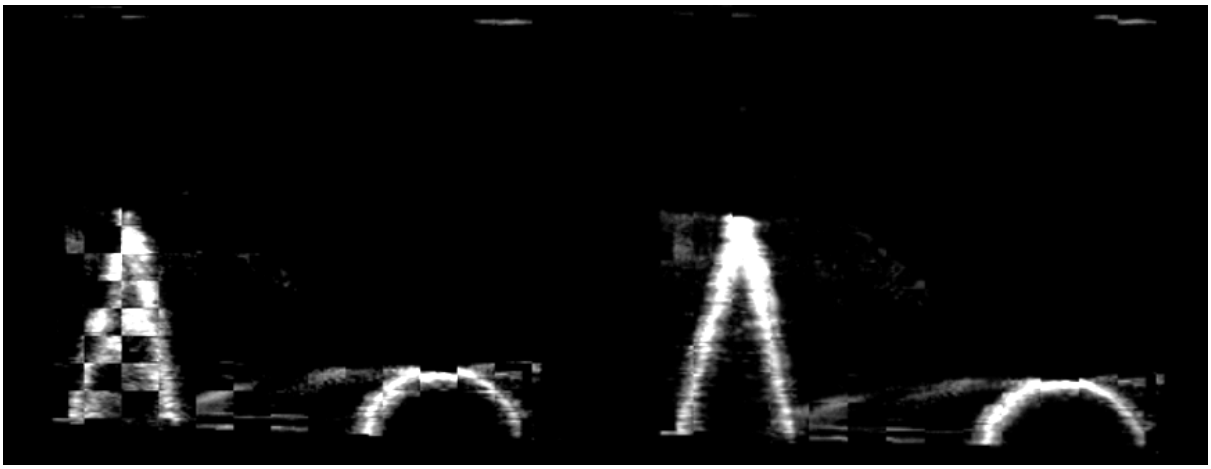

(a)

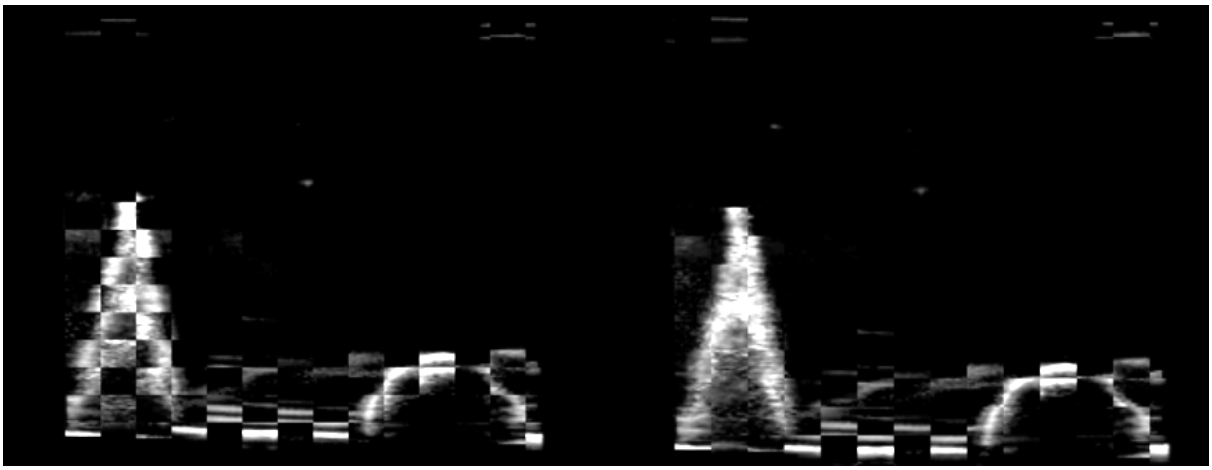

(b)

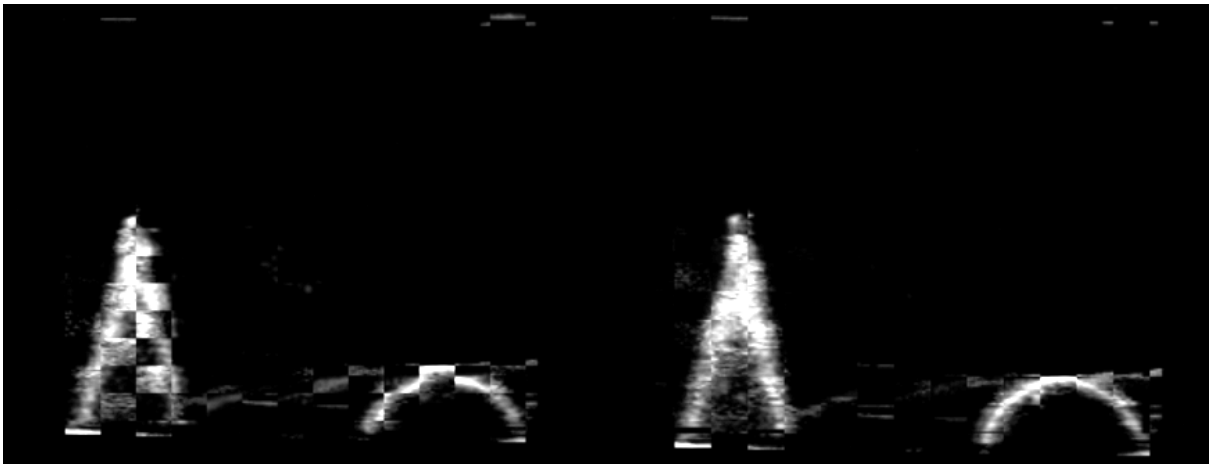

(c)

Figure 3.2: Image registration results of the figure phantom using checkerboard filter. The left image represents the checkerboard before image registration while the right image represents the checkerboard after image registration. (a): Phantom _1_5, (b): Phantom_2_3, (c): Phantom_2_4

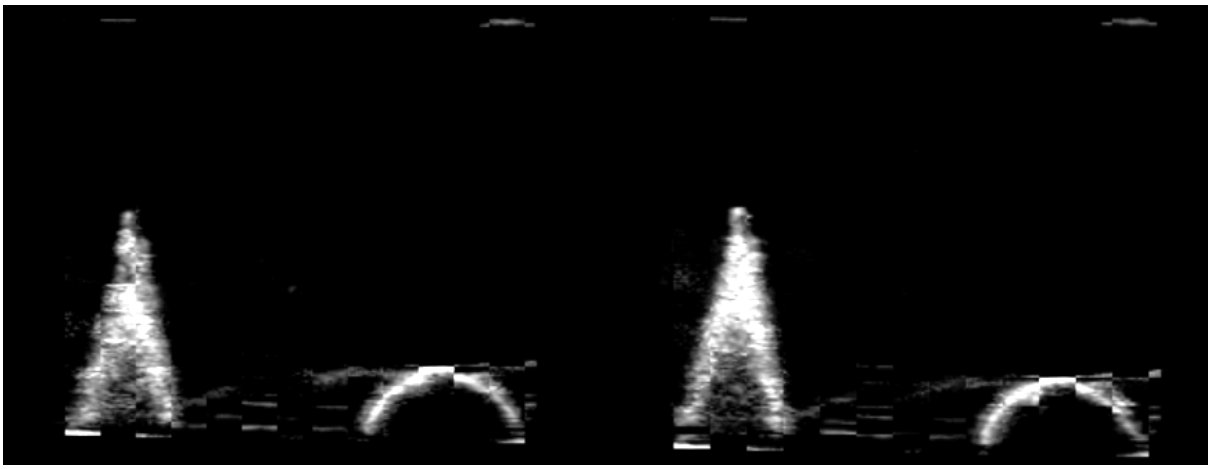

(a)

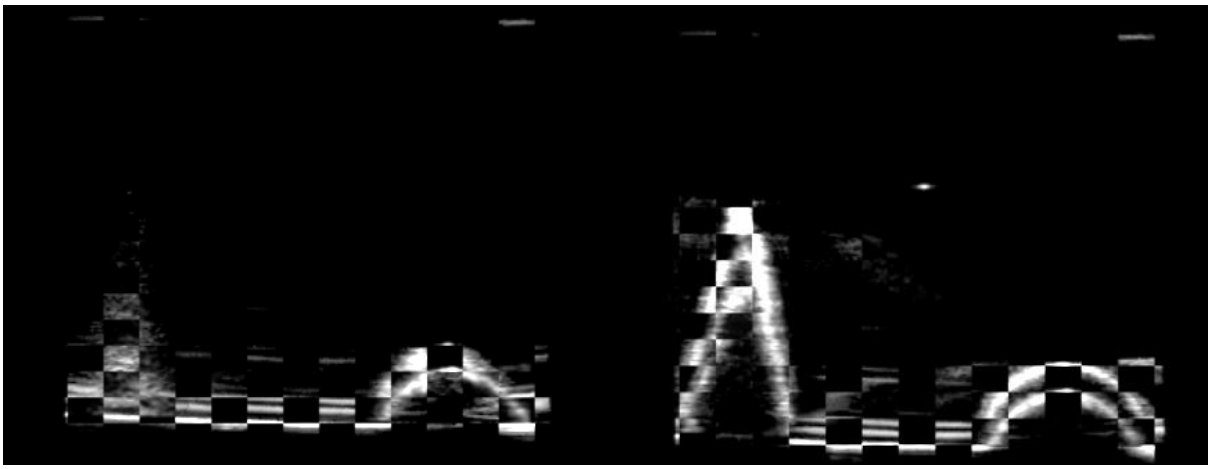

(b)

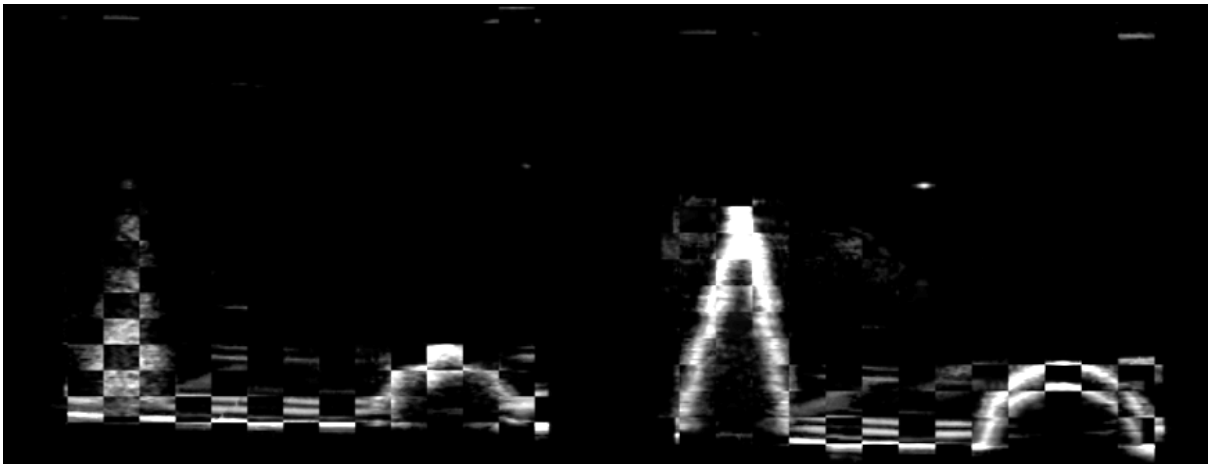

(c)

Figure 3.3: Image registration results of the figure phantom using checkerboard filter. The left image represents the checkerboard before image registration while the right image represents the checkerboard after image registration. (a): Phantom _2_5, (b): Phantom_3_4, (c): Phantom_3_5

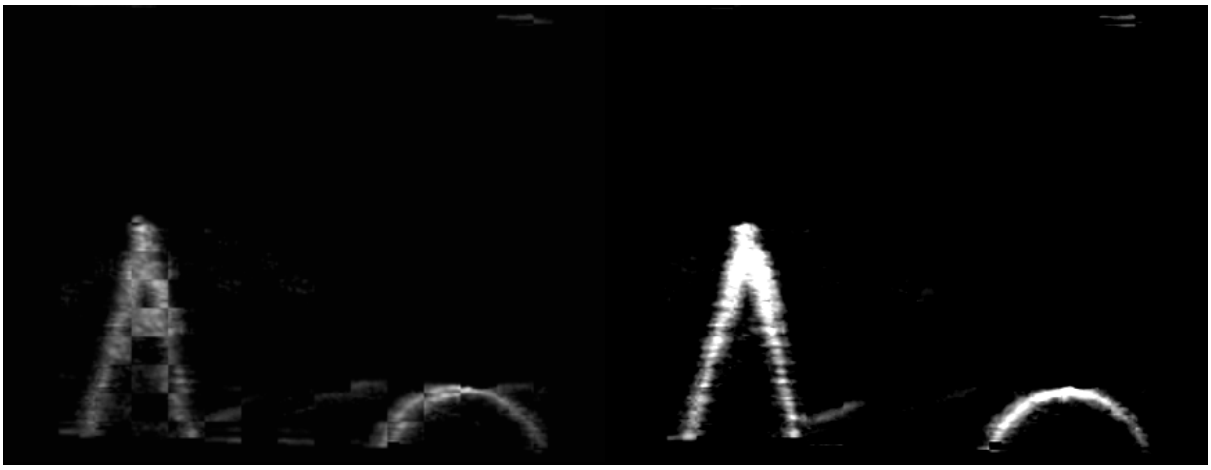

Figure 3.4: Image registration results of the figure phantom using checkerboard filter. The left image represents the checkerboard before image registration while the right image represents the checkerboard after image registration. Phantom_4_5

The measure of quality in terms of accuracy is not directly given by the checkerboard filter images but they give a clue of how well image registration was performed. It can be said that the better the images fit together the better the registration result and the more accurate the measure of misalignment of the coordinate systems given by the norm of the deviation vector. As aforementioned, the registration result not necessarily manifests in the checkerboard filter images but rather in the deviation vector of the registration transformation matrix. These results of the performed registrations can be seen in Table 3.1. The most left column represents the combination of image volumes for registration. X, Y and Z represent the translation in these directions of the reference coordinate system. $||\vec{t}||$ is the norm of the deviation vector and thereby stands for the overall shift of the images defined as the misalignment to the reference coordinate system as mentioned in 2.6.1 Details on Quality Measurement. The higher the calculated norm is, the higher the misalignment of the coordinate systems of the registered images is.

Phantom set	X [mm]	Y [mm]	Z [mm]	$\|\|\vec{t}\|\|$ [mm]
Phantom_1_2	-4,04	1,64	2,14	4,86
Phantom_1_3	-1,11	3,7	3,83	5,44
Phantom_1_4	8,49	3,63	1,39	9,34
Phantom_1_5	9,27	1,95	2,16	9,72
Phantom_2_3	-0,26	5,89	6,32	8,64
Phantom_2_4	8,28	2,33	-0,76	8,64
Phantom_2_5	7,9	-6,99	-7,57	12,98
Phantom_3_4	-7,87	-3,74	-4,43	9,78
Phantom_3_5	6,85	-2,46	-2,43	7,67
Phantom_4_5	-0,69	0,3	2,37	2,49

Table 3.1: Registration results of the deviation vector of the transformation matrix of the figure phantom

As the same procedures where used as in (Kaar, et al., 2013), with the exception that they used a 3D US machine, this data can be compared to those measured in Table 3.1. Compared to data taken from (Kaar, et al., 2013), where patient alignment error were measured, this are rather high values. As (Kaar, et al., 2013) used patient data rather than a figure phantom, this data may not be comparable at all but it gives a clue of how good the image quality in terms of accuracy of 3D US images reconstructed from 2D slices is. From the computed norms of the data, listed in Table 3.1, the mean can be calculated as well as the standard deviation. These are important statistical measure and thereby represent the mean image quality given the standard deviation with the processed method. These measures are listed in Table 3.2. This data states that the mean of the norm resulting from image registration of the figure phantom is 7.96mm whereas the standard deviation σ is 2.99mm. This states that the results from image registration differ in about 3mm which states, that the results are comparable to each other. But also outlier exists like Phantom_4_5 which has a norm of less than 2.5mm which connotes a rather good registration result and therefore good image quality. But the quality of the images is rather comparable. This can state that the acquired images of phantom 4 and phantom 5 fit because of missing artifacts or other matters.

μ [mm]	σ [mm]
7,96	2,99

Table 3.2: Mean and std. deviation of the norm ||t|| resulting from image registration of the figure phantom

3.2 Patient Data

To be able to compare the data in (Kaar, et al., 2013) more accurate, also patient data was acquired during the data acquisition procedure discussed in 2.4.2 Data Acquisition Procedure. As to compare most similar data, also the region of the prostate of a test patient was measured. In Sum 5 scans of the patient where taken. Two imaging sessions were carried out. During the first session the transducer was swept in parallel that way that the resulting 2D images are aligned parallel to each other. During the second session the transducer was not moved at all except of movement at the same position. Thereby a fan-shaped image was produced. Each image was registered to each other. It emphasized that the fan-shaped images could not get registered as the registration algorithm registered to boarders of the fan-shape structure. Hence the images resulting from the second session were not used. These 5 images of session one result in a total registration count of 10 registrations. Thereby the naming scheme used in 2.6.3 Quality Measurement Procedure was used. The results of the registration processes of the patient data can be seen from Figure 3.5 to Figure 3.8. On The left the checkerboard represents the image volume before image registration while on the right the result after image registration is depicted. The registration results appear to be comparable to the results of the figure phantom. The data sets Patient_1_2, Patient_1_3 and Patient 1_4 seem to be inaccurate in terms of the registration result, while the other results look rather good. But as with the figure phantom also with patient data the transformation matrix gives the information considering quality in terms of accuracy. The translational data from the deviation vector is listed in Table 3.3.

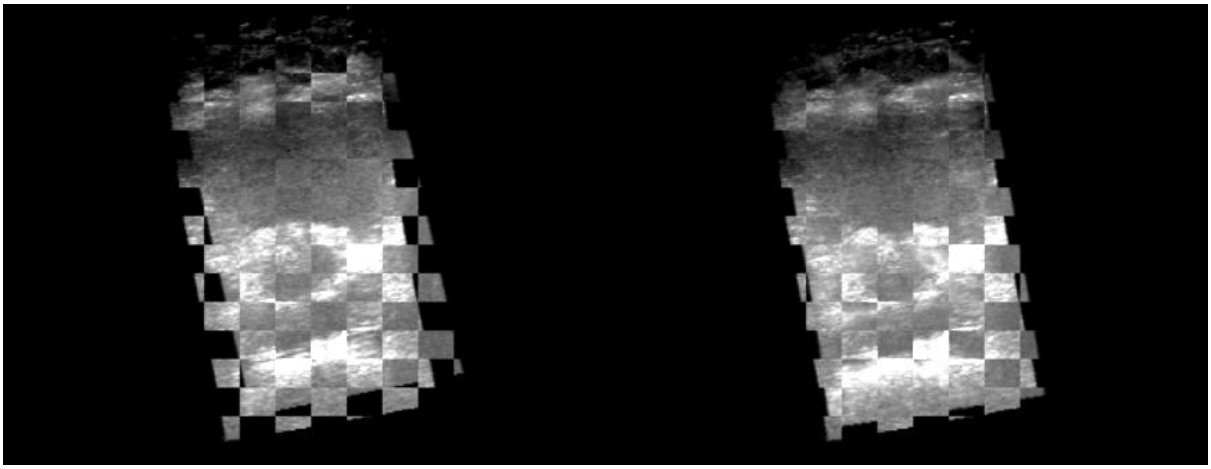

(a)

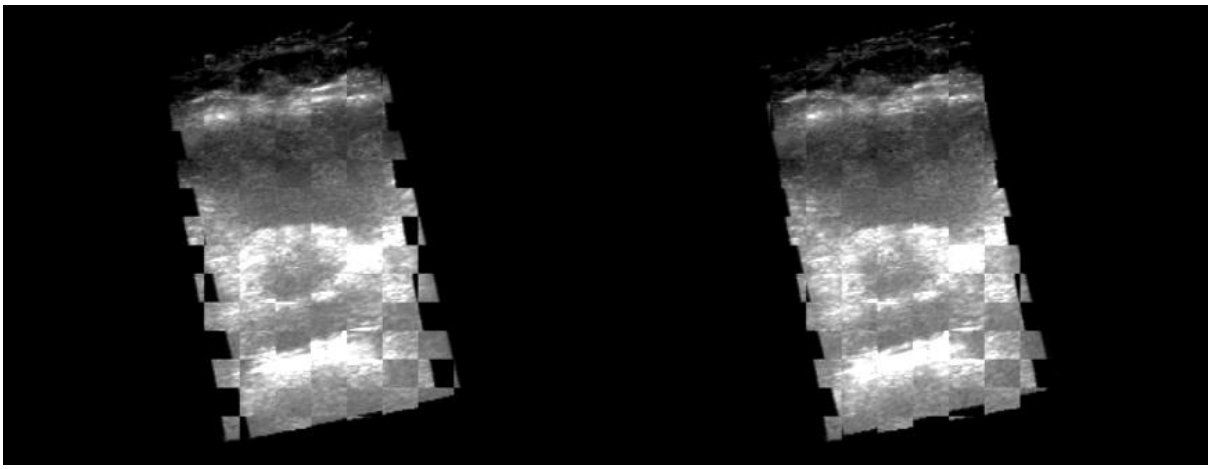

(b)

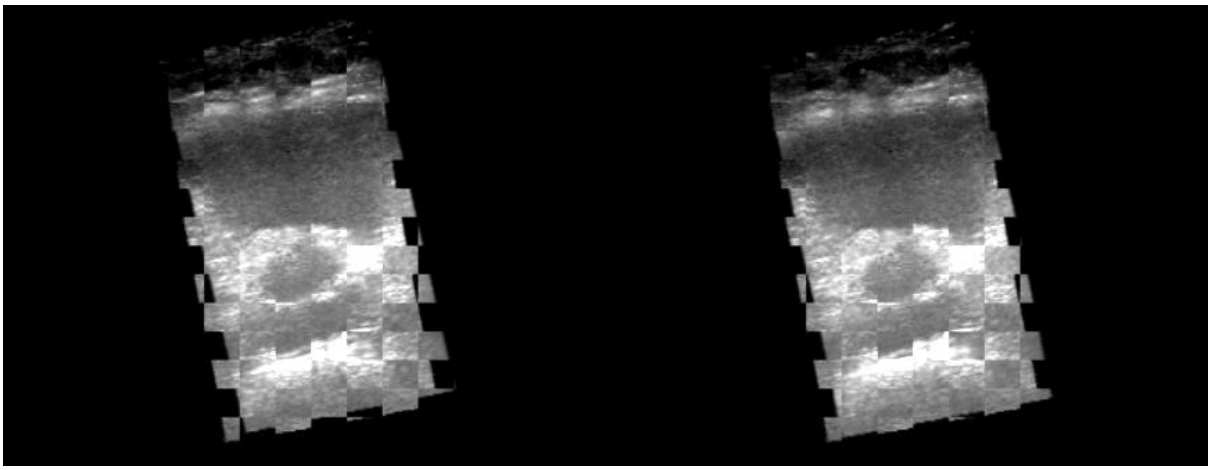

(c)

Figure 3.5: Image registration results of the patient data using checkerboard filter. The left image represents the checkerboard before image registration while the right image represents the checkerboard after image registration. (a): Patient_1_2, (b): Patient_1_3, (c): Patient 1_4

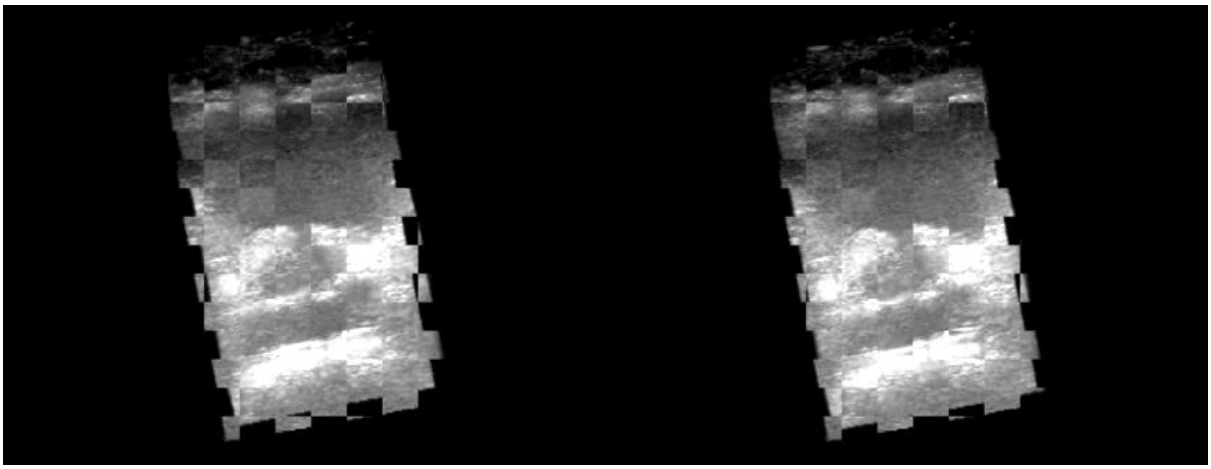

(a)

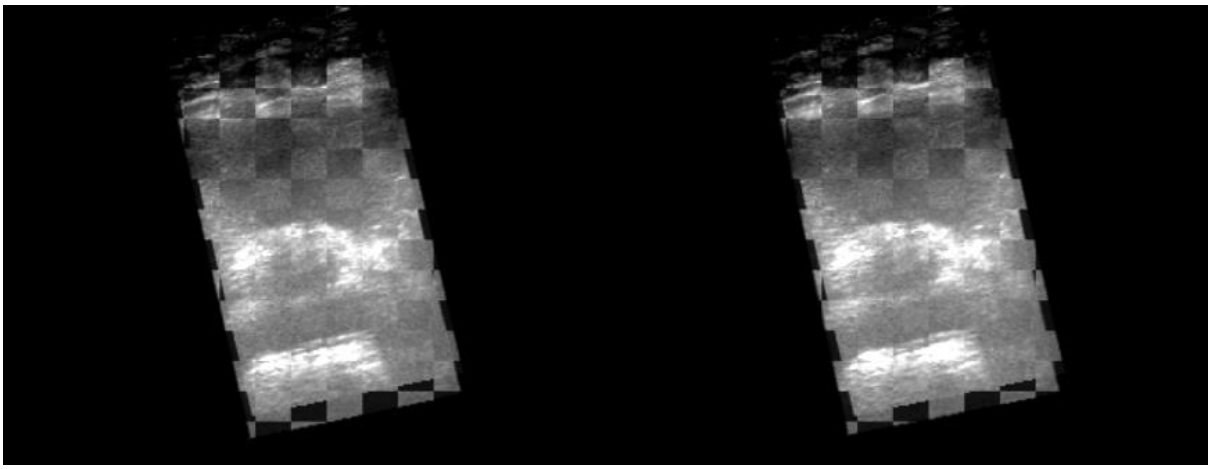

(b)

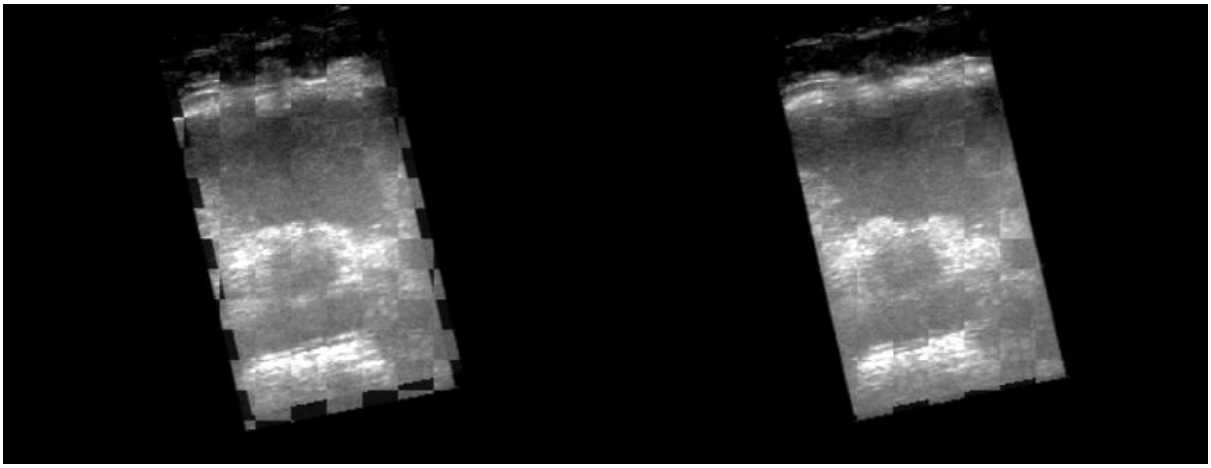

(c)

Figure 3.6: Image registration results of the patient data using checkerboard filter. The left image represents the checkerboard before image registration while the right image represents the checkerboard after image registration. (a): Patient_1_5, (b): Patient_2_3, (c): Patient 2_4

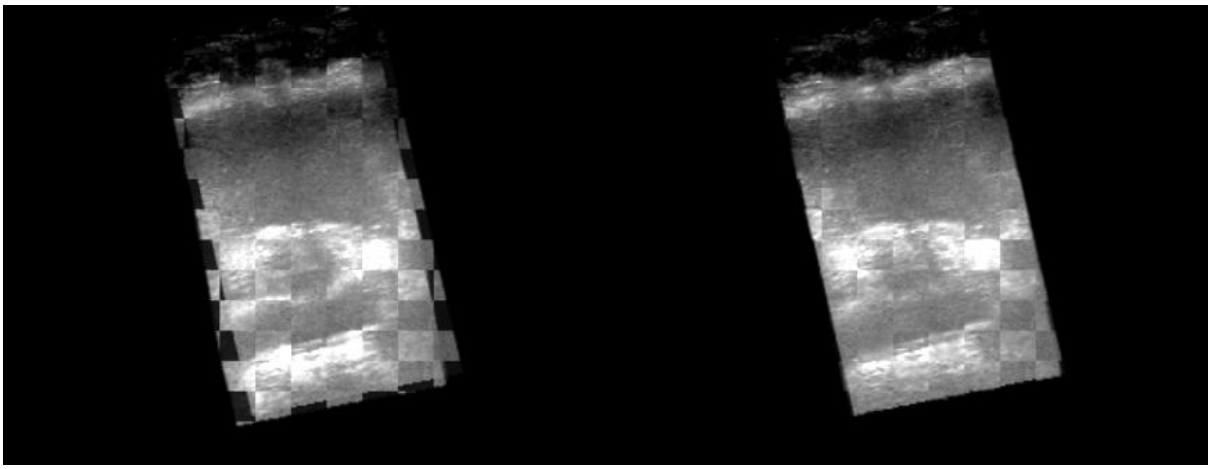

(a)

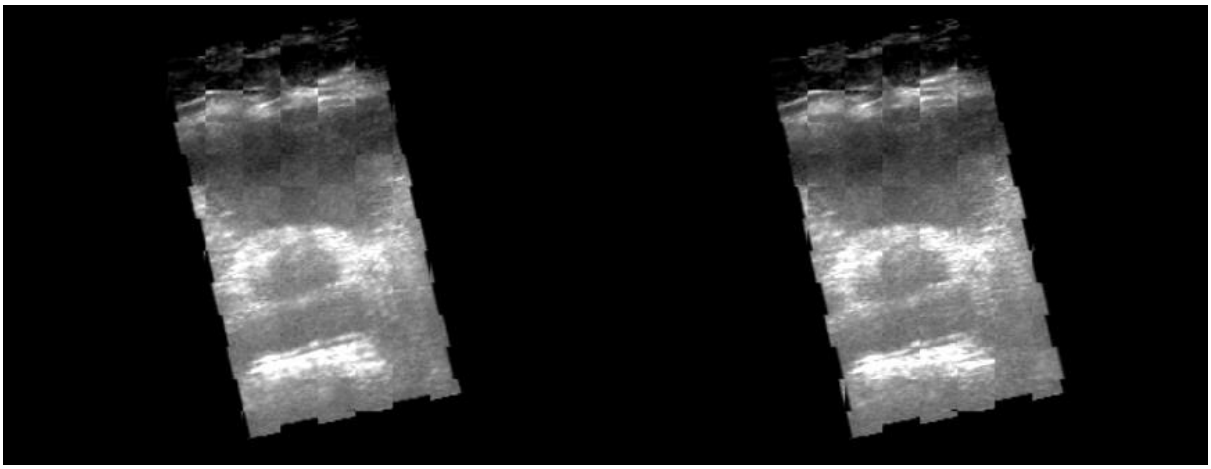

(b)

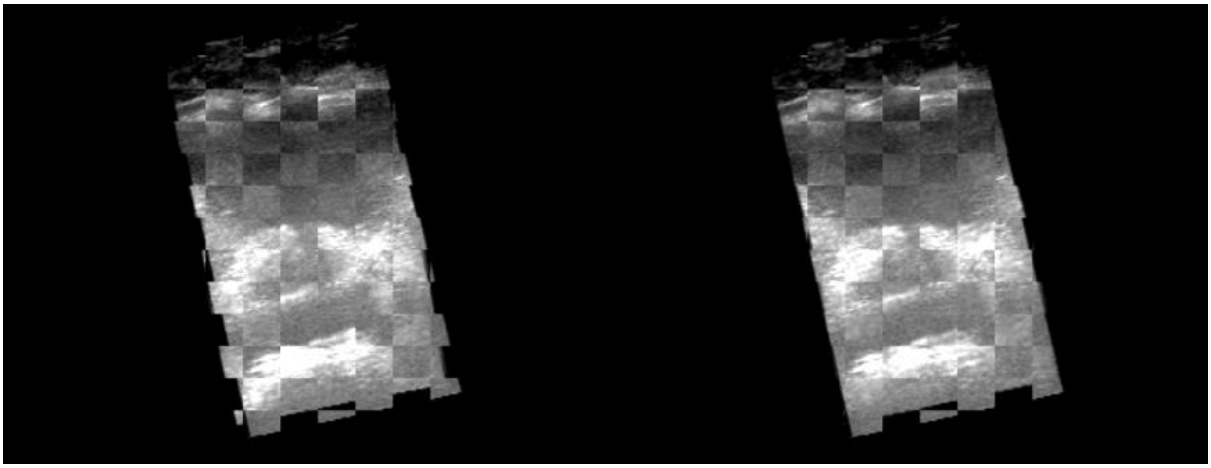

(c)

Figure 3.7: Image registration results of the patient data using checkerboard filter. The left image represents the checkerboard before image registration while the right image represents the checkerboard after image registration. (a): Patient_2_5, (b): Patient_3_4, (c): Patient 3_5

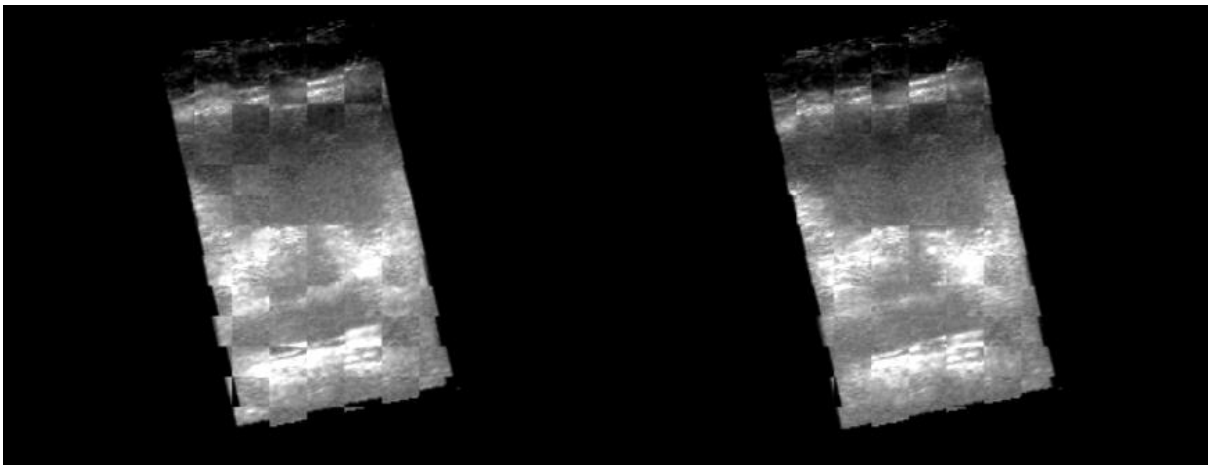

Figure 3.8: Image registration results of the patient data using checkerboard filter. The left image represents the checkerboard before image registration while the right image represents the checkerboard after image registration. Patient_4_5

As already mentioned with the figure phantom, the measure of quality in terms of accuracy is not directly given by the checkerboard filter images but they give a clue of how well image registration was performed. It can be said that the better the images fit together the better the registration result and the more accurate the measure of misalignment of the coordinate systems given by the norm of the deviation vector. Hence the registration result not necessarily manifests in the checkerboard filter images but rather in the deviation vector of the registration transformation matrix. These results of the performed registrations can be seen in Table 3.3. The most left column represents the combination of patient data volumes for registration. X, Y and Z represent the translation in these directions of the reference coordinate system. $||\vec{t}||$ is the norm of the deviation vector and thereby stands for the overall shift of the images defined as the misalignment to the reference coordinate system. It can be said the higher the calculated norm, the higher the misalignment of the coordinate systems of the registered images.

Patient set	X [mm]	Y [mm]	Z [mm]	$\|\|\vec{t}\|\|$ [mm]
Patient_1_2	1,92	-2,61	-11,09	11,55
Patient_1_3	-7,52	3,55	6,8	10,74
Patient_1_4	-13,73	-2,71	1,87	14,12
Patient_1_5	6,9	-1,29	-7,33	10,15
Patient_2_3	2,15	-2,09	-8,4	8,92
Patient_2_4	-11,73	-10,57	-13,94	21,06
Patient_2_5	-1,86	-9,56	-16,42	19,09
Patient_3_4	19,47	3,08	0	19,71
Patient_3_5	2,05	-0,95	0,62	2,34
Patient_4_5	-5,45	-4,97	-6,69	9,96

Table 3.3: Registration results of the deviation vector of the transformation matrix of patient data

This data, listed in Table 3.3, was measured using the same method (Kaar, et al., 2013) used. The only difference is that they used a general 3D US machine. Hence this data can be compared to those measured in Table 3.3. Compared to data taken from (Kaar, et al., 2013), where patient alignment error were measured, this are even higher values than measured with the figure phantom. From the computed norms of the data, again the mean and the standard deviation can be calculated. These measures are listed in Table 3.4. This data states that the mean of the norm resulting from image registration of patient data is 12.77mm whereas the standard deviation σ is 5.80mm. This states that the results from image registration differ in about 6mm which means, that the results are not necessarily comparable to each other. But again an outlier exists like Patient_3_5 which has a norm of less than 2.4mm which connotes a rather good registration result and therefore good image quality in terms of accuracy.

μ [mm]	σ [mm]
12,77	5,80

Table 3.4: Mean and std. deviation of the norm ||t|| resulting from image registration of patient data

The question now is, why these results, the figure phantom compared to the patient data, differs that much in quality in terms of accuracy, although the setup of both imaging sessions was the same. One can assume that the image volumes registered to each other do not fit, different from what the checkerboard filter images suggest. This may be a reason concerning the high values of the norm. It even is comprehensible as it is quite sophisticated difficult to register volumes from an anatomic region where the contrast is rather poor. The prostate is rather difficult to see in the image volumes. But this does not explain why there are still good registration results. Six to seven images out of 10 show a good registration result. It was mentioned, that the checkerboard images only represent a partial-region of the whole volume. So it is possible that the fitting of the volumes is not as good as thought. To ensure this, the volumes were observed with more detail by viewing different slices of the same volume. It appeared that the results of image registrations are the same when observing other image slices of each checkerboard filter volume. So difficulties during the registration process would not explain rather good registration results. It also attracts attention that some of the volumes even fit without performed image registration as can be seen in Figure 3.7 b and Figure 3.8. But the majority of the volumes show misalignment before image registration was performed. It also comes to one's mind that the results using the figure phantom is much better than using patient data. This allows for claiming the following hypothesis. Due to missing rigidly attached reference marker to the patient, it is possible that patient movement during data acquisition results in such high values of the norm $||\vec{t}||$. This would explain the overall good registration results in contrast to inaccurate alignment of the volume coordinate systems and hence poor image quality in terms of accuracy. Patient movement of up to 10mm does not necessarily attract one's attention when concentrating on image acquisition and parallel movement of the US transducer. Hence it is probably that mostly patient movement is the cause for such an inaccurate alignment of the coordinate systems of the registered images.

4 Discussion

The results show that there is a difference between the data using a figure phantom and patient data. As it was not possible to rigidly attach the reference marker to the patient, movement may be the cause for such inaccurate results when using patient data. This was discussed at the end of chapter 3.2 Patient Data. The conclusion of patient movement during the image acquisition sessions was made because the registration results showed rather good results in terms of conformity. Now to compare the resulting data listed in Table 3.3 with those measured from (Kaar, et al., 2013), this data is listed in Table 4.1. While they used a LCS instead of a reference marker, inaccuracies from movement of the patient during data acquisition can be precluded. Taken the hypothesis of patient movement into account it is not surprising that these results are much better compared to those underlying patient movement in Table 3.3. But also in the data measured from (Kaar, et al., 2013) an outlier exists, even though in the other direction. The data taken from Patient 3 results in a repositioning error of 9mm compared to results in the mean of 4.6mm as can be seen in Table 4.2.

Patient	X [mm]	Y [mm]	Z [mm]	$\|\|\vec{t}\|\|$ [mm]
1	4,91	1,72	2,65	5,84
2	3,74	1,75	1,71	4,47
3	6,44	4,88	3,96	9,00
4	2,71	0,3	0,82	2,85
5	5,64	0,73	1,09	5,79
6	0,79	1,23	-1,99	2,47
7	2,38	-1,24	-1,96	3,32
8	3,96	-1,43	-3,2	5,29
9	-0,36	1,1	-3,64	3,82
10	-2,81	-1,36	-1,33	3,39
11	0,68	0,61	-4,11	4,21

Table 4.1: Error in repositioning. Revised from (Kaar, et al., 2013)

From the computed norms of the data again, the mean and the standard deviation can be calculated. These measures resulting from data listed in Table 4.1 are listed in Table 4.2. This data states that the mean of the norm resulting from image registration of the figure phantom is 4.62mm whereas the standard deviation σ is 1.95mm. This states that the results from image registration differ in about 2mm which means, that the results are comparable to each other. But also here there is an outlier even if in the other direction. Patient 3 shows an error in repositioning of about 9mm which is rather high compared to the other results.

μ [mm]	σ [mm]
4,62	1,95

Table 4.2: Mean and std. deviation of the norm ||t|| resulting from image registration

To be able to compare the data measured to those taken from (Kaar, et al., 2013) another table is composed of the norm $||\vec{t}||$ from all data sets. This comparison is listed in Table 4.3. The data shows that the data measured by (Kaar, et al., 2013) is the most accurate one. Even the data measured with the figure phantom does not reach the measure taken from (Kaar, et al., 2013). To be able to make a more precise declaration one can compute the statistical measure of the mean and the standard deviation of the norm $||\vec{t}||$. This data is listed in Table 4.4.

data set	figure phantom	patient data	patient data Kaar et al.
1	4,86	11,55	5,84
2	5,44	10,74	4,47
3	9,34	14,12	9,00
4	9,72	10,15	2,85
5	8,64	8,92	5,79
6	8,64	21,06	2,47
7	12,98	19,09	3,32
8	9,78	19,71	5,29
9	7,67	2,34	3,82
10	2,49	9,96	3,39
11			4,21

Table 4.3: Comparison of the norms ||t|| from all three data sources

	figure phantom	patient data own	patient data Kaar et al.
μ [mm]	7,96	12,77	4,62
σ[mm]	2,99	5,80	1,95

Table 4.4: Comparison of the mean and the std. deviation from all three data sources

It can be seen that the data from the figure phantom differs in approximately 3mm from those measured by (Kaar, et al., 2013) at a rather comparable standard deviation. The data measured using patient anatomy differs in approximately 8mm while the standard deviation is also not comparable. Considering the possibility of patient movement during data acquisition and only comparing the results from the figure phantom with those taken from (Kaar, et al., 2013) this states that the accuracy of the acquisition method using 3D US reconstruction out of 2D slices using the material discussed in this thesis is lower than using a conventional 3D US. This may have different reasons. On the one hand using the reconstruction method involves inaccuracies from measuring the position of the US transducer by the optical tracking system. Also from calibration inaccuracies can arise. On the other hand the used US device was an elder 2D only model compared to a rather new US machine used by (Kaar, et al., 2013). This leads to the assumption when inaccuracies from the calibration procedure can be minimized and a more recent US device is used, the results may get better. But it has to be ensured that patient movement during data acquisition can be excluded and thus be neglected from the error chain. With the results given, the used procedure cannot be recommended for IGRT because these state that the inaccuracy measured using patient data is too high.

5 Conclusion

3D ultrasound is an interesting approach considering image-guided radiation therapy. The reason for this is the missing additional radiation that has to be applied when using other approaches. With respect to time effort it showed that using such an automatic repositioning system suggested in (Kaar, et al., 2013) will speed up the repositioning process compared to bulky and costly cone beam CT approaches. As the results show, 3D US reconstructed from 2D US image slices is an attractive method of 3D US image acquisition when image registration is of interest. Therefore it would be an interesting way to go. But the results also show that the accuracy of such measured images cannot compete with general 3D US devices. Also general 3D US systems cannot compete with systems like CBCT, as the accuracy of the latter system is higher compared to the 3D US approach. But it is a way that can be gone when no CBCT is available. It has to be mentioned that the access to general 3D ultrasound machines is also a matter of costs and therefore not every clinician has access to such a machine. Thus 3D US reconstructed from 2D image slices is also an interesting approach. But the results show, that the system which makes use of 2D US image acquisition lacks in terms of accuracy. The procedure used cannot compete with the system used by (Kaar, et al., 2013). As discussed previously, it can be seen that the data from the figure phantom differs in approximately 3mm from those measured by (Kaar, et al., 2013) while the data measured using patient data show a much worse result of approximately a difference of 8mm at a mean error of 12.7mm which cannot be neglected. This states that the accuracy of the system is rather low. As discussed, patient movement may be the cause. When only considering the results of the figure phantom it was also revealed that the accuracy cannot compete with systems using general 3D US machines. As accuracy is an important matter in IGRT this results cannot be ignored. Hence an application of a system which makes use of 3D volume reconstruction from 2D slices cannot be recommended in consideration of IGRT. It may be a way to go in the field of science when no other US device is available but using it for patient position in radiation therapy can lead to irradiation of healthy, normal tissue. To maximize the accuracy of the system one can try to lower the calibration error and minimize patient movement. But even if this is done it has to be ensured that the accuracy can compete with other systems still available on the market. As long as this is not ensured 3D US systems using reconstruction out of 2D slices should not be used in the field of IGRT although it is an interesting approach. The costs are low and compared to systems like CBCT or ExacTrac the mobility of the system is an advantage. Hence such a system can be used not only in the CTR or the TR but also in other environments. But to use the system in IGRT one has to overcome the lack in accuracy and ensure that it can compete with comparable systems.

Bibliography

Accuray. (2015). Retrieved 3 20, 2015, from TomoTherapy: www.tomotherapy.com

Active Silicon. (2015). Retrieved 3 22, 2015, from Active Silicon: www.activesilicon.com

Bathia, A. (2012). *3D Ultrasound Calibratioin and its Application in Radiation Therapy*. Vienna: Vienna University of Technology.

Best nomos. (2015). Retrieved 3 20, 2015, from Best nomos: www.nomos.com

Birkfellner, W. (2014). *Applied Medical Image Processing - A Basic Course - Second Edition.* CRC Press Taylor and Francis.

Boisvert, R. J., Gobbi, D., Vikal, S., Rohling, R., Fichtinger, G., & Abolmaesumi, P. (2008). n open-source solution for interactive acquisition, processing and transfer of interventional ultrasound images. *Systems and Architectures for Computer Assisted Interventions (MICCAI)*, 1-8.

Brainlab AG. (2015). Retrieved 03 20, 2015, from Brainlab: www.brainlab.com

Bronzino, J. D. (2006). *The Biomedical Engineering Handbook - Medical Devices and Systems.* CRC Press Taylor and Francis.

Bushberg, J. T., Seibert, J. A., Leidholdt, E. M., & Boone, J. M. (2012). *The Essential Physics of Medical Imaging.* Lippincott Williams & Wilkins.

Carbajal, G., Lasso, A., Gómez, A., & Fichtinger, G. (2013). Improving n-wire phantom-based freehand ultrasound calibration. *International Journal of Computer Assisted Radiology and Surgery, Vol 8*, 1063-1072.

Chen, T. K., Thurston, A. D., Ellis, R. E., & Abolmaesumi, P. (2009). A realtime freehand ultrasound calibration system with automatic accuracy feedback and control. *Ultrasound Med Biol, Vol 35*, 79-93.

Dawson, L. A., & Ménard, S. (2010). Imaging in Radiation Oncology: A Perspective. *The Oncologist*, 338-349.

Elekta AB. (2015). Retrieved 3 20, 2015, from Elekta AB: www.elekta.com

Gary, K., Ibanez, L., Aylward, S., Gobbi, D., Blake, M. B., & Cleary, K. (2006). Igstk: an open source software toolkit for image-guided surgery. *Computer, Vol 39*, 46-53.

Gobbi, D. G., & Peters, T. M. (2002). Interactive intra-operative 3D ultrasoud reconstruction an dvisualization. *MICCAI*, 156-163.

Hoffmann, R., Figl, M., Kaar, M., Bathia, A., Bhatia, A., Birkfellner, W., et al. (2010). Correction of Prostate Misalignment in Radiationi Therapy Using US-CT Registration. *Medical Imaging 2010: Visualization, Image-Guided Procedures, and Modeling, Vol. 7625*.

Hudson, R. M., Seeger, A., Weber, H., Juliano, J., & Helser, A. T. (2001). VRPN: A device-independent, network-transparent VR peripheral system. *Virtual Reality Software & Technology*, 15-17.

Kaar, M., Figl, M., Hoffmann, R., Birkfellner, W., Hummel, J., Stock, M., et al. (2013). Automatic patient alignment system using 3D ultrasound. *Medical Physics*.

Kaar, M., Kratochwil, A., Figl, M., Hoffmann, R., Bhatia, A., Bathia, A., et al. (2012). Automatic Patient Alighnemt for Prostate Radiation Applying 3D Ultrasound. *Medical Imaging 2012: Image-Guided Procedures, Probotic Interventions and Modeling, Vol. 8316, SPIE Press*.

Kapoor, A., Deguet, A., & Kazanzides, P. (2006). Software components and frameworks for medical robot control. *IEEE Int. Conf. Robotics and Automation ICRA*, 3813-3818.

Krieger, H. (2009). *Grundlagen der Strahlungsphysik und des Strahlenschutzes.* Vieweg & Teubner.

Lange, T., Kraft, S., Eulenstein, S., Lamecker, H., & Schlag, P. M. (2011). Automatic Calibration of 3D Ultrasound Probes. In *Bildverarbeitung für die Medizin* (pp. 169-173). Springer.

Lasso, A., Heffter, T., Rankin, A., Pinter, C., Ungi, T., & Fichtinger, G. (2014). PLUS: open-source toolkit for ultrasound-guided intervention systems. *IEEE Transactions on Biomedical Engineering; Vol 61*, 2527 - 2537.

Mathworks. (2015). Retrieved 3 27, 2015, from Mathworks Documentation: www.mathworks.com/help/

Mattes, D., Haynor, D. R., Veselle, H., Lewellen, T. K., & Eubank, W. (2003). PET/CT image registration in the chest using free-form deformations. *IEEE Transaction of Medical Imaging, Vol 22*, pp. 120-128.

MedicalExpo. (2015). Retrieved 03 13, 2015, from medicalexpo.com: www.medicalexpo.com

Mercier, L., Lango, T., Lindeseth, F., & Collins, L. D. (2005). A review of calibration techniques for freehand 3-d ultrasound systems. *Ultrasound Med Biol, Vol 31*, 143-165.

Mohan, R., Dong, L., & Zhang, X. (2006). Tecent Advances in Image-Guided Radiotherapy. *Radiotherapy and Oncology Volume 78*, 27-28.

OpenIGTLink. (2015). Retrieved 3 22, 2015, from OpenIGTLink: www.openigtlink

Oppelt, A. (2005). *Imaging Systems for Medical Diagnostics: Fundamentals, Technical Solutions and Applications for Systems Applying Ionizing Radiation, Nuclear Magnetic Resonance and Ultrasound.* Publicis Publishing.

Peters, T., & Cleary, K. (2008). *Image-Guided Interventions - Technology and Applications.* Springer.

PLUS Project. (2015). Retrieved 3 22, 2015, from PLUS Project: www.plustoolkit.org

Sawney, G. S. (2007). *Fundamentals of Biomedical Engineering.* New Age International.

Schroeder, W., Martin, K., & Lorensen, B. (2003). *The Visualization Toolkit, Third Edition.* Kitware Inc.

Slicer.org. (2015). Retrieved 3 21, 2015, from Slicer.org: www.slicer.org

SlicerIGT. (2015). Retrieved 3 25, 2015, from SlicerIGT user tutorial: http://www.slicerigt.org/wp/user-tutorial/

Spiczak, J., Samset, E., DiMaio, S., Reitmayr, G., Schmalstieg, D., Burghart, C., et al. (2007). Multimodal event streams for virtual reality. *SPIE Medical Imaging, Vol 6504*, 65040M-65040M-8.

Steiner, E. (2011). *Image-Guided Radiation Therapy of Prostate Cancer: Organ and Patient Movement Analysis.* Vienna: Vienna University of Technology.

Vaezy, S., & Zderic, V. (2009). *Image-Guided Therapy Systems.* Artech House.

Varian Medical Systems. (2015). Retrieved 3 20, 2015, from Varian Medical Systems: www.varian.com

Verellen, D., de Ridder, M., & Storme, G. (2008). A (short) history of image guided radiotherapy. *Radiotherapy and Oncology*, 4-13.

Abbreviations

2D	Two-dimensional
3D	Three-dimensional
API	Application programming interface
CBCT	Cone-beam computed tomography
CT	Computed tomography
CTR	Computed tomography room
DBS	Double strand break
DOF	Degrees of freedom
EMTS	Electromagnetic Tracking Systems
EPID	Electronic portal imaging device
GUI	Graphical user interface
Gy	Gray (radiation dose)
IGI	Image-guided intervention
IGRT	Image-guided radiation therapy
IGT	Image-guided Therapy
IM	Imaging modalities
IMRT	Intensity modulated radiation therapy
IP	Ion pairs
IR	Infrared
keV	kilo electron volt
LCS	Laser coordinate system
LED	Light Emitting Diode
LET	Linear energy transfer
LINAC	Linear accelerator
MDS	Multiple damaged sites
MeV	Mega electron volt
MMI	Mattes mutual information
MRI	Magnetic resonance imaging
MSE	Mean square error
NC	Normalized correlation
OTS	Optical Tracking Systems
ROS	Reactive oxygen species
RT	Radiation Therapy

PET	Positron emission tomography
PLUS	Public software Library for Ultrasound imaging research
PSNR	Peak signal to noise ratio measure
SSB	Singles strand break
SSIM	Structural similarity index measure
TR	Treatment room
US	Ultrasound
USB	Universal serial bus
VDR	Void detectability ratio
VfW	Video for Windows